ESA/SCI(2021)2
February 2021

THESEUS

Transient High-Energy Sky and Early Universe Surveyor

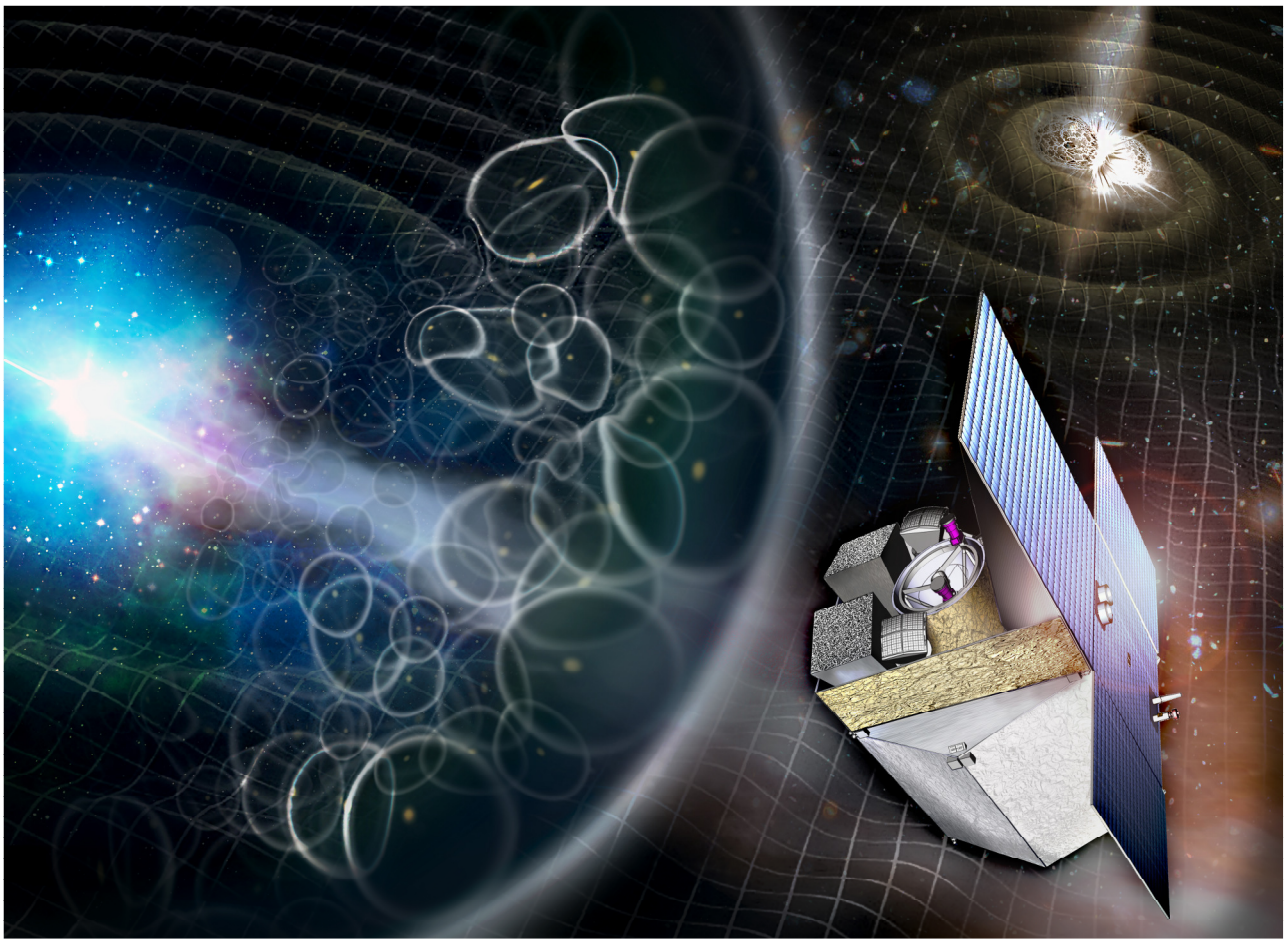

Assessment Study Report

European Space Agency

THESEUS Assessment Study – Mission Summary	
Key scientific goals	The THESEUS mission will use long Gamma-Ray Bursts (GRB) to solve key questions about the early Universe and will become a cornerstone of multi-messenger and time-domain astrophysics. Core science goals of THESEUS are summarized as follows. **Investigating the first billion years of the Universe through high-redshift GRBs,** thus shedding light on main open issues in modern cosmology, like: - Population of primordial low mass and luminosity galaxies; - Sources and evolution of cosmic re-ionization; - SFR and metallicity evolution up to the "cosmic dawn" and across Pop-III stars. **Providing a substantial advancement of multi-messenger and time-domain astrophysics** by enabling the identification, accurate localisation and study of: - Electromagnetic counterparts to sources of gravitational waves and neutrinos, which will be routinely detected in the late '20s and early '30s by the second and third generation Gravitational Wave (GW) interferometers and future neutrino detectors; - All kinds of GRBs and most classes of other X/gamma-ray transient sources. Under all these respects, **THESEUS will provide great synergies with future large observing facilities** in both the and multi-messenger domains. A **Guest Observer programme**, comprising Target of Opportunity (ToO) observations will expand the science return, to include, e.g., solar system minor bodies, exoplanets and AGN.
Reference core payload	**Soft X-ray Imager** (**SXI**, 0.3 – 5 keV), a set of two X-ray monitors based on MicroPore Optics (MPO) in "Lobster-eye" configuration and using large X-ray CMOS as detectors, covering 0.5 sr Field of View (FoV) with source location accuracy from 0.5 to 2 arc-min; **X/Gamma-rays Imaging Spectrometer** (**XGIS**, 2 keV – 10 MeV), a set of two X/gamma-ray monitors based on coded mask technique and Silicon Drift detectors (SDD) coupled to CsI crystal scintillator detectors, with imaging and source localization accuracy better than 15 arcmin in the 2 – 150 keV energy band and over a FoV of 2sr, a few μs time resolution; **InfraRed Telescope (IRT**, 0.7 – 1.8 m), an off-axis Korsch telescope with 0.7m primary mirror granting a FoV of 15x15 arc-min^2 and 1 arc-sec source location accuracy, providing imaging capabilities in five NIR filters (I, Z, Y, J, H), moderate (R~400 at 1.1μ) slit-less spectroscopy in 0.8 – 1.6 μm over a 2x2 arc-min^2 FoV and *on-board redshift measurement*. The payload system will also include the **Trigger Broadcasting Unit** (**TBU**), broadcasting transient alerts within a few tens of seconds.
Overall mission profile	THESEUS is designed to be launched with a VEGA-C vehicle into a **near equatorial Low –Earth Orbit** of 550-640 km altitude and 5.4° inclination. The main ground station will be Malindi (ASI). The ground segment will include a **network of VHF antennae** located around the Equator for receiving the data transmitted by the TBU. **The nominal mission duration is 4 years**, with no identified technical issues preventing an extension of at least 2 years. The concept of operations includes the spacecraft capability of **autonomously evaluating and performing fast (>7°/min) slews** for pointing the IRT to the GRB locations provided by SXI and/or XGIS. Pointing strategies maximizing the combined efficiency of GRB detection with the SXI and/or XGIS and follow-up observations by IRT, as well as facilitating the follow-up from ground facilities, have been identified. All scientific data will be public, except for those acquired during the early mission phases and those of GRBs at z>6 detected in the first 6 months from launch.
Description of Spacecraft	Industrial teams developed a bus design based on 3-axis stabilised spacecraft with box shaped structure and divided into a Service Module and a Payload Module, with a central IRT telescope surrounded by the SXI and XGIS cameras. The AOCS uses four star-trackers optical heads configuration with 2 always in tracking, coarse rate sensor and sun sensors. The spacecraft agility is obtained through (3N+1R) Reaction Wheels, with magnetic torquers for quasi-continuous desaturation. The field of regard corresponds to 60% accessibility of the sky at any time. The spacecraft dry mass at launch is 1900 kg, including contingency.

Foreword

The transient high energy sky has proven a remarkable source of discoveries in astrophysics, going back to the 1960s. In recent years, the Swift mission has demonstrated the power of autonomous, rapid-slewing satellites for discovery and localisation of short-lived transients, including GRBs, now detected over the whole of cosmic history back to the era of reionization. At the same time, extraordinary progress in multi-messenger astronomy have resulted in the historical observation of a kilonova both in gravitational waves and across the whole electromagnetic spectrum, as well as the first identification of extra-galactic neutrino sources.

The THESEUS mission will provide a step change in capabilities for wide-area detection and characterisation of transients over a very broad energy band (0.3 keV to 10 MeV), including on-board near-infrared imaging and spectroscopy, and is designed to be at the forefront of these science fields in the 2030s. It grew out of the recommendation following the ESA L2/L3 selection process: *"The SSC strongly endorses the need to continue pursuing in the future the discovery of GRBs"*. Although building on the legacy of previous missions designed to be GRB discovery machines, the crucial next step is to develop a multi-wavelength mission which can fully exploit GRBs to address central questions in astrophysics and cosmology. THESEUS is that mission, with its highest priority goals to: (a) discover a significant sample of long-duration GRBs (at least several tens) at $z>6$, providing a unique window on early star formation and galaxy evolution, allowing detailed study of the interstellar medium of even extremely faint host galaxies, and evaluating the role of stars in the reionization of the universe; and (b) discover and study EM counterparts of merging compact binaries also detected via gravitational waves, relying on the bright short-duration GRB emission to provide rapid localisation and potentially leading to redshifts for sources at distances such that they are invisible in other EM bands.

European leadership in this area builds on past success and ongoing investment: in addition to involvement in pioneering satellite missions (BeppoSAX, INTEGRAL, Swift, SVOM), Europe has been at the heart of developments in multi-messenger astrophysics (e.g., Virgo, KM3Net) and its electromagnetic follow-up via European led consortia (e.g., ENGRAVE, VINROUGE, STARGATE etc). THESEUS is inherently a mission with huge synergy with the premier future observatories, providing simultaneous wide sky monitoring, rapid follow-up and real-time triggers. From ELT to ATHENA, CTA to Einstein Telescope, the Rubin Observatory to the Roman Space Telescope, the science returns from combining observations with multiple facilities is a classic case of "the whole being much greater than the sum of the parts".

A broad range of other science programmes will also be enabled by THESEUS, including using observations of GRB emission as laboratories of ultra-relativistic matter, providing tests of fundamental physics, such as Lorentz invariance, and gathering statistics on large populations of other high energy sources and transients. Thus, THESEUS data will be of interest to a very wide user community, including through its open guest-observer programme.

The study, conducted by the THESEUS consortium and the ESA study Team, has led to detailed, workable and well qualified solutions for the spacecraft, its payload and operations. It has also demonstrated the technical and programmatic feasibility of accomplishing the core science goals with this mission concept.

In conclusion, THESEUS will be a really unique and superbly capable facility, one that will do amazing science on its own, but also will add huge value to the currently planned new photon and multi-messenger astrophysics infrastructures coming on-line in the 2020s and 2030s.

Authorship, acknowledgements

This report has been prepared by the *THESEUS* Team listed below.

ESA Science Study Team (SST)		
Name	*Affiliation*	*City, Country*
Lorenzo Amati (*Lead Scientist*)	INAF – OAS	Bologna, Italy
Stéphane Basa	LAM	Marseille, France
Maria Dolores Caballero-Garcia	IAA - CSIC	Granada, Spain
Lise Christensen	University of Copenhagen	Copenhagen, Denmark
Diego Götz	CEA – Irfu	Saclay, France
Lorraine Hanlon	University College Dublin	Dublin, Ireland
Paul T. O'Brien	University of Leicester	Leicester, United Kingdom
Stéphane Paltani	University of Geneva	Geneva, Switzerland
Andrea Santangelo	IAAT	Tübingen, Germany
Giulia Stratta	INAF – OAS	Bologna, Italy
Nial Tanvir	University of Leicester	Leicester, United Kingdom
Assessment Study Report Editorial Board		
Andrew Blain	University of Leicester	Leicester, United Kingdom
Enrico Bozzo	University of Geneva	Geneva, Switzerland
Giancarlo Ghirlanda	INAF – Osservatorio di Brera	Milano, Italy
Emerich Le Floch	CEA – Irfu	Saclay, France
Sandro Mereghetti	INAF – IASF Milano	Milano, Italy
Julian Osborne	University of Leicester	Leicester, United Kingdom
Piero Rosati	University of Ferrara	Ferrara, Italy

The ESA Team supporting the activities is composed by:

ESA Study Team		
Silvia Bayon, Gonzalo Saavedra Criado, Philippe Gondoin (Study Managers)	ESA	ESTEC, The Netherlands
Matteo Guainazzi (Study Scientist)	ESA	ESTEC, The Netherlands
Thibaut Prod'homme (Payload Manager)	ESA	ESTEC, The Netherlands
Guillaume Belanger (Science Operations Study Manager)	ESA	ESAC, Spain
ESA Coordinators		
Luigi Colangeli, Paul McNamara	ESA	ESTEC, The Netherlands

The authors acknowledge support by Y. Evangelista and Carlo Ferrigno for figures editing, the coordinators and members of the Consortium Science Working Groups, and further Members of the ESA Study Team.

Table of contents

1 Executive summary

Transformational science with THESEUS

The Transient High Energy Sources and Early Universe Surveyor (THESEUS) is designed to fully exploit the unique and breakthrough potentialities of Gamma-Ray Bursts (GRBs) for investigating the Early Universe and advancing Multi-Messenger Astrophysics, while simultaneously vastly increasing the discovery space of high energy transient phenomena over the entirety of cosmic history. The primary scientific goals of the mission will address the Early Universe ESA Cosmic Vision theme "How did the Universe originate and what is made of?" and will significantly impact on "The gravitational wave Universe" and "The hot and energetic Universe" themes. This will be achieved by a payload and mission profile providing an unprecedented combination of: 1) wide and deep monitoring of the high-energy sky in a very broad energy band (0.3 keV - 10 MeV); 2) focusing capabilities in the soft X-ray band providing large grasp and high angular resolution; 3) on board NIR capabilities for immediate low-frequency counterpart identification, arcsecond localization and redshift determination; and 4) a high-degree of spacecraft autonomy and agility, together with the capability of promptly transmitting to ground transient trigger information. In summary, the main scientific goals of the proposed mission are to:

a) Explore the Early Universe (cosmic dawn and reionization era) by building a representative sample of the GRB population in the first billion years; specifically, THESEUS will:

- Unveil and characterize the bulk of the population of low-luminosity primordial galaxies not (or marginally) accessible by current and future large telescopes (e.g., JWST and ELT);
- Provide a substantial contribution to assessing the global star formation history of the Universe up to z ~ 10 and possibly beyond;
- Investigate the re-ionization epoch, the interstellar medium (ISM) and the intergalactic medium (IGM) up to z ~ 6 – 10, thus shedding light on how did re-ionization proceed as a function of environment, if radiation from massive stars was its primary driver and how did cosmic chemical evolution proceed as a function of time and environment;
- Provide observational constraints on when did the first stars form and how did the earliest Population III and Population II stars influence their environment.

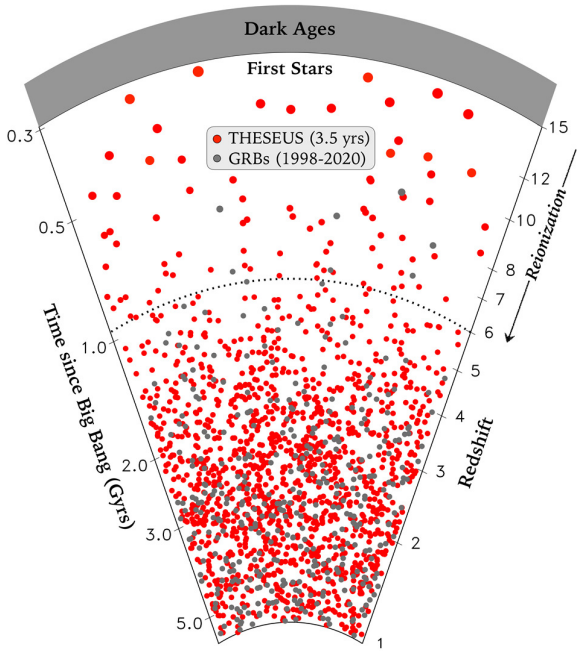

Figure 1-1 THESEUS capability of detecting and autonomously identifying high-redshift GRBs, as a function of cosmic age, in 4 years of operations (red dots) compared to what has been achieved in the last ~20 years.

b) Provide key observations to multi-messenger and time-domain astrophysics:

- Locate and identify the electromagnetic counterparts to sources of gravitational radiation and neutrinos, which will be routinely detected in the early '30s by second (2G) and third generation (3G) Gravitational Wave (GW) facilities (e.g., LIGO A plus, Advanced Virgo Plus, KAGRA; Einstein Telescope, Cosmic Explorer) and future large neutrino detectors (e.g., Km3NET and IceCube-Gen2);
- Provide real-time triggers and accurate (≤15' within a few seconds; ~1'' within a few minutes) positions of large numbers of (long/short) GRBs and other high-energy transients for follow-up with next-generation optical-NIR (ELT, TMT, JWST if still operating), radio (SKA), X-rays (ATHENA), TeV (CTA) telescopes;

- Get fundamental insights into the physics and progenitors of GRBs and their connection with peculiar core-collapse SNe and substantially increase the detection rate and characterization of sub-energetic GRBs and X-Ray Flashes;
- Allow a fundamental step forward in the comprehension of the physics of various classes of Galactic and extra-Galactic transients, e.g.: tidal disruption events (TDEs), magnetars / Soft Gamma-ray Repeaters (SGR), Supernovae (SNe) shock break-outs, Soft and Hard X-ray Transients, thermonuclear bursts from accreting neutron stars, novae, dwarf novae, stellar flares, Active Galactic Nuclei (AGN) and blazars.

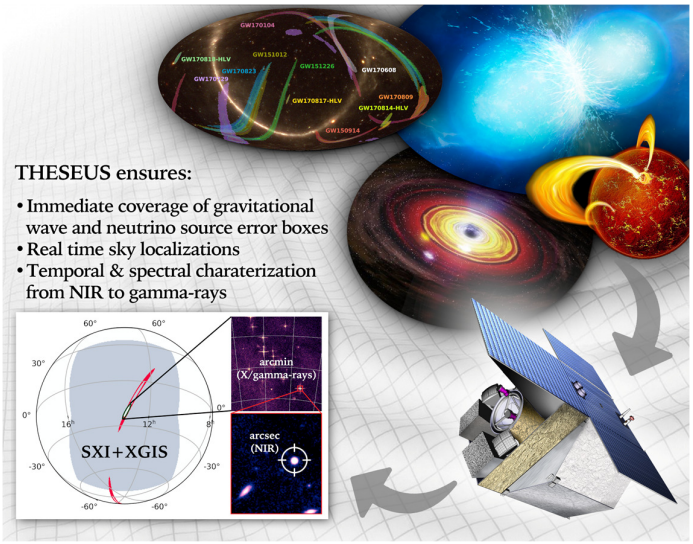

Figure 1-2 Examples of THESEUS capabilities for multi-messenger and time-domain astrophysics.

By satisfying the requirements coming from the above main science drivers, the THESEUS mission will automatically provide fundamental synergies with the future large multi-wavelength and multi-messenger facilities, allowing them to fully exploit their scientific capabilities. As outstanding examples, we remark that: a) THESEUS would operate at the same epoch as ATHENA, and would be the ideal space mission to provide the triggers required to fulfil some of the scientific objectives of that mission involving GRBs (progenitor environment, find Pop-III stars, enable high sensitivity absorption spectroscopy of the Warm-Hot Intergalactic Medium, WHIM) and high-energy transients of all kinds; b) THESEUS will provide high-energy transient survey capabilities complementary to those of the Vera C. Rubin Observatory (VRO; formerly known as the Large Synoptic Survey Telescope, LSST) in the optical; the joint availability of the two facilities in the next decade would provide a substantial advancement of time-domain astronomy. THESEUS will also enable excellent science as an observatory, including, e.g., performing NIR observations, long-term monitoring, and a rapid-response capability to external triggers, thus enabling strong community involvement.

THESEUS: a breakthrough mission concept

The scientific goals for the exploration of the early Universe require the detection, identification and characterization of several tens of long GRBs occurred in the first billion years of the Universe ($z > 6$) in the 4 years of nominal mission lifetime of THESEUS a giant leap with respect to what has been obtained (7 GRBs at $z>6$) in the last 20 years, using past and current GRB dedicated experiments (e.g., *Swift*/BAT, *Fermi*/GBM, Konus-*WIND*) combined with intensive follow-up programs from the ground with small robotic and large telescopes (e.g., VLT, Figure 1-1). This breakthrough performance can be achieved by overcoming the current limitations through an extension of the GRB monitoring passband to the soft X-rays with an increase of at least 1 order of magnitude in sensitivity with respect to previously flown wide-field X-ray monitors, as well as a substantial improvement of the efficiency of counterpart detection, spectroscopy and redshift measurement through prompt on-board NIR follow-up observations. At the same time, the objectives on multi-messenger astrophysics and, more generally, time domain astronomy, require: a) a substantial advancement in the detection and localization, over a large (>2 sr) Field-of-View (FoV) of short GRBs as electromagnetic counterparts of GW signals coming from Neutron Stars (NS), and possibly NS-Black Hole (BH), mergers, as demonstrated in the case of GW170817; b) monitoring the high-energy sky with an unprecedented combination of sensitivity, location accuracy and field of view in the soft X-rays; c) imaging up to the hard X-rays and spectroscopy / timing to the soft gamma-rays. The capabilities of THESEUS in this field are summarized in Figure 1-2.

Payload and mission profile

Based on the mission scientific requirements and the unique heritage and Consortium worldwide leadership in the enabling technologies, the THESEUS **payload** will include the following scientific instruments:

- **Soft X-ray Imager (SXI, 0.3 – 5 keV):** a set of two "Lobster-eye" telescope units, covering a total FoV of ~0.5sr with source location accuracy ≤2', focusing onto innovative large size X-ray CMOS detectors;
- **X-Gamma rays Imaging Spectrometer (XGIS, 2 keV – 10 MeV**): a set of two coded-mask cameras using monolithic SDD+CsI X- and gamma-ray detectors, granting a ~2 sr imaging FoV and a source location accuracy <15 arcmin in 2-150 keV, an energy band from 2 keV up to 10 MeV and few μs timing resolution;
- **InfraRed Telescope (IRT, 0.7 – 1.8 μm**): a 0.7-m class IR telescope with 15'x15' FoV, with imaging (I, Z, Y, J and H) and spectroscopic (resolving power, R~400, through 2'x2' grism) capabilities.

The instruments' **Data Handling Units (DHU)** will operate in synergy, thus optimizing the capability of detecting, identifying and localizing likely transients in the SXI, XGIS and IRT FoVs, as well as providing the unprecedented capability of on-board redshift measurements.

From the programmatic point of view, the SXI is led by *UK* (with contributions by *Belgium, Spain, Czech Republic, Ireland* and *ESA*), the XGIS is led by *Italy* (with contributions by *Spain, Denmark and Poland*) and the IRT is led by *France* (with contributions by *Switzerland* and *ESA*). *Germany* has the overall responsibility of instruments' DHUs.

The **mission profile** will include: a) the capability of promptly (within a few tens of seconds at most) transmitting to ground the trigger time and positions of GRBs (and other transients of interest) through the **Trigger Broadcasting Unit (TBU)** VHF transmitter, provided by *Italy*, and the **THESEUS Burst Alert Ground Segment (TBAGS)** network of VHF antennae, provided by *France*; b) a spacecraft autonomous *slewing capability >7°/min*. The baseline launcher / orbit configuration is a launch with Vega-C to a low inclination *(5.4°) Low Earth Orbit* (LEO, 550-640 km altitude), which has the unique advantages of granting a low and stable background level in the high-energy instruments, allowing the exploitation of the Earth's magnetic field for spacecraft fast slewing and facilitating the prompt transmission of transient triggers and positions to the ground. The main ground station will be in Malindi (Kenya), provided by *Italy.* The mission *nominal duration will be 4 years* (corresponding to about three and half years of scientific operations; cf. §5), due to programmatic constraints: no technological issues preventing an extension by at least 2 more years have been identified. The **Mission Operation Control** (**MOC**) and **Science Operations Centre** (**SOC**) will be managed by *ESA*, while the **Science Data Centre (SDC)** will be under the responsibility of the Consortium and responsibility of *Switzerland*, with contributions from the other Consortium members.

The baseline **mission operation concept** includes a *Survey mode*, during which the monitors are chasing GRBs and other transients of interest. Following a GRB (or transient of interest) trigger validated by the DHU system, the spacecraft enters a *Burst mode* (improved data acquisition and spacecraft slewing), followed by a pre-determined (but flexible) IRT observing sequence (*Follow-up* and *Characterization or Deep Imaging modes*). The *pointing strategy* during the Survey mode will be such to maximize the combined efficiency of the sky monitoring by SXI and XGIS and that of the follow-up with the IRT. Small deviations (of the order of a few degrees until core science goals are achieved) from the Survey mode pointing strategy will be possible so to point the IRT on sources of interest pre-selected through a *Guest Observer (GO) programme*. Scientific modes also include *external trigger (or ToO)* mode, in which the IRT and monitors will be pointed to the direction of a GRB, transient or, e.g., to the error region of a GW or neutrino signal, provided by an external facility. The overall compliance of the mission profile and instruments performances with high-level scientific requirements has been demonstrated through a sophisticated *Mission Observation Simulator* including the latest instrument performance estimates and all spacecraft and orbit constraints.

The **data policy** for *THESEUS* will allow to maximize the participation of the international community and minimize cost and complexity of the scientific ground segment. As in the case of the very successful *Swift* mission, the data will be reserved to the Instrument Teams only during the launch and Early Orbit Phase; data rights will be extended to scientists of the whole Consortium during the Performance Verification Phase. After that, data will be public as soon as they are processed, the only exception being data of GRBs at redshift higher than 6 detected in the first six months of mission operation, reserved to the Consortium for six months.

2 Scientific objectives

2.1 Introduction and general context

GRBs, surely amongst the most remarkable phenomena known to astrophysics, were shrouded in mystery, until the discovery of the first GRB afterglows in the 1990s allowed for precise localisation and redshift determination [1] [2] [3]. We now know that there are two main classes of bursts, which are distinguished by the characteristic duration and the spectral hardness of their emission: the long-duration GRBs (T_{90} > 2s, the time for 90% of the prompt gamma-ray emission in the observer frame), associated with the collapse of some massive stars, which allow us to probe star formation and gas physics over all redshifts, back to the era of reionization [4]; and the short-duration GRBs associated with neutron-star compact binary mergers, which are of exceptional interest as powerful sources of gravitational waves, and are perhaps the dominant sites of heavy element formation in the Universe [5].

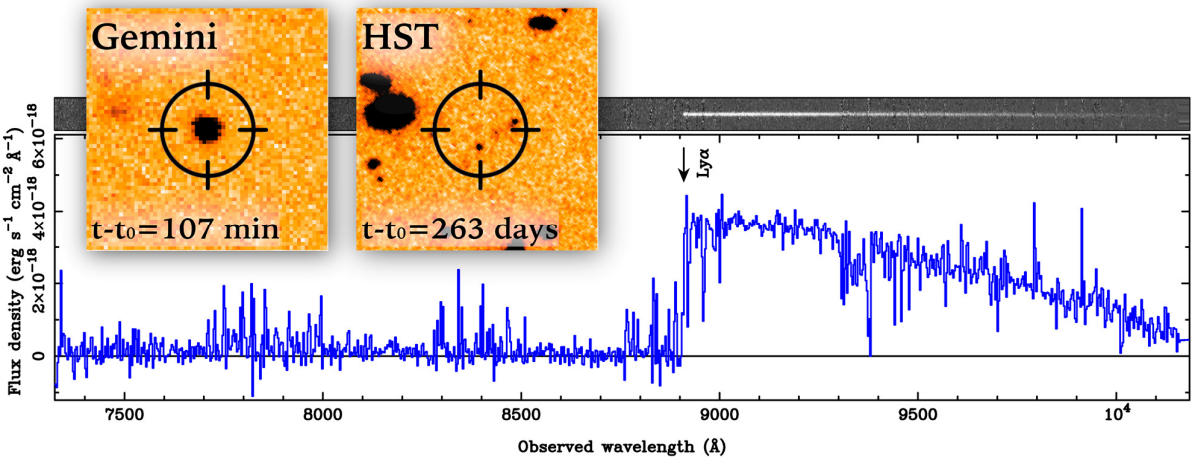

Figure 2-1 The bright afterglow of GRB 140515A at z=6.3 imaged from Gemini (left inset), contrasts with the much deeper HST image of the same region (right), which provides marginal (~3-σ) evidence of a host galaxy (m(AB)~28.3; [6]). The Gran Telescopio Canarias (GTC) afterglow spectrum (main panel) shows a sharp break at Ly-alpha, and detailed analysis of the spectrum places limits on the metallicity of Z<0.1 $Z_\odot$ ([7]; see also [8]).

These twin themes form the central motivation for the THESEUS mission: to use the incredibly bright prompt and afterglow emission of long-GRBs to explore star formation, chemical enrichment and the reionization of the intergalactic medium at high redshifts (Figure 2-1); and to become a cornerstone of multi-messenger astrophysics research in the 2030s (Figure 2-2). This will be achieved by an instrument complement designed to rapidly localise high energy transients at a much higher rate than any previous missions and obtain their detailed X-ray and NIR properties on board. A diverse range of powerful next generation electromagnetic (e.g. ELT[1], ATHENA, LSST/VRO, SKA, CTA etc.) and multi-messenger (e.g. advanced and 3rd generation GW interferometers, Einstein Telescope and Cosmic Explorer, and neutrino detectors, Km3NET, IceCube-Gen2) facilities will reach fruition in the 2030s, and will provide extraordinary complementary information, both responding to THESEUS discoveries and providing triggers to THESEUS. THESEUS will build on the well-established and highly successful model of *Swift*, which has demonstrated the power of rapid on-board localisation of high-energy transients. It will also follow other upcoming missions, such as SVOM (3-yr

[1] *Where we mention ELT, we also include the other 30-m class telescopes, the TMT and GMT, which have similar capabilities for follow-up of THESEUS discoveries.*

mission, launch mid-2022) and Einstein Probe (3-yr mission, launch end-2022), but will have greatly enhanced capabilities for high-redshift and short-hard GRB discovery, and multi-wavelength characterisation compared to these other missions, as summarised in Table 2-1.

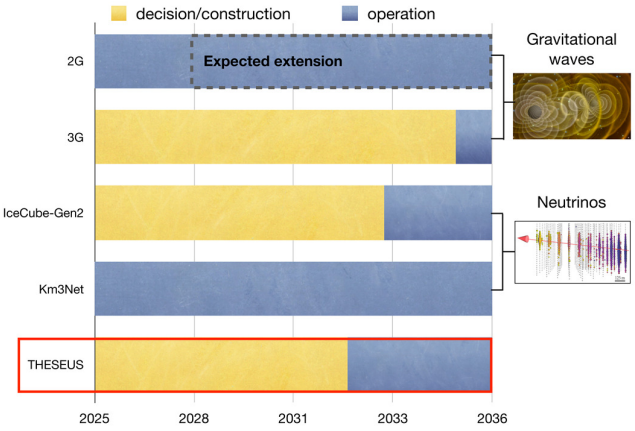

Figure 2-2 Expected timeline of construction and operation of the key multi-messenger facilities, namely the 2nd and 3rd generation gravitational wave networks, and the KM3NET and IceCube-Gen2 neutrino detectors.

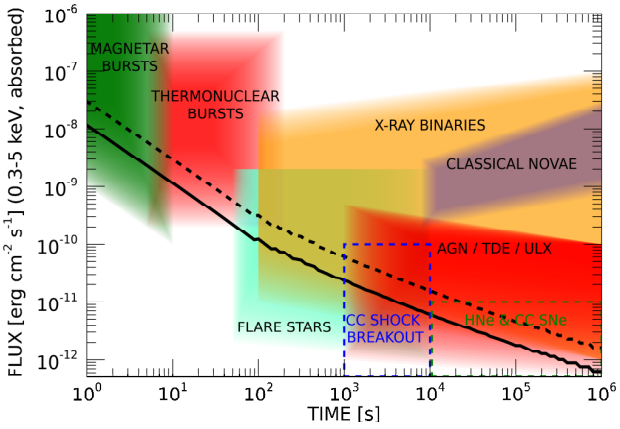

Figure 2-3 Typical variability time scales and soft X-ray fluxes of different classes of sources compared to the SXI sensitivity for a power law spectrum with photon index $\Gamma = 2$ and neutral hydrogen column $N_H = 5 \times 10^{20}$ cm^{-2} (solid) and 10^{22} cm^{-2} (dashed).

History has also shown that the transient high-energy sky is a natural discovery space, probing diverse sources such as supernova shock breakouts, relativistic tidal disruption events, magnetar giant flares possibly related to Fast Radio Bursts, etc. New breakthroughs can be expected in, for instance, the detection of relativistic jets from Pop-III collapsars, tests of fundamental physics (e.g. Lorentz invariance), and classes of transient not yet conceived. While monitoring the sky looking for GRBs, THESEUS will gather excellent data that offer a great opportunity to study the time variability of Galactic and extra-Galactic sources of various kind (see Figure 2-3) and to provide alerts to trigger observations with other facilities.

Thanks to the huge grasp (the product of effective area and FoV), high sensitivity and wide spectral coverage of its high-energy instruments, THESEUS will bring three great benefits not available to traditional X-ray telescopes:

- The frequent long-term monitoring opens up previously unavailable timescales for study, giving access to physical processes which would otherwise be missed.
- The high-cadence situational awareness of the sky enables the discovery of new rapid phenomena to be broadcast promptly to the world's greatest astronomical facilities for immediate follow-up, so catching vital source types in revealing new states.
- The very wide energy bandwidth provides a new opportunity to constrain the emission processes. The great sensitivity will vastly expand the classes of high energy emitters studied.

In the following sub-sections, we outline these key high-redshift (§2.2) and multi-messenger (§2.3) themes in more quantitative detail, together with other examples of transient classes addressed by THESEUS (§2.4 and 2.5). The potential for observatory science is discussed in §2.6. In §2.7 we elaborate on the discovery potential of THESEUS emphasizing the expected synergy with the global multi-wavelength and multi-messenger facilities in the 2030s.

Table 2-1 GRB detection performance of THESEUS compared with current and upcoming high-energy space missions. By the 2030's, THESEUS will be the only facility allowing both the rapid identification of GRBs and the spectral characterization of their optical/NIR counterparts for a sizeable population of bursts at low and high (z>6) redshift.

Mission	Autonomous rapid repointing	Arcsec localisation	Optical imaging	Near-IR imaging	Near-IR spectroscopy	On-board redshift broadcasting	<10 keV X-ray coverage	>10 keV X-ray coverage	MeV γ-ray coverage
Swift	✓	✓	✓	×	×	×	✓	✓	×
Fermi/GRB	×	×	×	×	×	×	×	✓	✓
Integral	×	×	✓	×	×	×	×	✓	✓
SVOM	×	×	✓	×	×	×	✓	✓	✓
Einstein Probe	✓	×	×	×	×	×	✓	×	×
eXTP	✓	✓	×	×	×	×	✓	×	×
THESEUS	✓	✓	✓	✓	✓	✓	✓	✓	✓

2.2 Exploring the Early Universe with GRBs

A major goal of contemporary astrophysics and cosmology is to achieve a detailed understanding of the formation of the first collapsed structures (Pop-III and early Pop-II stars, black holes and galaxies) during the first billion years in the life of the Universe. The birth and growth of these first structures is intimately connected to the reionization of the IGM and build-up of heavy chemical elements. The latter is very poorly constrained, and even in the JWST era, metallicity estimates at z>6 will rely on crude emission line diagnostics for only a limited number of the brightest galaxies ($M_{UV} \lesssim$ -19 mag). Regarding the former, measurement of the Thomson-scattering optical depth to the microwave background by the Planck satellite now suggests reionization substantially occurred in the redshift range $z \sim 7 - 8.5$ [9], whereas the observations of the Gunn-Peterson trough in the spectra of distant quasars and galaxies indicate it was largely finished by $z \sim 6.5$ [10]. Statistical measurements of the fluctuations in the redshifted 21 cm line of neutral hydrogen by future experiments, notably SKA-Low, are expected ultimately to provide further constraints on its time history [11].

The central question, however, remains whether it was predominantly radiation from massive stars that both brought about and sustained this phase change, or whether more exotic mechanisms must be sought? Even in the JWST/ELT era, the numerous galaxies populating the faint-end of the luminosity function ($M_{UV} \gtrsim$ -16 mag) in the re-ionization epoch (z>6) will be mostly out of reach. Gauging star formation occurring in these faint galaxies, the fraction of ionizing radiation that escapes its host galaxy, and the parallel build-up of metals, will still remain highly challenging problems. GRBs and their faint host galaxies can be found to very high redshifts (Figure 2-4) and provide multiple powerful probes of early star formation, metal enrichment and galaxy evolution, potentially even preceding reionization. GRBs are indeed detectable independently of the luminosity of their underlying host and can pinpoint the presence of massive star formation in distant galaxies below the sensitivity limit of even the most powerful facilities foreseen in the long-term future. Besides, their afterglow counterparts can be used as powerful background lighthouses probing in absorption both the IGM and the ISM of faint galaxies otherwise non accessible with other observing technics. We foresee that THESEUS will identify and locate between 40 and 50 GRBs at z>6 in 3.45 years of scientific operations, with photometric redshift accuracy better than 10% thanks to the identification of the Lyman break feature shifted to the IRT imaging sensitivity range (see §3.2.2). This will allow THESEUS to address major key questions of modern cosmology and structure formation, which we describe in the rest of this section.

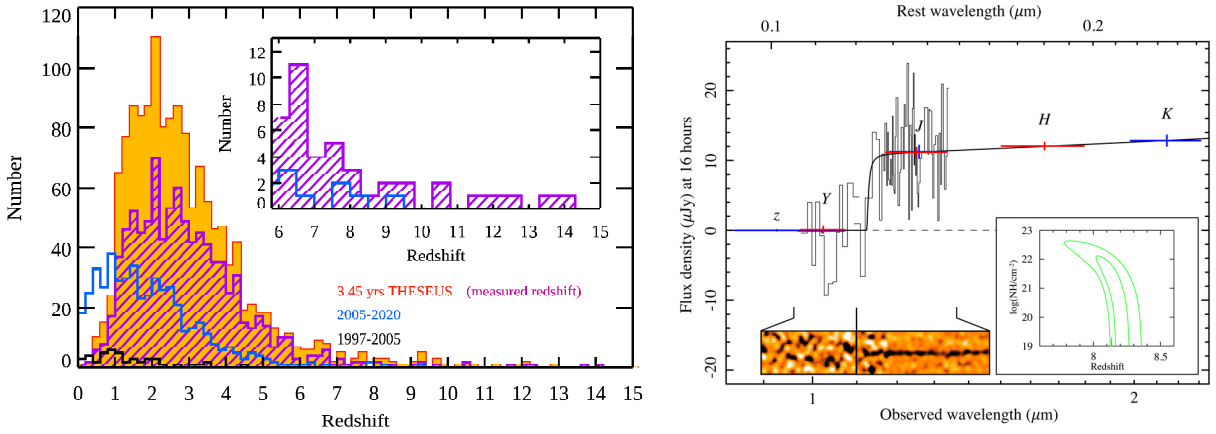

Figure 2-4 Left: Expected redshift distribution of long-duration GRBs detected by THESEUS in 3.45 yr of scientific operations (orange and purple histograms), compared with the redshift distribution obtained to date (blue and black histograms). Right: VLT spectrum of the afterglow of GRB 090423 at z=8.2. The Ly-alpha break between the Y and J bands is very well located in the spectrum, in perfect agreement with the photometric redshift derived with broadband imaging (blue and red points). As in this case, high-z afterglows observed with current facilities are often too faint to extract information on metallicity or column density. When THESEUS is in orbit, on-board identification of high-z candidates, and more powerful follow-up facilities, will largely eliminate this problem (cf the simulated ELT spectrum of a similar afterglow in Figure 2-7).

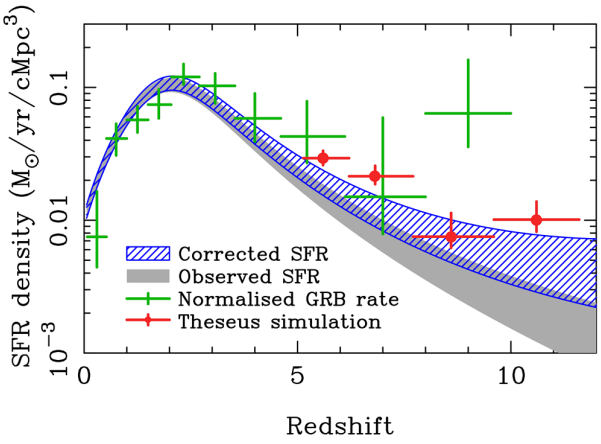

Figure 2-5 Comoving Star Formation Rate density as a function of redshift as derived from rest-frame UV surveys (shaded curve based on the observed galaxy population [12], blue hatched region accounts for galaxies below the detection limit) and from GRBs based on different assumptions (GRB rate to SFR ratio, GRB progenitor metallicity [13]). Green points show current constraints from the available GRB sample, which is very small at z>6 [14]; red points show corresponding estimates expected from a representative THESEUS sample.

2.2.1 Global star formation rate from GRB rate as a function of redshift

Long-duration GRBs are produced by massive stars, and so track star formation, and in particular the populations of UV-bright stars responsible for the bulk of ionizing radiation production. This makes them powerful probes of global star formation, and changes in the initial mass function (IMF).

Although there is evidence at low redshift that GRBs are disfavoured in high metallicity environments, it is likely that GRBs are tracing well the bulk of massive star formation beyond $z \sim 3$, since star-forming activity at such high redshifts predominantly occurs at low to moderate metallicity ([15], [14]). THESEUS will establish the GRB redshift distribution, $N(z)$, much more reliably at $z > 5.5$ than previous missions, thanks to significantly larger numbers and also more uniform selection via rapid on-board redshifts, and in many cases refinement of the redshift through follow-up with other facilities. Thus, accounting for the observational selection function, we will obtain the evolution of the global star formation rate density at redshifts where uncertainties from traditional galaxy observations begin to rise. Analyses of this sort have consistently pointed to a higher SFR density at redshifts z > 6 than traditionally inferred from UV rest-frame

galaxy studies ([14], [16]; Figure 2-5), which rely on counting star-forming galaxies and attempting to account for galaxies below the detection threshold. Although this discrepancy has been alleviated by the growing realisation of the extremely steep faint-end slope of the galaxy Luminosity Function (LF) at $z > 6$, it still appears that this steep slope must continue to very faint magnitudes (e.g. $M_{AB} \geq -11$), or the stellar Initial Mass Function (IMF) become more top-heavy (GRB progenitors being drawn from populations with birth masses ~25-40 $M_{\odot}$), in order to provide consistency with GRB counts and indeed to achieve reionization (something that can only be quantified via a full census of the GRB population; see §2.2.5). Evidence for variations in the IMF would be particularly intriguing, and suggestive of very low metallicity populations (see §2.2.5).

2.2.2 The galaxy luminosity function: detecting undetectable galaxies

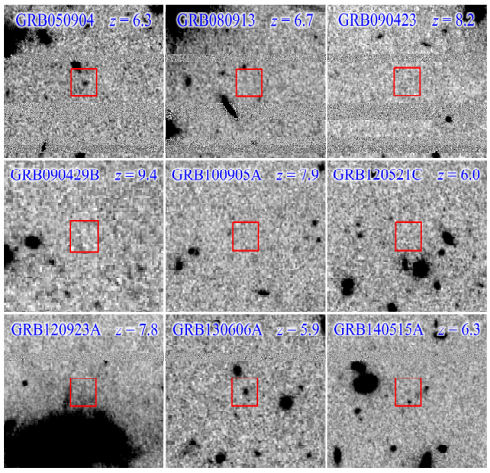

Figure 2-6 Mosaic of deep HST imaging of the locations of known GRBs at $z \gtrsim 6$, obtained when the afterglows had faded. Only in 2-3 cases is the host galaxy detected, confirming that the bulk of high-z star formation is occurring in galaxies below current limits. This approach allows us to quantify the contribution of the faint end of the galaxy luminosity function to the star formation budget, even in the absence of direct detections.

The intrinsically very small galaxies, which appear to increasingly dominate star formation at $z > 6$, are very hard to detect directly. GRBs circumvent this difficulty, signposting the existence and redshifts of their hosts, no matter how faint.

As discussed in §2.2.1, the faint end of the galaxy luminosity function is a key issue for our understanding of reionization since, to the depth achieved in the Hubble Ultra-deep Field (HUDF), it appears that the faint-end of the LF steepens significantly with redshift reaching a power-law of slope $\alpha \sim 2$ at $z > 6$ [17]. Thus, the value of the total luminosity integral depends sensitively on the choice of low-luminosity cut-off (and indeed the assumption of continued power-law form for the LF). By conducting deep searches for the hosts of GRBs at high-z we can directly quantify the ratio of star-formation occurring in detectable and undetectable galaxies, with the sole assumption that GRB-rate is proportional to star-formation rate (Figure 2-6). Although currently limited by small-number statistics, early application of this technique has confirmed that the majority of star formation at $z \geq 6$ occurred in galaxies below the effective detection limit of HST ([18], [6]) with expected magnitudes fainter than $m_{AB} \sim 30$, at the limit of what is reachable with JWST and the ELTs. Since the exact position and redshift of the galaxy is known from the GRB afterglow, follow-up observations to measure the host UV continuum are much more efficient than equivalent deep field searches for Lyman-break galaxies. If the luminosity function is modelled as a Schechter function with a sharp faint-end cut-off, then this analysis allows us to constrain that cut-off magnitude, even though the galaxies are too faint to be observed. As further discussed in §2.2.5, this technique applied to a sample of ~40 GRBs detected by THESEUS at $z \geq 6$ will yield much tighter constraints on that cut-off magnitude than obtained with GRBs so far (Figure 2-10, left).

2.2.3 The build-up of metals, molecules and dust

Bright GRB afterglows with their intrinsic power-law spectra provide ideal backlights for measuring not only the hydrogen column, but also obtaining exquisite abundances and gas kinematics probing to the hearts of their host galaxies [19]. Thus, they can be used to monitor cosmic metal enrichment and chemical evolution to early times, and search for evidence of the nucleosynthetic products of even earlier generations of stars.

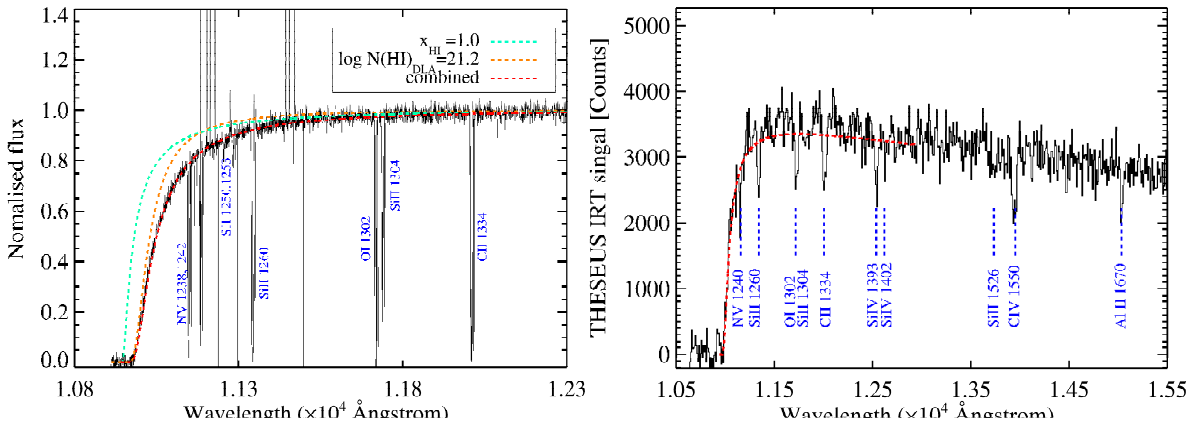

Figure 2-7 Left: simulated ELT 30-minute spectrum of a z=8.0 GRB afterglow with J(AB)=20 (typical after ~0.5 day). The S/N provides exquisite abundance determinations from metal absorption lines (in this example, 1% solar metallicity), while fitting the Ly-alpha damping wing simultaneously fixes the IGM neutral fraction and the host HI column density, as illustrated by the two overlaid models, a pure 100% neutral IGM (green,) and a log(N_{HI}/cm^{-2})=21.2 host absorption with a fully ionized IGM (orange). A well-fitting combined model is shown in red. Right: the same afterglow with a magnitude of 16 in a simulated IRT spectrum with a realistic spectral observing sequence at a total integration time of 1800 s, illustrating that the most prominent metal lines are also clearly detected.

First, follow-up of the brightest afterglows (H < ~17.5 mag) with the IRT spectroscopic mode (§4.3.5) will provide constraints within ~0.2 dex on the hydrogen column density along the GRB line of sight. The identification of metal absorption lines will also enable spectroscopic redshift determinations to <1% precision, which will help refining the IRT photo-z estimates and distinguishing cleanly between the GRBs at $z > 6$ and contaminants from dusty afterglows at lower redshifts. Further, taking advantage of the availability of 30 m class ground-based telescopes in the 2030s, and also of ATHENA to quantify the high ionization gas content, superb abundance determinations will be possible through simultaneous measurement of metal absorption lines and modelling the red-wing of Ly-α to determine host HI column density, potentially even many days post-burst (Figure 2-7). Using the sample of GRBs discovered by THESEUS to trace the ISM in galaxies at z>6 will be the only way to map in detail accurate metallicities and abundance patterns across the whole range of star forming galaxies in the early Universe, including those at the very faint end of the LF (Figure 2-8). The imprint of the dust in the host can be seen in the (rest-frame UV/optical) broad-band spectral energy distributions of GRB afterglows. Such studies have found a variety of dust laws, many reasonably approximated by the three canonical local laws (SMC, LMC, MW; e.g. [20], [21]), but along some sight-lines the extinction is unusual and harder to explain [22]. Thus, GRBs offer a remarkable route to assessing the dust content of even low mass galaxies in the early Universe [23]. At moderate redshifts, H_2 molecular absorption seen in GRB afterglow spectra, provides direct evidence of the state of the dense ISM in the host [24].

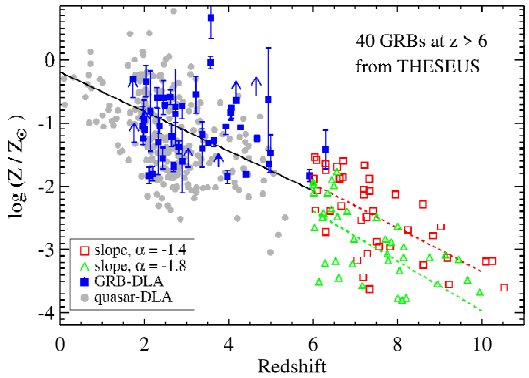

Figure 2-8 Absorption-line based metallicities relative to solar, corrected for dust depletion as a function of redshift for Quasar Damped Lyman-alpha Absorbers (DLAs, grey symbols) and GRB-DLAs (blue symbols) [adapted from [25], [26]]. Open square symbols show representative expectations for THESEUS, assuming continued evolution of the mass-metallicity relationship, and a dominant population of low mass galaxies at z>6 (green triangles and red squares assume faint-end slopes of -1.8 and -1.4 for the galaxy luminosity function, respectively). GRBs represent the unique way for probing evolution of ISM absorption–based metallicities in the first billion years of cosmic history.

Although this becomes unfeasible at high redshift due to the Gunn-Peterson trough obscuring the Lyman-Werner bands, other absorption tracers, notably vibrationally-excited H_2*, and neutral carbon, CI, provide reliable indicators of high molecular hydrogen columns [27].

We emphasize that using the THESEUS on-board NIR spectroscopy capabilities will provide, in addition to arcsec accurate location, the redshift estimates and luminosity measurements that are essential to optimising the time-critical follow-up observations using highly expensive next-generation facilities, allowing us to select the highest priority targets and deploy the most appropriate telescope and instrument.

2.2.4 The Lyman-continuum escape fraction

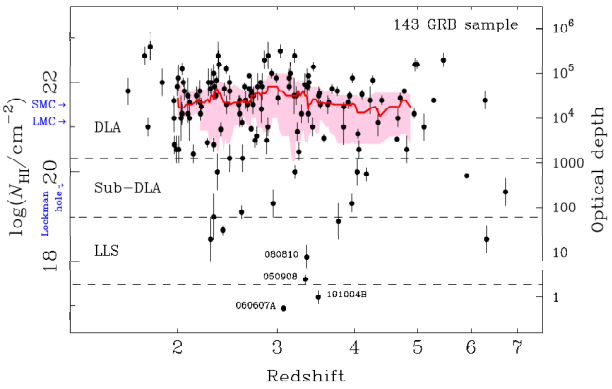

Figure 2-9 The host neutral hydrogen column densities measured from the Ly-alpha absorption line in the afterglows of 143 GRBs spanning a wide range of redshift. Typically, the columns imply a high optical depth to ionizing Ly-continuum radiation, and thus a low overall escape fraction (f_{esc}<2%). THESEUS will enable us to extend this plot with good statistics at z > 5 providing a direct estimate of the escape fraction on the lines of sight to massive stars in this era.

GRB afterglow spectroscopy allows us to measure the column density of neutral hydrogen in the host galaxy, thus providing a powerful probe of the opacity of the interstellar medium to EUV photons.

A key issue for the reionization budget is quantifying the fraction of ionizing radiation that escapes the galaxies in which it is produced. Even in the JWST/ELT era, direct observations of escaping Lyman continuum radiation at z > 5 will remain unfeasible for the low mass galaxies responsible for the bulk of star formation in the era of reionization. However, GRB afterglow spectroscopy allows us to measure the column density of neutral hydrogen in the host galaxy, thus providing a strong lower limit to the opacity of the interstellar medium to FUV photons (further EUV attenuation due to dust can also be estimated by modelling the afterglow SEDs). A statistical sample of afterglows can be used to infer the average escape fraction over many lines of sight, specifically to the locations of massive stars dominating global ionizing radiation production. Useful constraints have so far only been possible at z = 2-5, indicating a strong upper limit of f_{esc}< 2% (Figure 2-9; [28], [29]), although other studies contradict these conclusions [30]. However, future observations of the population of z > 5 GRBs detected by THESEUS, with both on-board spectroscopy and with 30 m class ground-based telescope follow-up observations, will provide much more precise constraints on the fraction of ionizing radiation that escaped galaxies *during* the epoch of reionization (see §2.2.5 and Figure 2-8).

2.2.5 Did stars reionize the Universe?

The evolution of the IGM from a completely neutral to a fully ionized state is intimately linked to early structure formation, and thus a central issue for cosmology. Answering the key question of whether this phase change was primarily brought about stars hinges on two subsidiary issues: how much massive star formation was occurring as a function of redshift, and, on average, what proportion of the ionizing radiation produced by these massive stars escaped from the immediate environs of their host galaxies? Both will be addressed through THESEUS GRB observations.

As discussed in §2.2.2, the former question about massive star formation as a function of redshift can be extrapolated based on observed candidate z > 7 galaxies found in HST deep fields, but two very significant uncertainties are, firstly, the completeness and cleanness of the photometric redshift samples at z > 7, and, secondly, the poorly constrained faint-end behaviour of the galaxy luminosity function (at stellar masses <~

10^8 $M_\odot$), especially since galaxies below the HST (and potentially even the JWST) detection limit very likely dominate the star-formation budget.

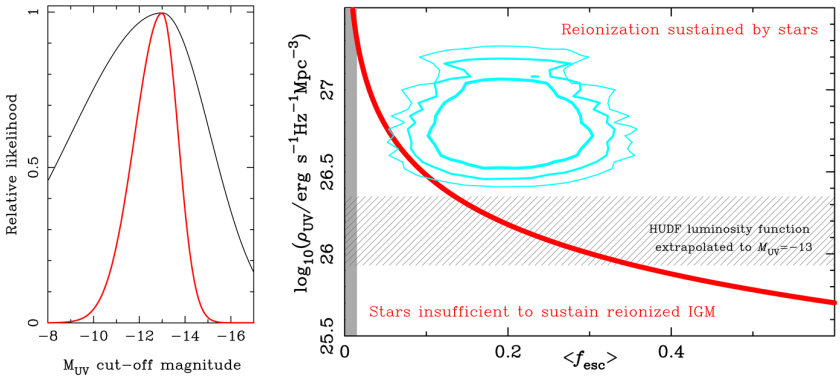

Figure 2-10 Left: constraints on the faint end cut-off of the galaxy luminosity function (assuming a Schechter function with abrupt cut-off and bright end constrained by galaxy observations). Black curve shows current constraints based on nine GRBs at $z \geq 6$; red curve shows a simulation after THESEUS, assuming deep host searches from 30 m class telescopes. Right: the UV luminosity density from stars at z~8 and average escape fraction $\langle f_{esc} \rangle$ are insufficient to sustain reionization [31] unless the galaxy luminosity function steepens to magnitudes fainter than M_{UV}=-13 (hatched region), and/or $\langle f_{esc} \rangle$ is much higher than that found from GRB studies at z~2-5 (shaded region). Even in the late 2020s, $\langle f_{esc} \rangle$ at z>6 will be largely unconstrained by direct observations. The cyan contour shows the 2-σ expectations for samples of 20, 30 and 50 GRBs (thin to thick contours) at z~7-9 for which deep spectroscopy provides the host neutral column and deep imaging constrains the fraction of star formation occurring in hosts below ELT limits. This sample would be sufficient to distinguish a Universe in which stars may sustain reionization from one with f_{esc} more consistent with lower redshifts.

Even though some constraints on fainter galaxies can be obtained through observations of lensing clusters [32], which will be improved further by JWST, simulations suggest considerable star formation was likely occurring in fainter systems still [33]. As discussed in 2.2.4, the second problem, that of the Lyman-continuum escape fraction, is even more difficult since it cannot be determined directly at these redshifts, and studies at lower redshifts have found conflicting results. Recent stacked spectroscopic analyses have suggested escape fractions as high as 10% [30], which could be sufficient to drive reionization [13], but it is unclear whether the samples of galaxies studied, at z~3, are representative of all star-forming galaxies, and in particularly of the typical, intrinsically fainter galaxies at z>7. As seen in Figure 2-9, GRB studies find that sightlines to massive stars are generally highly opaque to ionizing radiation, at least up to z~5.

The improvements in both the census of star formation and the escape fraction from THESEUS GRB studies will provide a strong test of the hypothesis that reionization was brought about by star light. Our detailed simulations indicate that THESEUS is expected to detect between 40 and 80 GRBs at $z > 6$ over a four-year mission, with between 10 and 25 of these at $z > 8$ (and several at $z > 10$). The on-board follow-up capability will mean that redshifts are estimated for almost all of these, and powerful next generation ground- and space-based telescopes available in this era will lead to extremely deep host searches and high-S/N afterglow spectroscopy for many (e.g. using ELT, ATHENA etc.). To illustrate the potential of such a sample, we simulate in Figure 2-10 (right) the precision in constraining the product of the UV luminosity density and average escape fraction, $\rho_{UV} f_{esc}$, that would be obtained with samples of 20, 30 and 50 GRBs at 7<z<9 having high-S/N afterglow spectroscopy and (~3hr) ELT depth host searches (for definiteness the ρ_{UV} axis corresponds to z=8). This will allow us to confidently distinguish between conventional models in which starlight brings about reionization, and models that fail (e.g. if the escape fraction remains as low as we find at lower redshifts).

2.2.6 Topology and timeline of reionization

In practice, it is expected that reionization should proceed in a patchy way, for example, ionized bubbles may form first around the highest density peaks where the first galaxies form, expanding and ultimately filling the whole IGM. The topology of the growing network of ionized regions reflects the character of

the early structure formation and the ionizing radiation field. With high-S/N afterglow spectroscopy, the red damping wing of the hydrogen Ly-alpha line can be decomposed into contributions due to the host galaxy and the IGM. The latter provides the hydrogen neutral fraction and so measures the progress of reionization local to the burst.

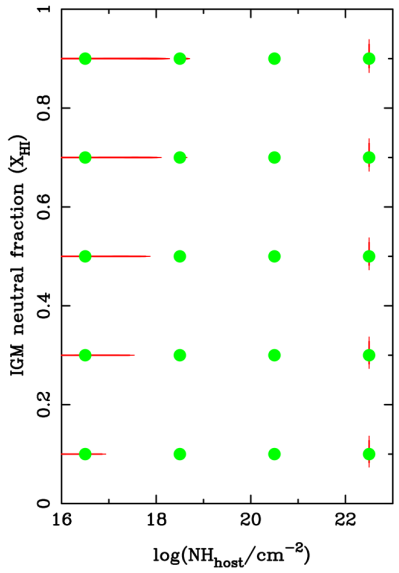

Figure 2-11 results of simulations showing how well the IGM neutral fraction X_{HI} and host HI column density can be retrieved from typical ELT-class afterglow spectra (Figure 2-8). The input values are shown as green points, and the resultant fits by the red contours. In nearly all cases the IGM neutral fraction is well recovered (within the symbol size), as are host columns for all but the lowest cases, although even here results should be sufficient to indicate a partially transparent sight line. The variance between sight-lines at the same redshift of IGM neutral fraction is expected to be up to δX_{HI}~0.3 at mid reionization [34], depending on the reionization model, which can be determined with the THESEUS sample.

With samples of several tens of GRBs at z > 6-9, we can begin to investigate statistically the redshift-dependence of the average and variance of the reionization process [34]. To illustrate the capability of follow-up spectroscopy to quantify both host HI column, and IGM neutral fraction, Figure 2-11 shows the results of simulating an afterglow with the characteristics of GRB 090423 (cf. Figure 2-8) with a range of different input parameters, for which the measured parameters over a large number of realisations are shown (green points). This demonstrates that the IGM neutral fraction can be recovered from such spectra, even in the presence of a fairly high host column, and similarly the host column can generally be well characterised except when very low.

2.2.7 Population III stars and primordial galaxies

High redshift GRBs provide several routes to exploring the earliest populations of metal-free and ultra-low metallicity stars, from direct spectroscopic determinations of ISM abundances, to changes in the numbers and properties of the bursts themselves, reflective of the increase in average and maximum masses expected for Population III stars.

In the current ΛCDM paradigm, the very first stars (the so-called Population III stars) are expected to form from pristine gas at redshift z~10-30 [35]. Because of the absence of heavy elements and the subsequent inefficiency of cooling at these early cosmic times, their mass is supposed to largely exceed those of Pop-I and Pop-II stars (M > 40 $M_\odot$, possibly reaching several hundreds of solar masses). When these first stars reach their final stage of evolution, their low-opacity envelope combined with limited mass loss from stellar winds may thus keep large amounts of gas bound until the final collapse, favouring the conditions for jet breakout and for the launch of a very energetic long GRB [36]. Models even predict that the total equivalent isotropic energy released by such Pop-III star explosions could exceed by several orders of magnitude that of GRBs from Pop-I/II progenitors, possibly reaching ~10^{56} –10^{57} erg and making them detectable up to the highest possible redshifts [37]. The large population of high redshift GRBs detected by THESEUS offer several routes to searching for these unique events, and their spectroscopic follow-up with the ELTs or JWST would provide us with a unique chance to probe for the very first time the ISM of primordial galaxies. Given the peculiar energetics and chemistry associated with Pop-III star GRBs, their observed properties should differ from GRBs at lower redshift. Their prompt emission could extend over much longer timescales, reaching in some cases that of ultra-long GRBs [38].

Similarly, the energy released by the jetted explosion could imply much longer times to dissipate. This could give rise to a luminous afterglow emission peaking much later and at higher fluxes than observed for Pop-II GRBs, which in particular would be extremely bright at radio wavelengths if happening in a high-density ISM

[39]. A luminous thermal component could also be produced if the jet deposits a large fraction of its total energy in the stellar envelope of the GRB progenitor.

Spectroscopy of such afterglows with 30 m-class telescopes or JWST may reveal ultra-low metallicity if their line of sight intersects pristine gas in their host galaxy, and these signatures would represent a direct piece of evidence for the association between a GRB and a Pop-III star progenitor. Similarly, gas cloud pockets enriched by Pop-III star explosions and highlighted by Pop-II GRBs might provide us with another way to explore the metal abundance patterns characterizing the ISM in which the very first generation of massive stars were born [40]. Such abundance patterns may in fact reveal if the first heavy elements were produced by typical core-collapse explosions or by other mechanisms such as pair-instability supernovae, hence constraining the Initial Mass Function up to the earliest cosmic epochs [41].

Predicting how many of such events THESEUS will identify throughout the duration of its science operations is particularly challenging since the probe of such first light sources still remains a fully uncharted territory. In the era of JWST and the ELTs, THESEUS might yet be the only experiment enabling the discovery of these first very massive star explosions, hence providing exquisite targets for further follow-up with larger telescopes. Pop-III stars likely played a major role in the growth of the very first bound structures at early cosmic times, through chemical feedback and metal enrichment of the primordial IGM, and they may have also contributed a head start to the cosmic re-ionization process. To date, no direct evidence of the connection between Pop-III stars and GRBs has been observationally established. The identification by THESEUS of even a single GRB with metal abundance unveiling a Pop-III star progenitor or a Pop-III star enriched medium would put fundamental constraints on the unknown properties of the first stars and represent a major breakthrough in our understanding of first-light sources.

2.2.8 Probing the expansion history of the Universe and dark energy with GRBs

While the standardised candle correlations proposed for GRBs exhibit larger scatter than those for SNIa, GRBs can be observed to much higher redshift, and thus provide much greater lever arm for testing cosmological world models.

By using the spectral peak energy – radiated energy (or luminosity) correlation ($E_{p,i} - E_{iso}$ or L_{iso}, [42], [43]), it has been demonstrated that GRBs offer a very promising tool to probe the expansion rate history of the Universe beyond the current limit of z~2 (Type-Ia SNe and Baryonic Acoustic Oscillations from quasar absorbers). With the present data set of GRBs, cosmological parameters consistent with the concordance cosmology can already be derived ([44], [45]). Current (e.g., Swift, Fermi/GBM, Konus-WIND) and forthcoming GRB experiments (e.g., SVOM) will allow us to constrain Ω_M and the dark energy equation of state parameters w_0 *and* w_a, describing the evolution of w according to $w = w_0 + w_a (1+ z)$, with an accuracy comparable to that currently obtained with Type Ia supernovae. The order of magnitude improvement provided by THESEUS on the size of the sample of GRBs, with measured redshifts and spectral parameters, will allow us to further refine the reliability of this method and, possibly, to characterize the equation of state with redshift independently of the functional form assumed to describe its evolution through cosmic time. Combined with the most recent constraints from the Cosmic Microwave Background, this will offer the unique opportunity to constrain the geometry, and therefore the mass-energy content of the Universe back to z~5, extending beyond the investigations of EUCLID and of next-generation large-scale structure surveys to the entire cosmic history.

2.3 Multi-messenger astrophysics

THESEUS will play a prime role during the 2030s due to its unique capabilities in detecting, localizing, and characterizing the electromagnetic counterparts of gravitational wave and neutrino sources which will be observed with unprecedented sensitivity by next generation detectors.

The newly born Multi-messenger astrophysics is becoming a major avenue to explore the Universe over a vast range of redshifts. The growing synergies between different probes is opening a new frontier capable of unveiling several aspects of fundamental physics and cosmology.

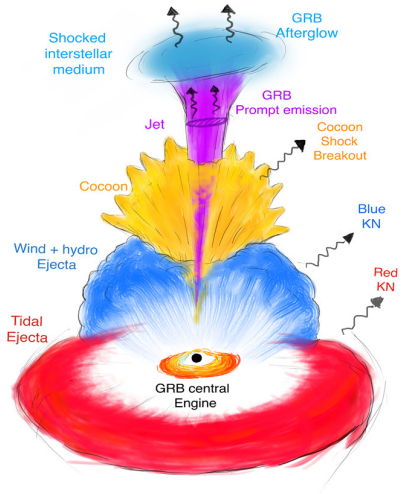

Figure 2-12 Cartoon on the current understanding of NS-NS merger emitting regions supported by the multi-messenger observation of GW170817 /GRB170817 (from [46]).

Compact binary coalescences (CBCs) have been confirmed as the most promising GW emitters in the frequency range covered by ground-based detectors (i.e. from about 10 Hz up to few kHz). Since the first GW detection of a coalescing binary stellar-mass black hole (BH-BH) system in 2015 [47], numerous other BH-BH mergers ([48], [49]), two confirmed binary neutron star (NS-NS) mergers, and one possible NS-BH merger ([50], [51], [52]) have been detected so far with Advanced LIGO (aLIGO, [53]) and Advanced Virgo (AdV, [54]). CBCs are also sources of potentially detectable electromagnetic (EM) radiation across the whole spectrum, from radio to gamma-rays. A breakthrough confirmation of such expectations was obtained on August 17th, 2017, when a GW signal consistent with a NS-NS merger 40 Mpc away (GW170817) was accompanied by the short gamma-ray burst GRB 170817A and later by further X-ray, optical, infrared, and radio emission ([55], [56]). This event was the first direct evidence of the progenitor of a short GRB, confirming past indirect evidence. The afterglow properties confirmed the formation of a relativistic, narrow jet after the NS-NS merger (half-opening angle of ~2°-4°, [57]), a result that theoretical studies and magneto hydro-dynamic simulations could not fully predict. Optical/NIR observations showed the first firm evidence of a kilonova (KN), with two ("blue" and "red") main emission components [58]. It was also the first GRB viewed from outside the core of the jet (i.e. the cone with very high Lorentz factor), as demonstrated by the rising and then slowly decaying afterglow [59]. The viewing angle has been estimated to be around 15°-30° away from the direction of propagation of the highly relativistic jet core [57]. Such a lateral view allowed us to identify the observed gamma-ray emission as directly originating from the mildly relativistic cocoon formed around the jet core via the interaction of the incipient jet itself with the surrounding material ejected during and after the NS-NS merger (Figure 2-12).

The last decade has also seen decisive discoveries in neutrino astronomy. The two major results are: the detection of a diffuse flux of astrophysical very-high-energy neutrinos (10 TeV-10 PeV) by IceCube [60], whose origin is still unknown ([61], [62]); and the first possible identification of a neutrino source at cosmological distance, the blazar TXS0506+056 [63] which adds to the only known non-solar source of neutrinos, the supernova SN1987A in the Local Group environment. These detections together with GW170817 show the huge power of identifying an electromagnetic counterpart of a GW or neutrino source.

By the end of the 2020s, the network of second generation (2G) GW interferometers, with Advances LIGO Plus (A+), Advanced VIRGO Plus (AdV+) and KAGRA [64], will see further upgrades and the addition of a fifth interferometer, LIGO-India, expected to start observations in 2025 [65]. The distances[2] up to which NS-NS and 10-solar-mass BH-BH mergers will be detected by the completed 2G network will be ~330 Mpc and ~2.6 Gpc, respectively. Within such distances, the expected detection rate of the most promising EM radiation emitters, NS-NS mergers, is in the range ~1-80 per year (updated to O3 results, [65]). Joint observations of short GRBs (as in the case of GW 170817) by current and future missions that will fly during the 2020s, like Fermi, INTEGRAL, or SVOM, are expected to be rare and likely much less than one per year due to the beamed emission even assuming a high jet production efficiency from such systems.

[2]*This is defined as the distance enclosing the CBC orientation-averaged spacetime volume surveyed per unit detector time, assuming a matched-filter detection signal-to-noise ratio (SNR) threshold of 8 in a single detector [65].*

In the early 2030s, at least ten times more sensitive third generation (3G) ground-based GW interferometers such as the Einstein Telescope (ET, [66]), and Cosmic Explorer (CE, [67]) are planned to be operational, allowing us to observe CBCs at distances nearly ten times greater than can the 2G network. Neutrino detectors are also experiencing significant upgrades with the KM3NeT in the Mediterranean Sea [68]. By 2030s, an upgraded version of the currently operating IceCube at the South Pole (IceCube-Gen2, [61]), and the Baikal Gigaton Volume Detector (Russia, [69]), will be completed, accessing flux levels expected from cosmic sources.

By that time, a major challenge for the identification of the EM counterparts of the discovered GW and neutrino sources will be the relatively poor sky localisation capabilities of such detectors. Indeed, 3G GW interferometer sky localization precision strongly depends on the number of interferometers in the network that will detect the source, ranging from a few up to more than several hundreds of square degrees [70]. For instance, the bulk of NS-NS mergers at z>0.3 observed with ET alone will have almost no sky localization (e.g. >1000 deg^2 uncertainty) and no events with accuracy better than ~10 deg^2 [71]. Neutrino detectors, on the other hand, can localise events to an accuracy that depends on neutrino flavour. Long tracks topology (for ν_μ) will provide angular resolution down to 0.1-0.2 deg and a 2π sr sky coverage, while cascade topology (for ν_e and most ν_τ) angular resolution will be typically 3-5 deg for the whole 4π sky. Therefore, in order to maximise the science return of the multi-messenger investigation during the 2030s, it is essential to have a facility that can: first, detect, accurately localize and disseminate EM counterparts independently from GW/neutrino triggers, second rapidly search with good sensitivity in the large sky areas indicated by the GW and neutrino detections. Moreover, given the still large uncertainties in the EM counterpart properties for both GW and neutrino sources, wide spectral coverage is a third essential requisite. These three combined requirements are uniquely fulfilled by THESEUS, with several advantages with respect to previous and current missions (Table 2-2).

The next sections describe the expected EM counterparts that THESEUS will detect in synergy with future GW and neutrino facilities, both in standard observing mode and via Target of Opportunity programs, allowing for fundamental and transformational knowledge on multi-messenger sources.

2.3.1 Electromagnetic emission from NS-NS and NS-BH mergers

2.3.1.1 Collimated electromagnetic counterparts: short GRBs

THESEUS will provide statistically significant samples of short GRBs with coincident GW observations. This will allow us to answer fundamental open questions on the nature of compact binary mergers, such as the efficiency to form a relativistic jet, the jet structures, the properties of the EM emission from merger remnants, the role of NS-NS/NS-BH mergers in the chemical enrichment of r-process elements in the Universe and in cosmology acting as "standard sirens" for luminosity distance measurements.

During its nominal mission lifetime, THESEUS/XGIS and SXI are expected to detect and accurately (<15') localize ~40 short GRBs (~12/yr assuming 3.45 years of scientific observations) inside their imaging field of view, plus numerous short GRBs at higher energies (>150 keV) with coarse or no sky localization. These numbers refer to short GRBs for which the line of sight falls inside the narrow core of the corresponding jet (aligned). Figure 2-14 shows the redshift distribution of these short GRBs (blue line). Joint short GRB+GW detections are obtained by considering, at each redshift, the GW detection efficiency for NS-NS mergers. In these computations, three scenarios for the 3G GW interferometers have been considered: 1) ET alone, 2) ET plus one CE (in USA), 3) ET plus two CE (one in USA and one in Australia). The expected numbers of short GRBs detected and localized with THESEUS and detected also by 2G and 3G interferometers are summarized in Table 2-3. These numbers are robust and based on the Mission Observation Simulator (MOS) results (see §3.3) and state-of-the-art NS-NS merger simulations for the GW detection efficiency estimates.

Since GW emission from CBCs depends only weakly on the inclination angle between orbital axis and line of sight, most GW detections will be misaligned, i.e. at viewing angles outside the narrow core of the putative jet. As a consequence, the possibility to observe also misaligned, short GRBs as in the case of GW170817, can greatly increase the number of coincident GW+EM detections.

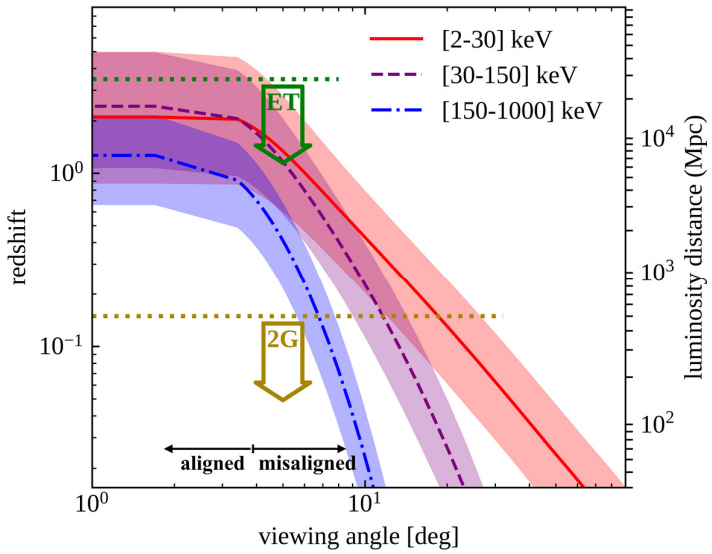

Figure 2-13 The pink, violet and blue stripes indicate the maximum distance/redshift for detecting with THESEUS/XGIS the prompt emission of a 170817A-like short GRB as a function of the viewing angle. Dotted horizontal lines indicate the ET and 2G maximum distance reach for NS-NS mergers, respectively. At 330 Mpc (typical 2G distance reach for random inclinations), for instance, THESEUS can detect up to a viewing angle of ~20°-40° (2-30 keV band), providing >25-100 times more detections with respect to a viewing angle within the jet core (<4°) [Credit: O. Salafia].

The richness of information inferred from GRB 170817A enabled us for the first time to quantify how the high-energy prompt emission becomes gradually softer and less energetic as the viewing angle increases with respect to the jet axis. From this information, by assuming GRB 170817A-like events, the maximum viewing angle at which THESEUS could detect the prompt emission depending on distance has been estimated. The unique capabilities of THESEUS offer excellent prospects for detecting the prompt emission from misaligned short GRBs, in particular in the 2-30 keV band (Figure 2-13) where we predict at least 80% more events with respect to the expected number of aligned short GRBs with accurate localizations[3] (i.e. from 41 to 73). The increment of joint short GRB+GW detections by including misaligned events is shown in Figure 2-14 (right panel). It is particularly evident at low redshifts where the maximum viewing angles at which THESEUS could detect a short GRB are larger and where GW interferometers are more sensitive for NS-NS merger detection. Table 2-3 shows the expected joint detections for aligned and misaligned short GRBs.

Soon after the main burst, the quickly fading soft X-ray tail interpreted as high-latitude emission from the jet, can be detected with SXI. In addition, the propagation of the GRB jet in the interstellar medium is known to produce a multiwavelength afterglow signal, from X-rays to radio, via synchrotron emission at the forward shock. By assuming a GRB 170817A-like jet, THESEUS SXI and IRT will be able to catch on-axis X-ray and IR afterglow emission up to z~1-2. Very accurate sky localization from SXI and IRT observations will allow facilities such as ATHENA, ELT, or SKA, to deeply monitor the source and thus to further characterize the following emission. Moreover, this synergy will significantly improve the chances of identifying the host galaxy and obtain a precise redshift measurement. For misaligned events, afterglow detection will also be possible at small distances. For instance, IRT can detect such emission up to a viewing angle of ~27° for an event at ~40 Mpc (i.e. the GW170817 distance) and up to ~8° at ~300 Mpc. Misaligned afterglows also peak at times that can be hours or days later than the prompt burst, in which case actual observations would require a dedicated re-pointing strategy (see §2.4). THESEUS has unique capabilities to detect and localize a statistically significant fraction of short GRBs. Together with GW observations, which will probe the nature and properties of the merging system and the remnant object, THESEUS will unveil the physics governing GRBs and its implications on relativistic astrophysics (see Table 2-3).

[3] *Computed by boosting the aligned short GRBs by a factor (1-cos $\theta_{view}(z)$)/(1-cos θ_{jet}), where θ_{jet} ~4° is the jet core half-opening angle (conservative choice from* [57]*) and θ_{view} (z) is the maximum detection angle at each redshift according to the results in Figure 2-13.*

Table 2-2 THESEUS role in the context of multi-messenger astrophysics during the 2030s

	The role of THESEUS	THESEUS vs other facilities
EM follow-up challenges: **The poor sky localizations of GW/neutrino cosmic sources during the '30s challenge searches for the EM counterparts and their identification and/or full characterization in the EM spectrum**	The large XGIS and SXI FoV and grasp will allow THESEUS to independently trigger the EM counterparts of several GW/neutrino sources and localize them down to arcmin/arcsec level.	THESEUS will independently detect the short GRB signal, similarly to Fermi/GBM for the case of GRB 170817A, but with respect to the Fermi/GBM, THESEUS will also provide accurate localisation down to the arcmin/arcsecond-level.
	The high cadence spectral observations across 0.3 keV - 10 MeV plus possible additional NIR observations, will allow to identify the nature of EM counterparts of GW and neutrino sources	THESEUS large spectral coverage is an advantage for transient identification w.r.t. other high-energy all-sky monitors operating on narrower energy bands, as e.g., Einstein Probe (0.3-4 keV) which is not optimized for the detection of short GRBs.
	THESEUS will disseminate accurate sky localization (arcmin/arcsecond uncertainties) within seconds/minutes to the astronomical community, thus enabling large ground- and space-based telescopes available by 2030s as SKA, CTA, ELT, ATHENA, etc. to observe and deeply characterise the nature of the GW/neutrino source as well as increasing the scientific output of these facilities.	The synergies of THESEUS with next generation neutrino and GW observatories will significantly increase the number of multi-messenger detections, allowing us to apply a first statistical approach to the study of multi-messenger sources and thus representing a major step forward with respect to other missions operating during the 2020s

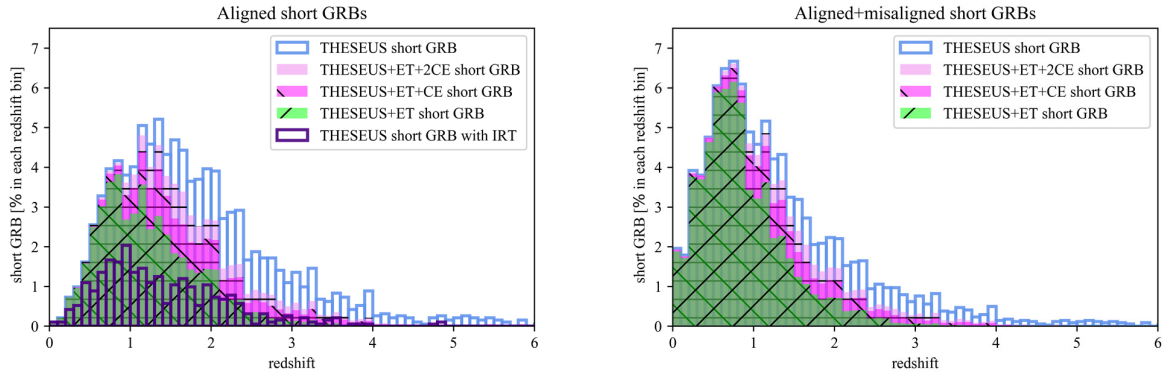

Figure 2-14 Left: The redshift distribution of well-localized aligned short GRBs (blue) from XGIS and SXI and those detected also with IRT (25%, indigo) [results from the MOS, credit A. Rocchi]. Joint short GRB+GW detections are obtained by considering, at each redshift, the GW detection efficiency for NS-NS mergers by ET (green, ~46% of THESEUS short GRBs), the ET+CE network and ET+2CE network (magenta and pink, ~62% and ~73%), respectively [credit: S. Grimm, M. Branchesi, J. Harms]. Right: same as the left panel where misaligned short GRBs are also included (see text). Including misaligned events not only increases the total number of THESEUS short GRBs, but also boosts the fraction of events with a joint EM+GW detection, leading to ~63% for ET, 76% for ET+CE and 83% for ET+2CE.

2.3.1.2 Additional electromagnetic counterparts of CBCs

Beside the short GRB prompt and afterglow emission, other EM signals are expected to be detected with THESEUS jointly with GW observations of CBC events. They have not yet been detected alone (i.e., with no short GRB) in association with GW emission, and so, predictions are more uncertain. However, these additional EM counterparts are of great interest since most of them are expected to be less collimated with respect to the prompt emission, and as such observable from the more frequent GW events observed from misaligned directions (that is, when the orbital plane is not perpendicular to the line of sight). This can significantly increase the number of multi-messenger sources detected. These additional EM counterparts are described in the following and include extended emission and plateau typically observed in short GRBs, whose origin is still matter of debate. The information carried by these additional signals when jointly detected with GWs are expected to provide fundamental clues on the nature of the post-merger remnant.

Table 2-3 The expected number of joint prompt GW+EM detections of NS-NS mergers/short GRBs for THESEUS and different GW detectors, assuming 1 or 3.45 years of joint observations. Number estimates of aligned short GRB+GW detections take into account the redshift distribution of THESEUS short GRBs from the MOS [credit A. Rocchi], and the NS-NS merger detection efficiency at each distance/redshift as predicted for the different GW detectors, assuming SNR=8 [credit: S. Grimm, M. Branchesi, J. Harms]. Number estimates of aligned plus misaligned short GRBs+GW detections take into account also the maximum viewing angle for misaligned short GRB detection at each distance/redshift (see text, Figure 2-13, Figure 2-14).

GW detectors	THESEUS+GW detectors plausible joint observation time	aligned short GRB+GW detections	aligned & misaligned short GRB+GW detections
2G network z<0.107 (500 Mpc)	3.45 yr	~0.04	1.8
ET	1 yr (3.45 yr)	5.6 (19.2)	13 (46)
ET+CE	1 yr (3.45 yr)	7.4 (25.7)	16 (55)
ET+2CE	1 yr (3.45 yr)	8.7 (30.1)	18 (61)

2.3.1.2.1 "Extended Emission" of Short GRBs

THESEUS is perfectly suited to observe the "Extended Emission" (EE) often accompanying short GRBs. The EE may be significantly less collimated than the prompt emission, implying the opportunity to catch a number of otherwise undetected events and thus increase the overall number of NS-NS/NS-BH mergers observed by THESEUS. A large sample of GRBs with detected and undetected EE will allow us to disclose the origin and the actual collimation of this mysterious component through synergic GW+EM data analysis.

EE of short GRBs refers to a softer and prolonged emission lasting a few tens up to hundreds of seconds [72] observed in a still uncertain fraction of short GRBs (2-25%, [73], [74], [75], [76]). It has been recently proposed to be present in >75% short GRBs if early X-ray observations are taken into account [77]. Figure 2-15 shows on the left an example of EE light curve for the short GRB 050724 at z=0.26 detected with Swift/BAT [78] that THESEUS would have detected with high significance.

The physical interpretation of the EE is still unclear. The long EE duration (e.g. 10-100s) challenges the BH-torus scenario after the merger of two NSs and supports the formation of a spinning down magnetar remnant ([79], [80]). In this scenario, the EE is expected to be much less collimated with respect to the main spike and as such it can also represent a possible "short GRB-less" EM counterpart of NS-NS mergers. Simulations performed on a sample of short GRBs with EE show that THESEUS/XGIS and SXI can detect such component up to z~2, with an average significance of ~50σ and ~10σ, respectively. The total number of EE that THESEUS can detect within a given distance depends on two uncertain parameters, namely the fraction of short GRBs with EE and its collimation. For instance, by assuming that EE has a 50% occurrence and a typical half-opening angle of 20°, we expect a few joint EE+GW detections within ~300 Mpc and ~100 detections up to the distance reach of 3G GW detectors.

2.3.1.2.2 X-ray plateaus

The soft X-ray "plateaus", commonly observed in association with short GRBs, are also possibly less collimated than the prompt GRB emission. Depending on how the emission weakens with the angular distance from the jet axis, the total number of detectable plateaus could be up to 1-2 orders of magnitude larger than that of short GRBs, thus potentially boosting further the number of EM counterparts of NS-NS/NS-BH detected by THESEUS. Joint GW+EM data analysis will definitively unveil the still unclear origin of this plateau component.

Table 2-4 Fundamental open questions on the nature of CBC sources and short GRB central engines that THESEUS will allow us to solve in synergy with the next generation GW interferometers.

How frequent is relativistic jet formation in NS-NS and NS-BH mergers?	THESEUS will allow for the detection of at least a few to about 10 or more short GRBs associated with GW-detected NS-NS/NS-BH mergers. The association of a short GRB with NS-NS/NS-BH mergers unambiguously marks the formation of a relativistic jet. Along with detections, THESEUS will also allow for confident non-detections in case of face-on mergers without a short GRB (based on the binary system inclination extracted via the GW signal).
What is the jet launching mechanism in NS-NS/NS-BH mergers?	The time delay between the GW merger epoch and the GRB peak flux is a powerful diagnostic indicator for the jet launching mechanism [56]. The significant number of short GRBs observed by THESEUS in synergy with GW detectors will allow us to uniquely characterize this important parameter and highlight differences between NS-NS and NS-BH systems.
What is the nature of the short GRB central engine and the origin of the still unexplained extra-features (e.g. "Extended Emission", "Plateaus")?	For short GRBs detected by THESEUS, the subsequent X-ray emission will be observed via the on-board SXI and/or by communicating the accurate sky localization to X-ray telescopes such as ATHENA. In presence of a coincident GW detection, a combined analysis will be possible, shedding light on the nature of the merger remnant (i.e. BH or NS). This unprecedented collection of information will also unveil the origin and statistical properties of puzzling X-ray features like the Extended Emission and the X-ray plateaus.
Do jets have a universal structure and are there any systematic differences between NS-NS and NS-BH mergers?	The afterglow properties of short GRBs viewed from outside the core of the jet strongly depend on the jet structure. THESEUS will detect and localize down to arcmin level several misaligned short GRBs (see Table 2-3). The afterglow profile of the brightest and most nearby sources will be monitored with SXI and IRT. Moreover, synergy with powerful facilities, as the contemporaneous mission ATHENA, will allow for deep and long afterglow monitoring.
What is the role of NS-NS and NS-BH merger systems in the chemical enrichment of the Universe?	Kilonova observations provide crucial information on the r-process element formation in the Universe. THESEUS accurate sky localization of several NS-NS/NS-BH mergers will allow for kilonova detection and characterization through the follow-up with the onboard NIR telescope and/or through ground-based follow-up campaigns.

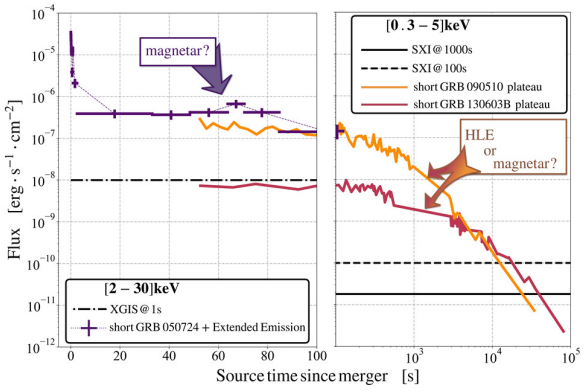

Figure 2-15 Left (linear temporal scale): X-ray light curve of a short GRB with "Extended Emission" (EE, GRB 050724, violet). Right (logarithmic temporal scale): X-ray light curves of two short GRB afterglows with "plateau" rescaled at 200 Mpc distance (GRB 090510, orange; GRB 130603B, red; data from Swift XRT repository, [81]). Both EE and plateaus are extra-features not explained by the standard GRB fireball model. Arrows indicate possible theoretical interpretations of EE and plateaus that predict poorly collimated or nearly isotropic emission (see text) [credit: S. Vinciguerra].

A potentially high fraction (>50%) of short GRBs are followed by a persistent soft X–ray emission characterized by a rather shallow decay in the light curve (so-called 'plateau' phase) and lasting from hundreds to several thousands of seconds (two examples are shown in Figure 2-15). Being inconsistent with the standard fireball model [82], the origin of such X-ray plateaus is still debated. Common interpretations include, for instance, (i) the emission sustained by prolonged (rather than nearly instantaneous) energy injection from a newly-born spinning down magnetar [83] and (ii) the high-latitude emission (HLE) from a structured jet whose energy and bulk Lorentz factor decrease with the angular distance from the jet axis ([84], [85]). While a magnetar emission could be nearly isotropic, the HLE would be observable, for a given distance, up to a maximum viewing angle estimated to be also several times the jet core aperture [46]. Understanding how plateaus are produced would require the ability to detect or exclude the presence of a plateau associated with GW-detected mergers for a large number of events and within a wide range of

possible inclinations. In the case of a magnetar origin, plateaus might be detected by THESEUS as "short GRB-less" X-ray transient sources, with lifetime of the order of ~1-10 ks up to 1 day and with ~10s-1ks temporal delay with respect to a spatially consistent GW event from a NS-NS/NS-BH source.

The 0.5 sr SXI field of view contains typical sky-localizations of signals detected by at least 2 GW interferometers ([70], [71]). Based on Swift/XRT X-ray plateau observations with known redshift, it can be inferred that about 90% and 30% of these plateaus can be detected with THESEUS/SXI with 1 ks of exposure within the 2G and the ET GW distance reach for NS-NS mergers, respectively. In the case of a HLE origin, a misaligned event observed with SXI will yield a steep X-ray decay transient with peak time ranging from a few 100 s up to >1 ks depending on the viewing angle, with a phenomenology similar to long GRBs (see §2.4). Joint detections of THESEUS and 3G GW detectors (able to detect the post-merger signal from the remnant) will unveil the connection among NS mergers and new-born magnetars and all the associated EM signatures.

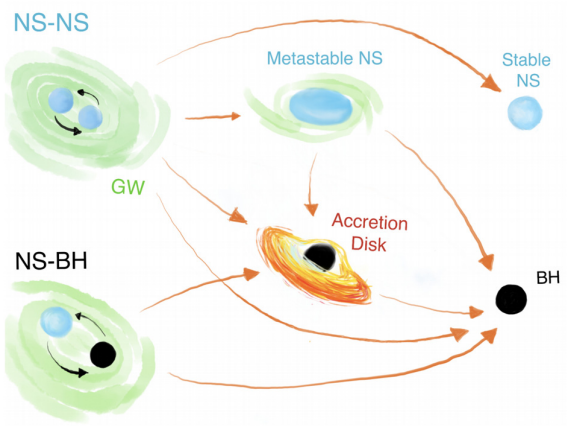

Figure 2-16 Cartoon on the NS-NS/NS-BH possible remnant formation channels (from Ascenzi et al. 2020).

2.3.1.2.3 Spin-Down Powered Transients

In the case a NS-NS merger produces a long-lived millisecond magnetar, nearly isotropic soft X-ray to optical transients with timescales of minutes to days can be powered by the magnetar EM spin-down emission. THESEUS/SXI can detect such transients up to redshift z~1.3

A potentially powerful nearly-isotropic emission is expected if a NS-NS merger produces a long-lived millisecond magnetar, i.e. a remnant object that does not collapse to a BH for as long as minutes, hours, or more (see Figure 2-16). Soft X-ray to optical transients can be powered by the magnetar EM spin-down emission reprocessed by the baryon-polluted environment surrounding the merger site ([86], [83]). In soft X-rays, such spin-down powered transients (SDPTs) can last for a timescale of minutes to days and their expected luminosities are up to 10^{46}–10^{48} erg/s [83], which would be reachable by SXI up to 0.9-9 Gpc with 1ks exposure.

One or more unambiguous detections of this type of emission after a NS-NS merger would indicate that the remnant is long-lived, allowing us to achieve significant constraints on the NS equation of state and other key properties of the remnant itself ([87], [88]). Moreover, it would provide crucial information to estimate the currently unknown fraction of mergers forming a long-lived NS remnant. Finally, it would clarify the possible connection with the extended emission and/or the X-ray plateaus of short GRBs. In the case of GW170817/GRB 170817A, no evidence for a SDPT was found in the soft X-ray band. However, the first deep pointed observations at ~keV photon energies only started as late as ~15 h after merger with Swift/XRT [89], and the earlier constraints provided by MAXI 4.6 h after merger with a flux limit of ~8.6 10^{-9} erg/cm^2/s [90] were not able to exclude a SDPT. The combination of the THESEUS/SXI sensitivity at ~keV energies and its field of view about 10^4 times larger than Swift/XRT will offer much better prospects for a detection within minutes/hours after a GW trigger.

2.3.1.2.4 Kilonovae

THESEUS/IRT can detect the kilonova emission associated with nearby short GRBs detected with XGIS/SXI, ensuring the binary merger sky localization down to the arcsecond level. This will allow next generation powerful telescopes, such as the ELT, to take high-detected-quality spectra and extract chemical abundance information, ultimately defining the role of NS-NS/NS-BH mergers in the cosmic enrichment of r-process elements.

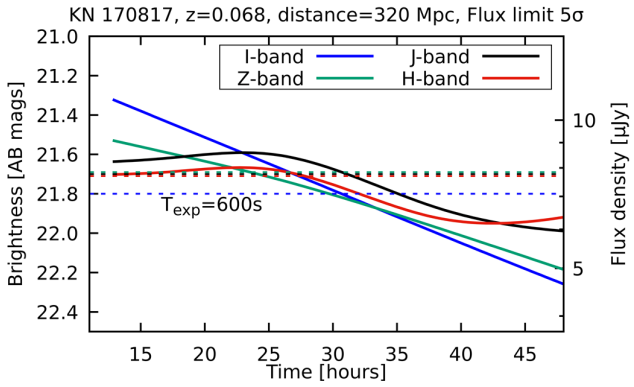

Figure 2-17 Multi-band light curves of the kilonova AT2017gfo [91] compared with THESEUS/IRT sensitivity. THESEUS can detect a kilonova like AT2017gfo with 5 sigma up to 320 Mpc in all bands with 600s of exposure, within 1-2 days from the merger epoch. Near-IR spectra (H<17.5, 1800 s) can be obtained for the most nearby sources (i.e. <40 Mpc).

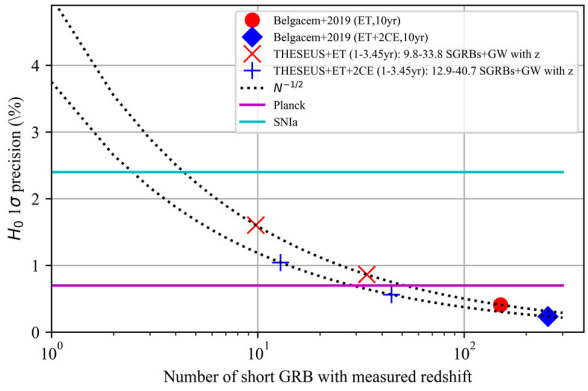

Figure 2-18 Hubble constant 1 sigma precision level as a function of the number of compact binary mergers for which the redshift and the luminosity distance can be measured from the electromagnetic and gravitational wave emission, respectively. In this plot, the electromagnetic counterpart comes from aligned and misaligned short GRBs (see last column of Table 2-3) for which redshift can be measured. These numbers are conservative estimates from afterglow simulations performed with "afterglowpy" (see text).

Neutron-rich matter released from NS-NS/NS-BH mergers undergo rapid neutron capture (r-process) nucleosynthesis, leading to the formation of very heavy elements such as gold and platinum. Radioactive decay of the newly-formed and unstable heavy nuclei powers a rapidly evolving, nearly isotropic thermal transient known as a ''kilonova'', the observation of which not only witnesses cosmic nucleosynthesis of heavy elements, but can also probe the physical conditions during and after the merger phase [92]. So far, the only robust observation of a kilonova, among a few other candidates [93], was the optical and infrared counterpart of GW170817, named AT2017gfo ([94], [95], [96], [97]). With an exposure of ~150 s, an AT2017gfo-like kilonova would be detectable by THESEUS/IRT for a NS-NS merger up to ~200 Mpc away (Figure 2-17).

2.3.1.3 CBC redshifts and prospects for H_0 measurement

THESEUS, in synergy with GW detectors and ground-based EM observatories, will allow us to build up a large sample of CBCs with measured redshift. Combining the redshifts with the luminosity distances measured from the GW waveform will lead to an independent measurement of the Hubble constant with the level of precision required to resolve the current tension.

Independent measurements of the Hubble constant H_0 are of utmost importance in order to understand if the current tension [98] is due to possible systematics or is the sign of a cosmological crisis that requires new paradigms. The detection of GWs from CBCs and the measurement of their redshift through their electromagnetic counterparts has already been proven to be a new probe for H_0 in the case of GW170817 [99]. To solve the current tension, a precision level at least of the order of ~1% should be reached and a large number of CBCs with measured redshift are needed. In this context, THESEUS observations of a large number of short GRBs in synergy with 3G interferometers represents a unique opportunity. Simulations of NS-NS mergers observed with the 3G network along with an instrument like THESEUS/XGIS have been performed by [100]. Their results predict a number of joint detections of ~130-300 in ten years, from which H_0 can be measured with a precision of 0.2% - 0.4% by assuming that a redshift can be measured for all events via either optical or X-ray spectroscopy: with this assumption, Figure 2-18 shows that, by rescaling these precision levels as $1/\sqrt{N}$, the goal of $\Delta H_0/H_0$~1% can be reached with N~15 events jointly observed with the 3G network (ET+CE+CE) and N~25 events jointly

observed with ET only (the lower number of events providing $\Delta H_0/H_0$~1% with the ET+CE+CE network with respect to ET only is due to the better parameter estimation with the former network). In reality, as we learned from past observations, the redshift cannot be measured for all short GRBs due to host galaxy identification challenges. This will likely not affect the ~25% of THESEUS short GRBs detected with IRT since their sky localization to arcsec accuracy will enable unambiguous identification of the host galaxy and measure the redshift. For the remaining 75%, the large number of galaxies contained in the XGIS or SXI error boxes for almost all short GRBs (i.e. at distances >50-100 Mpc) severely challenges the identification of the host galaxy if no transient optical afterglow is detected.

In order to quantify the chances to perform successful ground-based afterglow follow-up, 1000 optical aligned and misaligned afterglow synthetic light curves have been generated[4] assuming GRBs with equivalent isotropic radiated energy $>10^{50}$ erg and mean value ~2×10^{51} erg and then compared with the magnitude limits of different telescopes that may operate at the epoch of THESEUS[5]. Results show that, for aligned short GRBs with no IRT detection, ~50% will have a detectable optical afterglow (that unambiguously pinpoints the host galaxy) by providing a ground-based telescope follow-up reaction time of a few hours. With the same assumptions, ~13% of misaligned short GRB will have a detected optical afterglow. In conclusion, we estimate that ~73% of all short GRBs detected by THESEUS should have a redshift measurement. By taking into account our results on the expected fraction of aligned and misaligned short GRBs with measured redshift (Table 2-3), H_0 will be measured with ~1% accuracy (at 1 sigma) with 1yr of synergy with the ET+2CE network or 3.45yr with ET (Figure 2-18).

2.3.2 Other GW sources

Core-collapsing massive stars and isolated neutron stars are additional high-frequency GW sources and among the primary targets of THESEUS. Their GW emission will likely be observed only with the upcoming ~10 times more sensitive 3G detectors. THESEUS will ensure coincident electromagnetic counterpart detections and accurate sky localisation, both crucial for the challenging search of burst GW signals and for providing unprecedented insights on the physics of such events through a multi-messenger view.

GWs from core-collapse supernovae (CCSNe) encode crucial information on the explosion inner dynamics, inaccessible to electromagnetic observations [101]. Predictions on the burst GW signal and its detectability are much more uncertain than for CBC sources since they strongly depend on the rather unknown SN explosion mechanism. If the core-collapse results in the formation of a millisecond spin-period NS, strong GW emission may be expected from the remnant, although the rate of such an occurrence is uncertain ([102], [103], [104]). Realistic estimates predict a few GW detections within a several tens of Mpc with 3G interferometers during the nominal THESEUS lifetime (considering extreme emission core-collapse models or the GW signal from a new-born magnetars). For those events, THESEUS will offer the opportunity to catch the accompanying high-energy signal. In particular, the formation of a highly magnetized spinning NSs, as well as their predicted surface instability episodes, are expected to be accompanied by X-ray transients [103] that could be detectable with THESEUS/SXI. Long GRBs, in particular the expected nearby low-luminosity GRBs [105], shock breakout signals, Soft Gamma Repeaters, and ultra-long GRBs are also promising target signals for THESEUS which may have a detectable GW counterpart (see §2.4 and 2.5).

2.3.3 Neutrino sources

A major contribution to the observed diffuse neutrino flux is thought to originate from extragalactic

---

[4] *Using the python module afterglowpy [229] that however does not take into account possible "rebrightenings" observed in several optical afterglows, the origin of which is not yet fully understood (therefore, provided estimates are conservative) [Credit: L. Salmon].*

[5] *In this simulation we considered: LSST/VRO, the Liverpool Telescope and GTC/OSIRIS*

sources: AGNs, starburst galaxies, and GRBs. THESEUS will provide deep sky surveys in an era of ~10 times more sensitive next-generation neutrino detectors such as IceCube-Gen2 and KM3NET. The identification of temporally and spatially consistent EM transients will eventually disclose the origin and composition of the neutrino diffuse flux.

AGNs are thought to produce the largest fraction of the diffuse neutrino emission and are among the THESEUS transient targets. The joint detection of large numbers of neutrino and EM emission sources, feasible only during the 2030s with next generation neutrino detectors, will allow us to answer long-standing questions on the acceleration mechanisms inside these systems, on whether (hadronic vs leptonic) processes characterize the photon and neutrino production, and on the role of these events in producing the diffuse neutrino flux. Another, smaller, fraction of diffuse neutrino emission is expected to originate from SNe in starburst galaxies that are expected to behave as calorimeters [106]. The sky region localized by a neutrino event may thus contain starburst galaxies, a large fraction of which is detectable with THESEUS/IRT up to z~0.6. NIR observations will allow us to infer the level of ongoing star formation in each galaxy, which is directly connected to the rate of supernova explosions. For the brightest high-redshift galaxies IRT photometry will probe the UV emission, perhaps identifying the brightest star forming galaxies as the best candidates for originating the neutrino event.

A still very uncertain fraction of neutrino diffuse emission can originate from GRBs. If during the GRB prompt phase a non-negligible fraction of baryons is accelerated at internal shocks [107], neutrinos are likely to be produced in pγ interactions, given the intense radiation field of the jet. So far, no neutrino event has been detected in correlation with a GRB ([108], [109]), indicating a limited neutrino production in the most powerful sources [110], and strengthening the case for extending this investigation to fainter sources. For this reason, low-luminosity GRBs may be better candidates than bright GRBs to account for the IceCube diffuse neutrino flux, although likely not dominant [111]. THESEUS' sensitivity and extended energy bandpass are thus fundamental to probe the poorly-sampled fraction of intrinsically soft and low-luminosity GRBs. In short GRBs, pp collisions in the post-merger accretion disc are also expected to take place and contribute to the neutrino emission. As for long GRBs, so far, no neutrino event has been detected to coincide with a short GRB ([108], [109], [110]). Recent studies have suggested that high-energy neutrinos can be efficiently produced during the "Extended Emission" phase of short GRBs [112], a target that THESEUS/XGIS will detect up to large distances (see §2.3.1).

2.3.4 External triggers

THESEUS can also react to an external trigger from neutrino and/or GW detectors within about 12 hrs (with a goal of 4 hrs) after the alert[6]. The excellent THESEUS sky localization capabilities of GW and neutrino EM counterparts will allow for the activation of dedicated follow-up campaigns with terrestrial optical and radio facilities such as ELT, SKA, etc., as well as space-based telescopes such as ATHENA.

GW and neutrino sources can produce electromagnetic emission on timescales that require dedicated Target of Opportunity observations. Table 2-5 summarizes some examples of such expected electromagnetic components from GW-detected CBC sources and neutrino events.

2.4 GRB physics

THESEUS will unveil the physics of GRBs. Temporal and spectral studies, extending from 0.3 keV to 10 MeV, will probe the nature of the prompt emission process, constrain the structure of the relativistic jets and the nature of the energy dissipation mechanism, and explore the chemical composition of the ambient medium enriched by the progenitor.

---

[6] *Early GW detection from nearby CBCs during the inspiral phase, up to few hours before the merger epoch* [71]*, will be possible with 3G interferometers, allowing THESEUS/SXI to be ready to detect the post-merger X-ray emission right after merger, during the brightest phase.*

Table 2-5 Examples of possible EM counterparts of GW/neutrino sources that THESEUS can detect with a latency of a few hours in reacting to an external trigger (see §2.3.1 and 2.3.3 for further details on each component).

External trigger	Expected emission components on timescales longer than 4-12 hrs
NS-NS/NS-BH merger from GW interferometers	• X-rays from possible magnetar remnant or HLE from structured jet • X-rays and NIR misaligned afterglow (peak flux ~within 1 week)
Kilonova candidates from optical surveys (e.g. LSST/VRO)	• NIR kilonova monitoring/SED
Neutrino event	• X-rays from AGN flares with timescales of hours-days • NIR observations of starbursting galaxies within neutrino sky localization region (for well localized events only, i.e. <1 deg^2) • Aligned afterglows

2.4.1 Physics of the prompt emission

The unique combination of the wide energy range and the high sensitivity will constrain the overall spectral shape with high accuracy. At the low energy end, the possible presence of key synchrotron features like the "cooling break" and the appearance of a transient thermal component will constrain the physical parameters of the emission region and the jet energy content.

The radiative process responsible for the production of the prompt emission of GRBs has not been identified yet [113]. The spectral shape of the prompt emission, typically observed in the 10keV-10MeV energy range, is inconsistent [114] with expectations from the synchrotron process [115]. This triggered the flourishing of a wide range of possible alternatives (e.g. thermal emission from sub-photospheric dissipation) or modifications of the standard synchrotron scenario (e.g. inverse Compton scattering, peculiar magnetic field configuration in the emission region, [116], [117]). The extension of the spectral analysis below 10 keV has recently revealed the unexpected presence of a spectral break at low energies, with the bonus of reconciling the overall shape of the prompt spectrum with synchrotron radiation ([118], [119], [120], [121], [122]). Besides pointing to the synchrotron process as the mechanism producing the radiation, the detection of this spectral break, interpreted as the signature of the cooling frequency of emitting electrons, opened for the first time the possibility to constrain the physical properties of the emission region (magnetic field intensity, number of emitting particles and their characteristic energy, and localization of the emitting region).

However, the identification of this spectral break has been possible only for the small sub-sample of GRBs promptly followed by the Swift/XRT [119] or for relatively bright Fermi/GBM bursts ([121], [122]).

A prototypical example, GRB180720B at z=0.65 (Figure 2-19 top left panel) observed by Fermi/GBM, revealed [123] a steep electron energy distribution (inferred from the slope β of the high energy power law spectrum) and a relatively small comoving frame magnetic field, which challenge the acceleration mechanisms, the common understanding of the jet composition, and the standard electron-synchrotron scenario [107].

Using GRB 180720B as a template and moving it to different redshifts, simulations show that THESEUS will constrain with unprecedented accuracy the spectral parameter values (solid lines in Figure 2-19 right panel): e.g. at z~2, corresponding to the peak of the THESEUS-detected population, the break energy will be constrained with an accuracy of 20% (compared to >50% of Fermi - dashed lines in Figure 2-19 right) with a typical error on the spectral slopes of the power law segments of the photon spectrum (α_1, α_2, β) of 0.01-0.1 (a factor of 10 smaller than Fermi). The extension of the spectral window down to 0.3 keV with SXI will provide unique constraints on the Hydrogen equivalent column density, thus relieving the degeneracy with low spectral break values. The unique sensitivity of THESEUS in the 0.3-50 keV energy range, will be the key to reveal and study the possible thermal component arising from the photosphere (now revealed in a handful of GRBs, [124]), in order to constrain the jet magnetic energy content [125]. For slightly off-axis bursts, the soft X-ray band will contribute to unveil the cocoon emission produced by the jet shock break out [126].

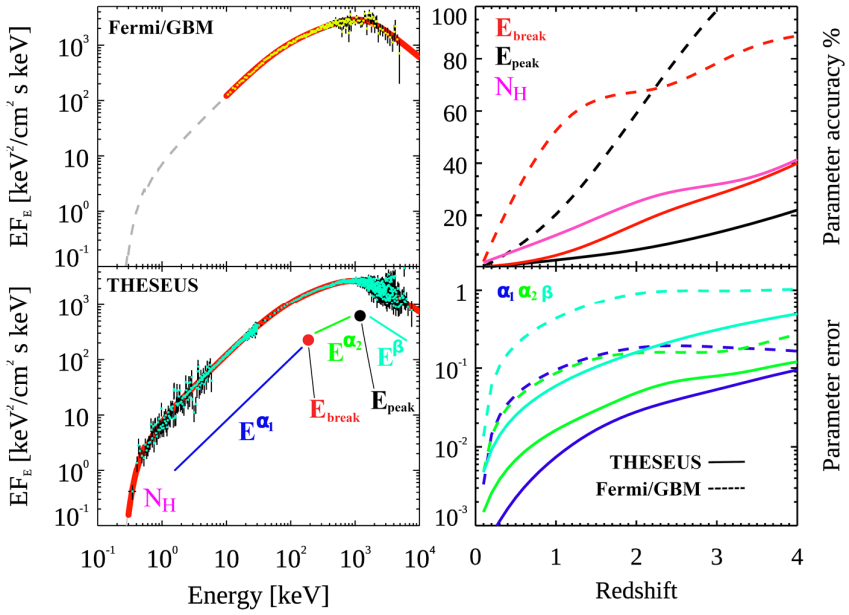

Figure 2-19 Simulated prompt emission spectrum of GRB 180720B [123] as observable by Fermi/GBM (top left panel) and by THESEUS/SXI+XGIS (bottom left panel). The red line is the simulated spectrum consisting of three power-law components and two smooth breaks (shown with the colour coded sketch in the bottom left panel) and a total absorption $N_H=10^{22}$ cm^{-2} (assuming solar metal abundances). Right panel: percent precision on model parameters, obtained by simulating GRB 180720B at different redshifts, for THESEUS (solid lines) and Fermi/GBM (dashed lines). The advancement of THESEUS, exploiting its wider energy range (0.3 keV-10 MeV) and larger effective area with respect to Fermi/GBM, will provide accurate estimates of the key parameters of the prompt emission spectrum and, therefore, of the underlying physical parameters.

The iron absorption edge revealed so far only in GRB 990705 by BeppoSAX [127], can be detected with unprecedented high statistics by THESEUS (Figure 2-20 main panel) providing additional constraints on the source redshift and the circumburst metal abundance (Figure 2-20 insert panel) paving the ground to unprecedented insights into the progenitor's explosion nucleosynthesis [128].

2.4.2 Structure of relativistic jets produced by GRB progenitors

The soft X-ray extension by the SXI will probe the early fast decay flux evolution.

THESEUS, combining SXI and XGIS, will systematically monitor the spectral evolution of the prompt gamma-ray emission towards softer energies and will cover the transition from prompt to afterglow emission. The cessation of prompt emission is usually associated with a steep drop in flux (so called "steep phase") produced, most likely, by the temporal delay/energy softening of photons emitted at large angles with respect to the line of sight (so called high latitude emission, [129], [130], [131]). A possible further effect which could have a relevant role in shaping the observed steep phase is the spectral evolution of the prompt emission consisting in the overall softening of the spectrum [132]. The possible angular structure of the jet imprints further characteristic signatures to the observed soft X--ray light curve [46]. As shown in Figure 2-21, THESEUS/SXI can sample the initial decay of the soft X--ray light curve, even for observing angles much larger than the jet core angular size). THESEUS will detect off-core GRBs, whose light curves will peak in the soft X-ray band but will likely be orphan of a detectable gamma-ray emission. The systematic study of the on- and off-axis emission on a wide population of GRBs will allow to constrain the jet structure and test its universality, as well as to constrain the long GRB rate in the local Universe.

THESEUS will detect a large number of GRBs at z<5 and ~20% of these will have a relatively small luminosity (<10^{50} erg/s) and a soft spectrum (peak energy <50 keV). This sample will provide unique insights on the nature of soft GRBs/X--ray flashes/X--ray rich events [133] and of low luminosity GRBs ([134], [135], [136]) whose origin is still unclear.

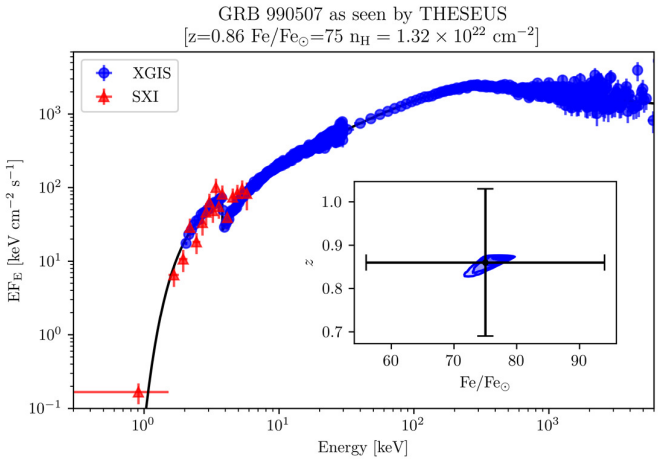

Figure 2-20 Simulated prompt emission spectrum of GRB 990705 [127] as observable by THESEUS SXI (magenta) and XGIS (blue). The assumed source parameters (in addition to those in the subtitle) are those in [42]. Exposure time is 10 seconds. The best fit model (solid red line) shows a prominent absorption edge due to the K-shell Fe transitions at 3.4 keV (observer frame). Insert: posterior sampling on the 2D constraints on the iron abundance (solar units) and redshift. The shaded grey and coloured (1,2,3σ) contours are compared to the uncertainty obtained from the BeppoSAX observation (orange cross).

2.4.3 Jet internal dissipation mechanism

The broadband capabilities and large effective area of XGIS will offer a systematic base for deciphering the dynamics that rule GRB light curves thanks to the uninterrupted monitoring of prompt and early X-ray flares.

The variety of GRB light curves along with early-time X-ray flares have poorly been understood, thus remaining mostly undeciphered. On the one side, some metrics that quantify the degree of variability are found to correlate with luminosity with considerable scatter, though ([137], [138]). Also, power density spectra, both average and individual, are suggestive of turbulence ([139], [140]) and correlate with E_p [141]. On the other side, a characterization as a stochastic process is still in its infancy, mostly hampered by the highly non-stationary, short-lived nature. In this context, it was found that the common waiting time distribution of GRB gamma-ray pulses and X-ray flares can be interpreted as the result of a unique time-dependent Poisson process, providing clues on the way the inner engine works [142]. Attempts to find evidence for self-organized criticality processes, that are invoked in the cases of solar and stellar flares, pulsar glitches, or even in the asteroid belt and in Saturn rings in the Solar System [143], have provided some clues from the study of energy, duration, and waiting time distributions of GRB X-ray flares [144]. Yet, a much larger data set for a statistically robust assessment is required. Other attempts have also been made to find evidence for the presence of deterministic signal as opposed to a pure random one [145]. In this respect, no compelling evidence has been found yet of periodic signals hidden in GRB light curves ([146], [147], [148], [149]). The delay in the arrival times between high and low energy photons from cosmic sources can be used to test the violation of the Lorentz invariance (LIV), predicted by some quantum gravity theories, and to constrain its characteristic energy scale E_{QG} that is of the order of the Planck energy. GRBs and blazars are ideal for this purpose thanks to their broad spectral energy distribution and cosmological distances ([150], [151], [152]). THESEUS spectral coverage, large effective area and relatively high temporal resolution will contribute to test LIV possibly through statistical studies that exploit the samples of long and short GRBs with measured redshift.

2.5 Exploring the time-domain Universe with THESEUS

The unprecedented grasp, high sensitivity, and wide spectral coverage of the THESEUS high-energy instruments offer a great opportunity to study the variability properties of several classes of sources on timescales from seconds to years. Currently, no X-ray all-sky monitors are planned for the 2030 timeframe. THESEUS will trigger observations with other facilities, not only when new sources are discovered, but also when interesting phenomena (e.g. outbursts or spectral state changes) are observed in the known sources that will be regularly monitored. Additionally, the use of the IRT for selected sources, through the implementation of a Guest Observer Program (see §2.6), further broadens the scientific scope by allowing for unique multi-wavelength monitoring.

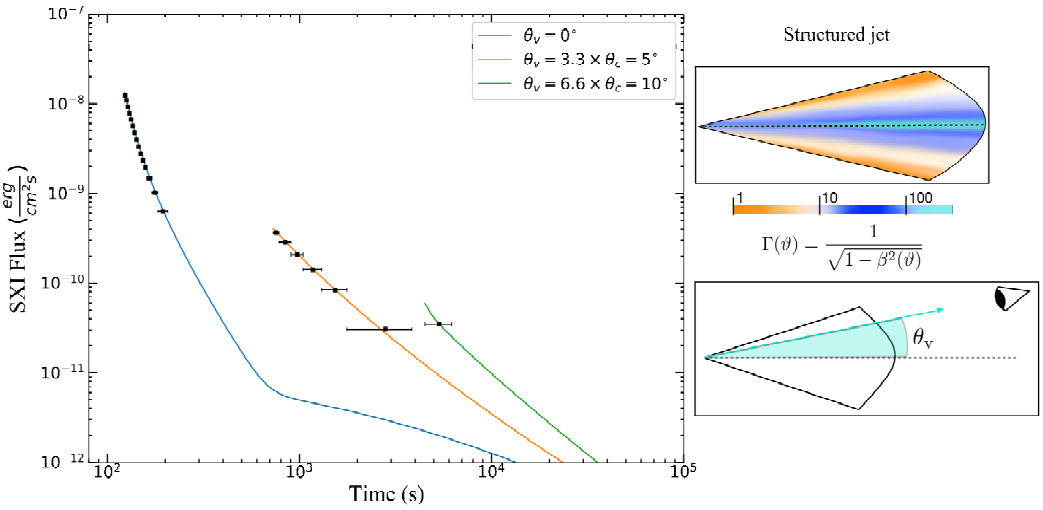

Figure 2-21 SXI temporal sampling of a light curve produced by the high latitude emission of a structured jet, observed at different inclination angles with respect to the symmetry axis of the jet. The adopted parameters for the jet structure are derived fitting the XRT light curve of GRB 060729. Each light curve is rescaled at redshift z=1.

2.5.1 Shocks and shock breakouts in Novae and Supernovae

THESEUS will constrain the physics of shocks and, thanks to its extensive monitoring, likely discover the thermonuclear runaway breakout predicted to occur in novae, but never observed to date.

The explosive burning of partly degenerate accreted matter on a White Dwarf (WD) causes a nova. The non-destructive nature of the explosion allows them to repeat; recurrent novae are classical novae for which this has been observed. Both types are feature-rich emitters of high-energy radiation, with ejecta shocks causing hard X-ray and even GeV emission [153], while the burning-heated WD photosphere can be a very bright super-soft X-ray source [154]. One aspect of their importance is that they are strong candidates to be the currently unknown progenitor of SN Ia [155].

THESEUS observations will constrain the shock physics via at least two methods. The SXI will measure the X-ray temperature and luminosity, using absorption measurements to monitor the shock progress through the progenitor wind, so measuring the energetics of the explosion (Figure 2-22). In combination with the orders-of-magnitude improvement in sensitivity of the CTA compared to the Fermi LAT, the acceleration of the highest energy particles will be characterised. In combination with SKA, the ejecta geometry and energetics can be further constrained. In addition, for the novae detected at higher energies by the XGIS, the buried shock hypothesis [156], in which the bright optical emission of novae is powered by deep ejecta shocks, can be definitively tested. Soft X-rays from the heated photosphere constrain the WD properties and ejecta mass ([157], [158]), but the ultimate promise of THESEUS is the discovery of the thermonuclear runaway shock breakout. Predicted by [159], this has yet to be seen because of its unpredictable timing, preceding the optical outburst. Current observational constraints are weak, being derived from a distant nova in M31 [160]. The wide FoV of the SXI makes it the ideal instrument to be first to characterise the pre-maximum state of Galactic novae via their ~10^{38} erg/s shock breakout, hence providing the temperature, a crucial parameter to derive the WD mass (see Figure 2-23).

The rate of Galactic novae is known within a factor of two, i.e. ~25-50 per year [161]. With the baseline THESEUS pointing strategy, most Survey Mode pointings will have a typical duration of 2.3 ksec, corresponding to a SXI detection threshold of a few 10^{-11} erg/cm^2/s. The Swift XRT detects 15% of the novae it observes at fluxes above this level. Therefore, we estimate that ~4-8 nova outbursts per year will be found by THESEUS on the basis of their WD or shocked ejecta emission.

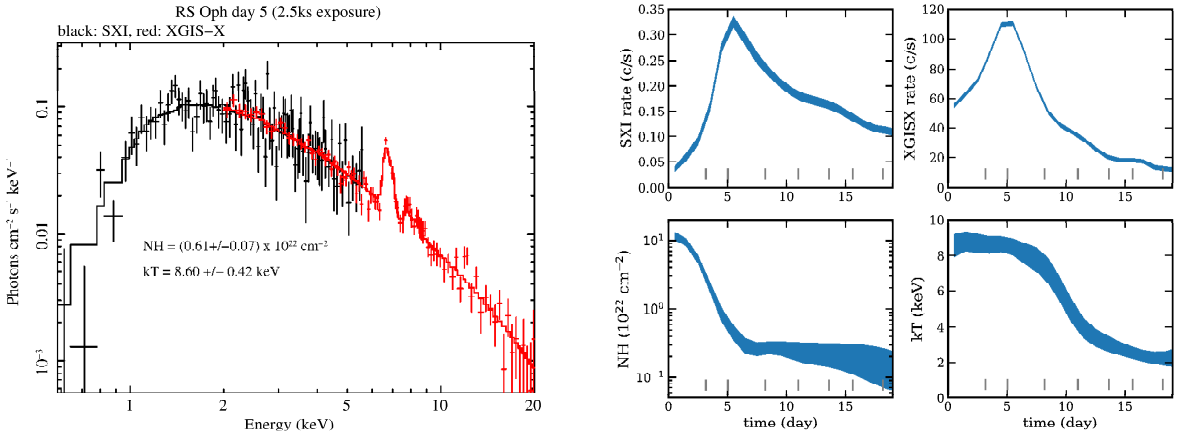

Figure 2-22 Left – SXI and XGIS predicted spectra of the ejecta shock of the recurrent nova RS Oph at peak shock brightness as it emerges from the wind of its red giant companion, based on the results of the Swift observations of [162]. Right – Top: the SXI and XGIS predicted count rates due to the ejecta shock emission of RS Oph based on the Swift observations. Bottom: The 90% confidence constraints derivable from SXI and XGIS spectra for the absorbing column and shock temperature. Swift observation times are marked below. While the individual spectral constraints are similar to those from Swift, THESEUS will observe up to 50x more frequently, allowing much tighter diagnostics of the shock evolution. By day 30 the soft X-ray count rate increases by 50x due to the emergence of the heated WD surface [163]. Although this specific nova may not erupt in the THESEUS nominal mission, other novae show similar patterns and can be followed for many weeks with THESEUS.

Nova shock breakouts are detectable for all WD with mass above 0.6 $M_\odot$, suggesting at least a couple of detections per year. Type Ia SNe are understood as explosions of WD in binary systems, disrupted by thermodynamical burning fronts. The apparent homogeneity in optical light curves and spectra is a direct result of the nuclear physics that governs the WD structure and the explosion. A 'stellar amnesia' masks the diversity. Potential progenitor systems include two WDs or a single WD with a non-degenerate donor. The triggering mechanisms of the explosion of the C/O WD may be compressional heating in the centre leading to the favoured scenarios of: a) reaching the Chandrasekhar mass, b) the surface He detonation triggering the C/O ignition in sub-Chandrasekhar mass, or c) friction during the dynamical merging of two WDs. However, the connection between progenitor systems and environment is largely unknown. A direct probe of the connecting layers requires advances in time domain astronomy. Thermonuclear burning temperatures and ejecta interactions with >10,000 km s^{-1} require X-ray observations. The system physical size sets the timescales to 0.1 seconds - weeks. THESEUS will uniquely and directly probe this uncharted territory in thermonuclear supernovae. The yearly SNe rate is 0.75, 6 and 750 for distances of 10, 20 and 100 Mpc [164]. Depending on model specifics, the values below are best estimates in the realm of unknowns. Potentially detectable sources include: a) the thermonuclear shock breakout [165], b) the interaction between the SN and the matter bound in the system [58], and c) the interaction between the SN ejecta and the direct environment ([166], [167]).

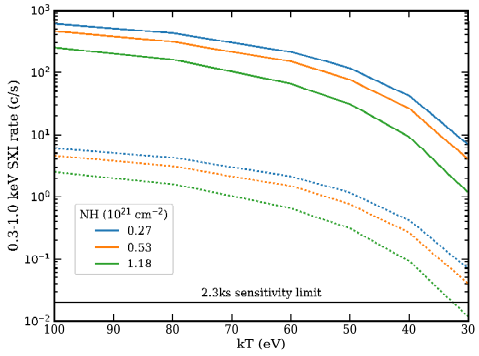

Figure 2-23 Predicted SXI count rates from the as-yet undiscovered classical nova shock breakout derived from the model of [160]. The upper and lower sets of curves correspond to distances of 1 and 10 kpc, the typical Galactic range. The colours refer to differing absorbing column densities, corresponding to 25%, median and 75% of the cumulative distribution of Galactic HI values from the HI4PI 21 cm survey [168]. The SXI detection limit for the standard unbroken observation length in the baseline Survey Mode strategy is shown. The peak temperature of the shock breakout is a measure of the mass of the white dwarf, the range displayed covers the nova range of 0.6-1.3 $M_\odot$.

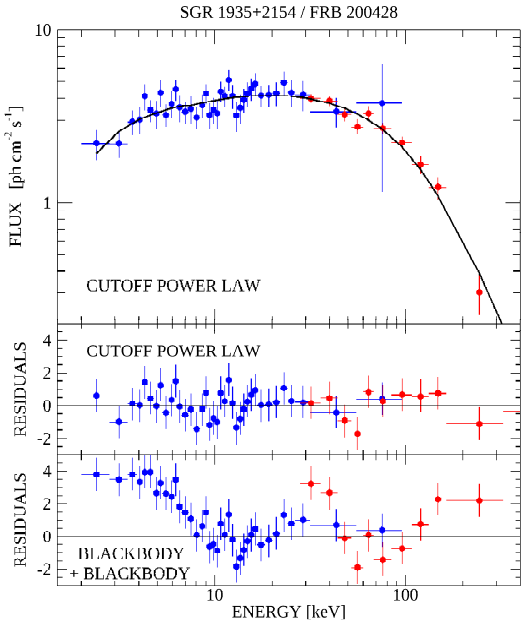

Figure 2-24 Simulated XGIS spectra of SGR1935+2154/FRB 200428 [169]. Thanks to the extended spectral coverage, THESEUS can discriminate between alternative spectral models (cut-off power law vs. sum of two blackbodies) that are equally acceptable when only data above ~10 keV are available. Despite the high absorption (N_H ~ 2 10^{22} cm^{-2}) this burst would yield about 40-50 counts in the SXI. More counts are of course expected for closer and/or less absorbed magnetars.

The timescale for the breakout is governed by cooling and nuclear burning. Similar to short GRBs, the spectral peaks shift within the XGIS band on time-scales up to ~1 s, followed by a tail in SXI for ~10 min. For pure C/O mixtures, rapid cooling combined with very low tail fluxes allow the detection of one SN Ia within 3-5 Mpc over 3 years. In both single- and double-degenerate scenarios He-layers mixed with C are expected. Burning time scales for $^{12}C(\alpha,\gamma)^{16}O$ are about 0.1 s, resulting in strong heating during the phase of early expansion and in large luminosity increases by about a factor of 100, leading to about 5 potential detections per year with XGIS and SXI.

2.5.2 Magnetars / Fast Radio Bursts

THESEUS will provide excellent wide band data on Galactic magnetars and can detect extragalactic magnetars in the local Universe as potential counterparts of Fast Radio Bursts (FRBs).

Magnetars, isolated NS with magnetic fields as high as 10^{15} G [170], are characterized by extreme variability on all timescales, from milliseconds to years. Although it is now well established that their persistent and bursting emission is powered by magnetic energy, many aspects of their rich multiwavelength phenomenology are still to be explained, both concerning the physical processes responsible for the bursts, giant flares, and outbursts, and their evolutionary connection with other classes of NS. Magnetars have also been invoked in models for a variety of other sources, such as GRBs (e.g., giant flares in nearby galaxies can mimic short GRBs; newly born magnetars can provide extended energy injection), super-luminous supernovae, and FRBs. Magnetars are also potential sources of neutrinos, high-energy cosmic rays and gravitational waves. The number of known magnetars (currently ~30 in the Milky Way and Magellanic Clouds) will at least double by the time of THESEUS launch because most magnetars are transients, discovered during their active states (typically a new one is discovered every year). THESEUS will give immediate alerts of outbursts from both known and newly discovered magnetars, through the XGIS detection of bursts and/or the SXI detection of the enhanced thermal emission that occurs when magnetars activate. Quick repointing with the IRT is a unique feature useful to identify and study the counterparts, taking advantage of the small absorption in the NIR. As shown in Figure 2-24, broad energy band coverage, rarely available up to now, is crucial to clarify the spectral shape of bursts and flares (e.g. if the emission is thermal or non-thermal). Magnetar giant flares could account for a fraction of short GRBs, since the extremely bright (up to ~10^{46} erg), short (<0.2 s), and spectrally hard initial spikes of these events appear similar to short GRBs. Proposed candidates in M31, in the M81 group and in the Sculptor Galaxy have been identified ([171], [172], [173], [174]). Similar events are easily detectable by the XGIS and, for the closest ones, the SXI can also detect the typical pulsating tails. The detection of these events, at the bright end of the luminosity distribution of magnetar bursts, has relevant implications for the origin and physical processes responsible for giant flares. The discovery of a bright X-ray/radio burst from the magnetar SGR1935+2154 on 18 April 2020 [169], has provided strong observational support to the connection between magnetars and FRBs, predicted by several models. The new generations of radio telescopes will detect hundreds of FRBs each day, many of which will fall in the SXI/XGIS field of view.

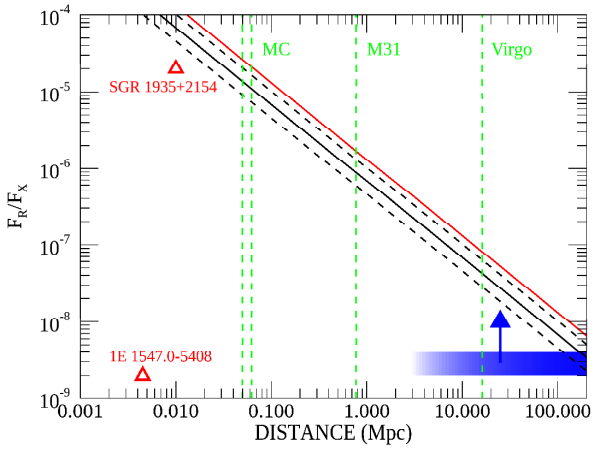

Figure 2-25 Maximum distance at which SXI (black) and XGIS (red) can detect an FRB-like burst similar to that of April 28, 2020 from SGR 1935+2154 as a function of the ratio between radio and X-ray fluences. The dashed lines give the range due to uncertainties in the spectrum and absorption. The triangles indicate the values of F_R/F_X observed Galactic magnetars, while the blue lower limits correspond to typical values inferred from the known FRB not seen in X-rays. The vertical green lines indicate the distances of the Magellanic Clouds, the Andromeda galaxy and the Virgo cluster.

Combining THESEUS with the wide-field sensitive radio monitoring will allow us to investigate this connection. With its frequent and sensitive coverage, THESEUS will provide robust constraints on the activity duty cycle of Galactic magnetars and possibly discover periodicities, which is particularly relevant for the sub-class of repeating FRBs. Although it is possible that, by the '30s, the mystery of FRBs will be solved and their multiwavelength study may be mature, only the availability of large samples allows sound applications to cosmology and fundamental physics problems, as it has been demonstrated with GRBs. The sensitivity of THESEUS for extragalactic magnetars is thus highly important. Figure 2-25 shows the predictions for the detectability of soft X-ray emission of FRBs by THESEUS.

2.5.3 Tidal disruption events

THESEUS will extensively sample the soft X-ray light curves with high cadence for more than 50 Tidal Disruption Events (TDEs) per year. The simultaneous infrared and hard X-ray data will provide crucial information on the geometry and jet orientation.

A TDE occurs when a star approaches so close to a black hole that the tidal forces across the star overcome its self-gravity (for a recent review see [175]). The star is destroyed and forms a stream of material whose subsequent evolution and fall back to the black hole gives a radiation signature in the X-ray, UV, optical, IR and sometimes radio bands. First discovered in the ROSAT survey [176], dozens of TDEs have been identified to date, with X-ray spectra typically modelled with a black-body of kT=40-100 eV. Observing TDEs is possibly the only way to directly reveal and study nuclear SMBHs in non-active galaxies allowing the BH mass to be estimated from the shape of the light curve [177] and X-ray emission temperature [178] and allowing the spin to be constrained [179]. Mass accretion rates are thought to vary from super-Eddington to sub-Eddington rates on timescales of weeks and months to years. In rare cases, highly luminous TDEs (log(Lx/(erg/s)) =46-48) with emission at hard X-rays (detectable with XGIS) and in the radio have been seen, interpreted as a relativistic jet ([180], [181]). In the coming decade the TDE sample is expected to increase significantly, as demonstrated, for example, by eROSITA [182], and future facilities such as Einstein Probe [183] in X-rays and the VRO [184] in the optical band.

The SXI instrument is well suited for the discovery and monitoring of TDEs with an expected detection rate of ~50-80 per year. XGIS may detect several jetted TDEs during the mission. X-ray and optical detection of TDEs are highly complementary as the X-ray bright sources strongly select fast spinning BHs (prograde) while the optically bright/selected TDEs are nearly agnostic about BH spin [179]. THESEUS, in synergy with optical surveys, will improve our diagnostic of the origin of the very different X-ray light curves seen in optically selected TDEs compared to those from X-ray selected events. Using the IRT to detect TDE counterparts will help to understand if differences in viewing angle explain the different appearance of TDEs across the electromagnetic spectrum, or if other factors are at work. IR flare detection with IRT will allow source identification, while IR dust echoes can provide information about the geometry, origin and composition of the material (stellar debris vs pre-existing circumnuclear). Real-time discovery of TDEs will be important to ensure multi-wavelength follow-up, including with ATHENA, and for long-term monitoring. THESEUS will also

provide X-ray spectral information (also providing a handle on SMBH mass) and distance to the host Galaxy through follow-up with IRT (if required), which will allow deeper study of individual TDEs of interest. Follow-up observations, especially at radio, should be able to discriminate relativistic TDEs from blazar flares. Discovery and follow-up of jetted TDEs, especially at radio wavelengths, will allow the investigation of processes through which relativistic jets are born.

2.5.4 Black holes on all mass scales

THESEUS offers the promise of studying accretion and ejection processes over an extremely large range of black hole masses, ranging from several solar masses (in X-ray binaries) up to ten billion solar masses (in AGNs).

Variability studies, an important diagnostic for the processes occurring near BHs, will be optimally done by THESEUS during the bright outbursts of galactic X-ray binaries, but many extragalactic sources will also be detected by the SXI (one or two in each typical ~2.3 ks pointing, increasing rapidly with longer integration), so providing important information at high cadence on a large sample of AGNs.

Accretion in AGN likely occurs sporadically [185], but observational constraints on duty cycles are lacking. We do not even properly understand how the accretion flow structure and radiative efficiency evolve with global accretion rate, undermining our knowledge of how SMBHs get fed. "Changing-look AGN" (CLAGN) have recently provided the first insight: optical monitoring of large samples of Seyferts and quasars has yielded a handful of cases wherein we observe radical changes in the coronal X-ray flux, optical/UV continuum accretion disc flux, and/or optical Broad Line Region emission over months to years. THESEUS can monitor many thousands of AGNs at low redshift ($z \leq 0.3$), and catch new CLAGN events in the act, allowing us to probe the response of AGN structural components to drastic changes in accretion rate.

THESEUS can also monitor for, and identify, sudden changes in coronal X-ray luminosity associated with disruptions of the inner disc and corona, as thought to have occurred in the CLAGN 1ES 1927+654 [186]. Such events can reveal the interaction between accretion disc and corona and allow us to determine timescales for destruction or formation of the corona. Quasi-Periodic Eruptions (QPE) have been recently discovered in a couple of AGNs, including the Narrow-Line Seyfert 2 in GSN 069 which showed two orders of magnitude X-ray eruptions lasting one hour with recurrence time of 9 hr [187]. Proposed explanations for the QPEs include the radiation-pressure disc instability affected by the presence of outflows ([188], [189]), Lense-Thirring precession of the inner torus, and TDE-driven outbursts. THESEUS discovery of similar events in more AGNs will be key to identifying the primary physical processes.

2.5.5 X-ray binaries

X-ray binaries containing compact objects provide a wealth of phenomena for which the extensive monitoring, triggers, and follow-up with THESEUS will be fundamental.

The outburst cycle of dwarf novae and low mass X-ray binaries provides insight into the physics of accretion discs and their boundary layers. The widely accepted disc instability model faces a significant challenge in explaining the quiescent behaviour of these binaries: the expected increase in accretion rate throughout quiescence has never been observed [190]. While low states are well covered in the optical, the few available X-ray observations have so far failed to reveal a consistent pattern [191]. Only a handful of sources have been observed with sufficient cadence and duration in X-rays to allow a systematic study of dwarf novae outbursts, quiescent variability, and high and low states.

Supergiant Fast X-ray Transients (SFXTs, [192]) are high-mass X-ray binaries which exhibit extreme variability on short timescales (up to 10,000x within minutes). The origin of this variability is still largely unclear because the limited sensitivity of current all-sky X-ray monitors is insufficient to detect short, low intensity flares, while the low duty cycle of SFXTs makes dedicated observations essentially unfeasible. The SXI will open a new horizon here, expanding the SFXT sample, and allowing detailed study of the statistics of

the known population, such as their duty cycles, duration and intensity distribution of the flares, and their dependence on orbital phase.

Other interesting targets for THESEUS variability studies are the thermonuclear super-bursts in low mass X-ray binaries [193], the transitional millisecond pulsars [194], and the Ultra-Luminous X-ray sources [195]. THESEUS will have the sensitivity to detect also the Very faint X-ray transients, a class of galactic sources reaching low peak luminosities ($<10^{36}$ erg/s) and of still unknown nature [196].

2.5.6 Stellar flares

THESEUS will yield a large homogeneous sample of flares from active stars and, thanks to the combination of its three instruments complemented by simultaneous multi-wavelength data obtained following its triggers, it will provide breakthrough capabilities for the understanding of the most energetic "super-flares".

Stellar flares will undoubtedly constitute the most numerous class of transient events discovered by the SXI. A catalog containing the sky coordinates of known and candidate flaring stars will be used by the on-board software to avoid too many undesired automatic satellite slews. However, the SXI and XGIS will continue to operate normally, thus acquiring useful data on the observed flares. These will constitute an unprecedentedly large database for the statistical characterization of flares from all the classes of active stars. Most studies of this kind carried out up to now at X-ray energies were based on relatively small samples and/or concentrated on specific observations of stellar clusters and star forming regions. THESEUS will instead permit a thorough statistical characterization of the X-ray flare properties, and, in particular, of their rate of occurrence as a function of stellar type and age, based on a large and unbiased sample. Note that the level of X-ray flaring activity has important implications for the habitability zone of exoplanets.

While the most energetic solar flares have total radiated energies exceeding 10^{32} erg and maximum coronal temperatures of a few tens of MK [197], large stellar flares can be 10^6 times more energetic than this [198] and reach temperatures around 100 MK ([199], [200]). X-ray flares with energy up to $2x10^{35}$ erg have been found in very young low mass stars [201] and up to 10^{38} erg in active binary systems [202]. These "super-flares", with X-ray luminosity increases of more than two orders of magnitude above the quiescent coronal emission level, occur less frequently but are of particular interest. Super-flares can be efficiently discovered by THESEUS and, being recognized as such by the on-board triggering software, can be rapidly placed in the IRT field of view. The long duration of super-flares discovered by THESEUS will also allow their follow-up by ground-based observatories.

The correlation of light curves at different wavelengths is an important diagnostic of the particle acceleration and emission processes taking places in the flares. The Neupert effect, an empirical correlation between the soft X-ray flux and the time-integrated flux in radio and optical bands, was first discovered in solar flares [203] and later seen also in flares from UV Ceti and Proxima Centauri [204]. Chromospheric evaporation is thought to be responsible for this correlation: the high-energy electrons, accelerated where magnetic reconnection occurs, travel along the field lines, where the large pitch-angle population generates prompt gyro-synchrotron emission and the small pitch-angle one impacts onto the chromosphere producing prompt radio/V(IR) band emission. The hot thermal plasma (seen in soft X-rays) evolves as a consequence of the accumulated energy deposition, hence the integral relation. Recently this relationship has been observed for the Swift BAT hard X-ray emission as well, in powerful flares from DG CVn ([205], [206], [207]). However, the detection of hard X-ray emission following the integral of the impulsive optical emission is unexpected in the chromospheric evaporation model. It indicates, contrary to what was understood, that either the plasma heats up to E >15 keV or the particles emit radiation following a non-thermal kinetic distribution. Further observations of optical/soft X- and hard X-ray delays, as can be provided by THESEUS, are crucial for the correct diagnosis of the nature of these exceptional events.

2.6 THESEUS as an Observatory

THESEUS is going to provide a very special opportunity for agile NIR and X-ray observations of a wide range of targets, from asteroids to the most distant AGNs. Space-borne, sensitive NIR spectroscopy is an extremely useful capability, and wide-field sensitive X-ray monitoring can identify changes and priorities for follow-up studies.

While in Survey Mode, the IRT, SXI and XGIS will be gathering data, with IRT pointed at a specific target. Hundreds of thousands of suitable targets are already known, and eROSITA*, Euclid,* VRO and SKA will deepen and extend the range of relevant catalogues. Many targets for THESEUS as an observatory have a time-domain aspect, and so have already been discussed in §2.5.

A space-based infrared, and X-ray spectroscopic facility will be attractive to a wide range of investigators and address important questions in a plethora of scientific areas. While less powerful than *JWST* and ATHENA, the chance to use THESEUS to observe substantial samples of interesting sources, both known and newly-discovered, to appropriate depths and cadences, while the mission is searching for GRBs, provides opportunities for additional science. A user community interested in scales all the way from the Solar System to distant AGN can provide abundant desired targets for THESEUS as an observatory.

THESEUS will maintain a list of core-programme targets, augmented with targets from a competed GO programme, with all observations planned and executed by the THESEUS mission operations team, while THESEUS operates in Survey Mode. The sensitivity of SXI and IRT are well matched and deliver images and spectra to useful depths in a fractional orbit spent staring at a specific target field. Existing catalogues of tens of thousands of targets will grow from the forthcoming very large wide-field VRO optical and eROSITA X-ray catalogues prior to launch. The numbers of known exoplanets continue to grow, and new generation of radio facilities are providing rich catalogues as precursors to the imaging of the SKA.

2.6.1 Key observatory science

We now consider the range and numbers of suitable targets for THESEUS as an observatory during the nominal mission, working out in cosmic distance. The co-alignment of the IRT with the part of the SXI FoV where the two units overlap ensures that the best X-ray spectra/limits will be obtained alongside every IR imaging/spectral target.

A space-borne IR spectrograph is able to investigate a range of cometary emission and absorption features, without being restricted to specific atmospheric bands, and with full access to all water and ice features, impossible from the ground. Several tens of comets per year are likely to be observable as they pass through the inner solar system, evolving through their approach to and recession from perihelion.

IR spectra of large samples of stars with transiting planets can be obtained by THESEUS. By 2030, tens of thousands of transiting planets will be known, spread widely over the sky, and with well-determined transit times, which can be scheduled well in advance to search for potential atmospheric signatures in IR absorption spectroscopy. IRT is more sensitive than the Atmospheric Remote-sensing Infrared Exoplanet Large-survey mission (ARIEL), and so carefully chosen extended planetary transit observations can be made for known targets, and for a substantial number of transiting planetary targets can be included in the observatory science target catalogue.

X-ray binaries and flaring stars can be discovered as bright X-ray and IR spectral targets by THESEUS, or highlighted by other observatories, and then confirmed and studied using THESEUS's spectroscopic capabilities. Found predominantly in the Galactic Plane, many hundreds of bright events will occur during the nominal mission.

A prompt spectroscopic IR survey for supernovae that are found taking place out to several 10s of Mpc, unencumbered by atmospheric effects, is likely to remain attractive beyond 2030, and will help to resolve

remaining questions about the impact of environment and metallicity on the nature of supernovae and their reliability as standard candles. Without sensitive IR spectroscopy, these questions might not be resolved.

The availability of the full spectral window is particularly helpful for observations of emission-line galaxies and AGN, for which key diagnostic lines are redshifted out of the optical band from the ground at redshifts z~0.7. Even ELTs cannot beat the atmosphere, and huge candidate samples will be catalogued over large fractions of the sky, colour-selected from VRO surveys, in concert with the coverage of eROSITA, SKA and WISE. IRT will enable Hα spectral surveys of interesting classes of the most luminous galaxies, and AGN all the way to z~2-3. Furthermore, the THESEUS mission will provide a useful time baseline out to several years, to see potential changes in the appearance of AGN spectra, and to confirm any changes by revisiting selected examples.

While it will be impossible to include more than a few thousand galaxies and AGN in a spectral monitoring programme, the results of combining the wide-area data from VRO and WISE in the optical and IR, and with eROSITA in the X-ray, with the serendipitous wide-area coverage of SXI and XGIS, will allow new insight into the X-ray variability of large samples of AGN.

There will be demand for tens of thousands of IRT spectral targets, from comets to distant AGNs. A practical number of targets, given that several spectra can be obtained per orbit, and thus up to of order 1000 targets each month, and tens of thousands of observations in parallel to Survey Mode during the nominal mission.

2.6.2 Mission operations for observatory science

THESEUS can observe tens of thousands of Galactic and extragalactic targets, as its survey operations model covers a large fraction of the sky (see §6.4). Changing survey-mode pointing two or three times per orbit, and with pointing ranging over a wide area of sky ensures that initial degree-scale offsets from nominal survey mode pointing will make observatory science possible, since the large number of sources of interest over the sky from eROSITA*, Euclid*, VRO and SKA, ensure that suitable targets can always be found. As the primary science goal of detecting high-redshift GRBs is met, the operations model foresees a wider range of pointing angles with respect to the nominal survey strategy being possible, and thus to even more flexibility in observatory science operations. While specific targets cannot always be observed, samples are sufficiently large that suitable and representative candidates will be available.

It is likely that a number of novel science opportunities will arise during the mission lifetime, and that associated targets of opportunity can be handled and scheduled using existing plans for interruptions to the Survey Mode. The possibility of IR and X-ray spectroscopy of any nearby supernovae, unusually proximate/bright novae and dramatic flaring and accretion events of binary systems and blazars can be included to boost THESEUS's scientific return, by taking advantage of its core mission capabilities.

2.6.3 Serendipitous detections

THESEUS will operate with a very substantial field-of-view in a Survey Mode when wide-field optical surveys with VRO are mature, the eROSITA reference map of the X-ray sky is available, and the SKA will be generating very deep radio images in the South. Many hundreds of thousands of interesting serendipitous sources that will be detected using THESEUS's SXI and XGIS instruments automatically during the mission, providing regular monitoring of a wide range of non-GRB transient sources, for comparison against known high-energy sources. These classes of targets include not only the transients and variables discussed in §2.5, but also interesting new targets from wide-field X-ray sky coverage, building on the eROSITA map of the sky. Furthermore, THESEUS's sensitive IR/X-ray monitoring capability will provide a very useful tool for selecting targets for ATHENA and possible future large optical-NIR facilities.

2.7 Synergies with the large facilities of the '30s

The combination and coordination of THESEUS with multi-wavelength, multi-messenger facilities expected to be operating in the thirties will open new avenues of exploration in many areas of astrophysics, cosmology and fundamental physics, thus adding considerable strength to the overall scientific impact of THESEUS.

We briefly discuss specific synergies, not addressed in previous sections, between THESEUS and such major facilities.

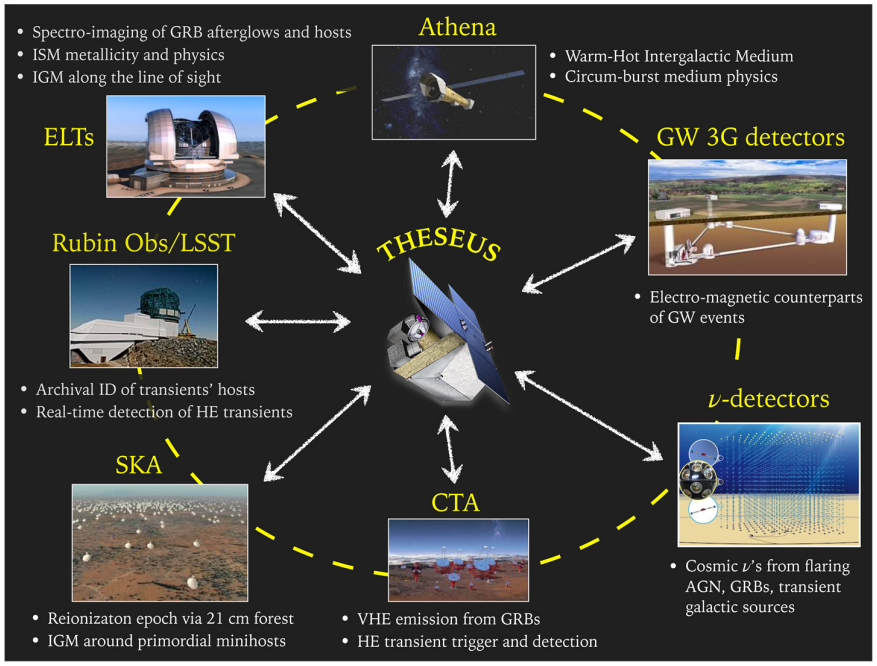

Figure 2-26 THESEUS will work in synergy on a number of themes (bullets) with major multi-messenger facilities in the 30ties and will provide targets and triggers for follow-up observations with several of these facilities.

2.7.1 ATHENA

ATHENA has a number of primary science requirements which exploit high-energy transients to probe physical questions. These include: probing stars in the early Universe; using GRBs as backlights to probe the WHIM; and probing galactic and extra-galactic variable sources, such as TDEs, AGN and stellar binary systems. For events with a sufficiently small error box, ATHENA can also contribute significantly to the area of multi-messenger astrophysics. To maximise the role of ATHENA, it is therefore essential that it promptly receives information on the location, brightness, redshift and object class for a newly discovered transient. ATHENA must in some cases be provided with targets very quickly (within a few hours) while others can be provided on timescales of days – weeks. THESEUS is ideally posed to deliver this information to ATHENA.

Extragalactic transients are sufficiently rare that intrinsically large field of view instruments are needed to identify sufficiently sizeable samples of bright objects. The Swift-BAT and the Fermi-GBM lack on-board redshift determination capability, and critically, they are unlikely to be operational in the ATHENA era as they were launched in 2004 and 2008, respectively. The upcoming transient discovery missions SVOM and Einstein Probe could still be operational (although beyond their design lifetimes), but they lack multi-wavelength redshift determination capability on-board. Only the multi-wavelength THESEUS, due for launch very close in time to ATHENA, can find transients, determine redshifts on-board, conduct a soft X-ray survey and find multi-messenger counterparts in the X-ray and IR, while rapidly communicating discoveries to other facilities.

Although independent missions, the combination of ATHENA and THESEUS in the early 2030s would greatly enhance the science return of both. Two prominent ATHENA science objectives ideally match the capabilities of THESEUS, by requiring very rapid (target sent to ATHENA within a few hours) identification of bright GRBs with redshift determination:

1. Probe the first generation of stars (Cosmic Dawn), the formation of the first black holes, the dissemination of the first metals and the primordial IMF. This is to be achieved by determining the elemental abundances of the medium around high-redshift GRBs. The ATHENA requirement is to observe 25, z>7 GRBs (Figure 2-27).
2. Measure the local cosmological baryon density in the WHIM to better than 10% and constrain structure formation models in the local density regime by measuring the redshift distribution and physical parameters of WHIM filaments. The ATHENA requirement is to observe 100 filaments towards bright GRBs up to z=1.

To enable a statistically reliable study of the period of cosmic dawn with ATHENA requires raising the current high-redshift GRB detection rate by more than an order of magnitude, a requirement well met by THESEUS but well beyond the capability of any other current or approved future mission. ATHENA and THESEUS also have similar fields of regard so prompt follow-up is achievable.

If followed-up within half a day, a 50 ksec exposure using the ATHENA/X-IFU will typically contain hundreds of thousands of photons from the brightest high-redshift GRBs. The rate of GRB discovery from THESEUS would readily provide the required rate of very bright low-redshift GRBs for the ATHENA WHIM science requirements. For the very brightest GRBs, if followed up within half a day, a 50ksec ATHENA/X-IFU spectrum would contain over a million photons.

ATHENA has multiple science requirements that assume the availability of astrophysical high-energy transients which it can follow-up on timescales of days to weeks depending on the object class. Examples include: (a) studying the nature of stellar disruption and subsequent accretion onto super-massive black holes during TDEs, (b) observing stellar stellar-mass and super-massive black holes in both quiescence and outburst to probe the accretion process and (c) studying the counterparts to multi-messenger (GW and neutrino) events.

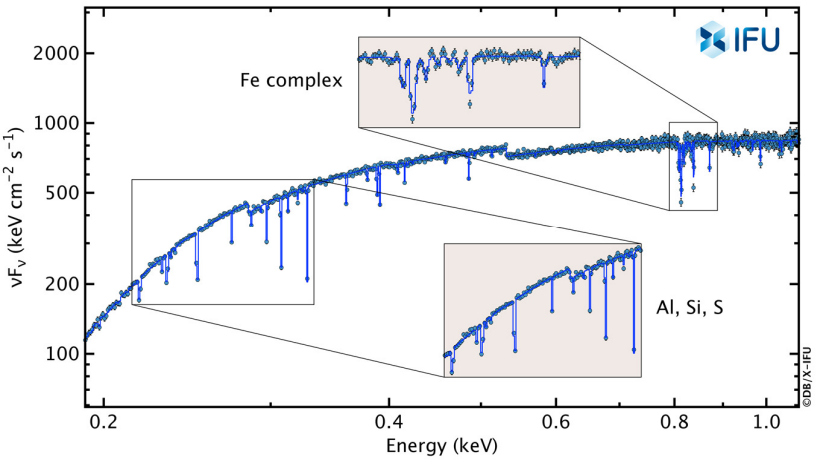

Figure 2-27 A simulated ATHENA/X-IFU spectrum of a medium bright (fluence: $4x10^{-7}$ erg cm^{-2}) z=7 GRB afterglow characterized by deep resonant lines from the ISM of the GRB host galaxy. An effective intrinsic column density of $2x10^{22}$ cm^{-2} was assumed [credit: ATHENA/X-IFU Consortium].

To this end, it is critical to monitor large areas of sky in real-time to know the current accretion state of either known or new examples of such systems. These ATHENA science requirements are highly synergistic with those of THESEUS, which has a primary science objective to perform an unprecedented real-time, high-cadence deep monitoring of the X-ray transient Universe in order to identify a wide variety of extragalactic and galactic transients and to identify the counterparts to multi-messenger sources. The two monitors on THESEUS will simultaneously observe the sky over an energy range exceeding a factor of five orders of magnitude and will be particularly sensitive to the softest energies down to 0.3 keV, providing a perfect complement to the ATHENA observing bandpass. The THESEUS/IRT can also provide complementary data for source monitoring and classification. THESEUS will detect tens of TDEs per year, many magnetars/SGRs, SN shock breakouts, SFXTs, thermonuclear bursts from accreting neutron stars, Novae, dwarf novae, stellar flares, AGNs and blazars. The data will be available within days from the THESEUS data processing system.

THESEUS will fly in the era when the next generation of gravitational-wave and neutrino detectors will provide routine detections. Counterparts of such events found by THESEUS will have location accuracies far superior to those of the multi-messenger observatories and will be observable by ATHENA in a single pointing.

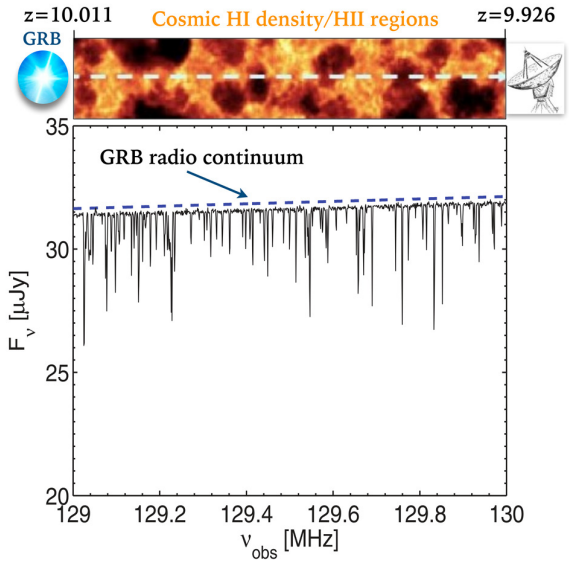

Figure 2-28 Representation of the 21 cm absorption lines (known as the "21 cm forest") produced by non-linear structures during the early stage of reionization.

2.7.2 SKA and other Radio Facilities

The SKA, expected to be fully operating in the 30ties, will enable an ideal technique to study the evolution of cosmic reionization via the measurement of the 21 cm radiation from neutral hydrogen atoms (due to the hyperfine structure of the triplet and the singlet levels of the hydrogen ground state). The 21 cm sky contains fluctuations around the mean ("global") signal, which encode information on the physical state of hydrogen, largely representative of all baryons, in the Dark Ages and in the Epoch of Reionization (EoR, [208]).

Canonical tools to study reionization include the polarization of the Cosmic Microwave Background, and most relevant here, absorption line spectra of bright sources, typically quasars, located in the reionization epoch. However, the paucity of these objects at early epochs, particularly in the first billion years of cosmic history, has prevented a comprehensive study of the EoR. The large sample of high-z long GRBs from THESEUS will open a complementary way to explore the reionization process avoiding the proximity effects. This has been made possible for the first time after the detection of GRBs at z >5 [209], and specifically demonstrated by the studies by [210], and [211], who have used this source to constrain the ionization state of IGM at high redshift by modelling its optical afterglow spectrum.

An even more exciting prospect is provided by 21 cm radio observations of GRB afterglows, particularly with SKA. This idea was first explored by [212] who investigated the 21 cm absorption lines (known as the "21 cm forest") produced by non-linear structures during the early stage of reionization, i.e. the starless minihaloes and the dwarf galaxies (see Figure 2-28). The infalling gas velocity around minihaloes/dwarf galaxies strongly affects the line shape and, with the low spin temperatures outside the virial radii of the systems, gives rise to horn-like line profiles. The authors compute synthetic spectra of 21 cm forest for the radio afterglows of GRBs. Broadband observation against GRB afterglows can also be used to reveal the evolving 21 cm signal from both minihaloes and dwarf galaxies. The number, strength and clustering of 21 cm absorption lines depend very sensitively on the intensity of the X-ray background produced by e.g. high-mass X-ray binaries or early black holes (as further illustrated in Figure 2-28). This experiment will then offer a unique opportunity to explore cosmic dawn and the rise of the first structures, including black holes. The synergy between THESEUS and SKA will be fundamental to achieve these ambitious goals.

2.7.3 Vera C. Rubin Observatory LSST/VRO

The VRO project will carry out the LSST, a 10-yearlong survey which will create a multi-colour, dynamic view of the Universe [213]. With its large field of view of 9.6 deg^2, it will cover around 10000 deg^2 each night, in six optical bands (u, g, r, i, z and y), thus mapping the entire visible Southern sky in just a few nights. With its 8.4 m diameter primary mirror, it will reach very faint magnitudes (up to 24.4 in r band) in a single exposure. Its surveys will produce a catalogue of 37 billion objects: 20 billion galaxies, 17 billion stars and orbits for 6

million bodies in the Solar System. It is very likely that Rubin observations, with emphasis on variable and transient sources, will continue after the first 10 years of operations.

Science operations of the VRO are planned to start in 2024 and continue through the next decade. Its four main science drivers are: (1) understanding dark matter and dark energy, (2) hazardous asteroids and the remote Solar System (3) formation and structure of the Milky Way, and (4) variable and transient sources. In particular, it will be a revolutionary and powerful transient machine: a stream of 1-10 million time-domain events per night are expected to be detected with real-time data analysis. They will be transmitted within 60 seconds of observation. A number of observing strategies are under study, with different combinations of cadence and sky coverage, to provide adequate discovery space for a variety of classes of transients.

THESEUS has survey capabilities for high-energy transient phenomena complementary to VRO in the optical. Their joint availability in the next decade will enable a remarkable scientific synergy between them. Specifically:

a) The catalogue of 20 billion galaxies provided by the VRO (combined magnitudes $r < 27.5$ and time resolved measurements to $r < 24.5$) – characterized in shape, colour, and variability – will be an invaluable resource for identification studies of THESEUS transients, including location and properties of the host galaxies of GRBs, GW events, TDEs etc. and their galactic environments.
b) Real-time observations of various classes of high energy transients will be possible. Although triggering and follow-up observations with the Rubin Obs-LSST/VRO are not envisaged, a wealth of unique data will be available in the LSST images taken (serendipitously) just prior, during or soon after transient events detected by THESEUS (GRBs, GW events, TDEs, magnetars/SGRs, SN shock break-outs, SFXTs, thermonuclear bursts from accreting neutron stars, Novae, dwarf novae, stellar flares, AGNs and Blazars). LSST will conservatively generate thousands of transient alerts of interest to HE scientists every night and will support public distribution of these alerts. The success rate of such simultaneous observations will depend on the adopted cadence strategy.

2.7.4 Cherenkov Telescope Array

The Cherenkov Telescope Array [214] is a global, next-generation observatory studying very-high-energy (VHE) gamma rays in the energy range from tens of GeV to hundreds of TeV. The observatory will consist of a range of Imaging Air Cherenkov Telescopes (IACTs) in two sites (Paranal, Chile and Canary Islands, Spain), and will have unprecedented sensitivity as well as unique angular and energy resolutions over a large energy range. CTA is building on the success of the current generation of IACTs, namely H.E.S.S., MAGIC, VERITAS and FACT. Its construction is expected to be completed around 2025. After a number of Key Science Projects defined by the CTA Consortium are completed, the fraction of the time allocated to guest observer programs will increase rapidly. It is thus expected that CTA will be a fully open observatory at the timescale of the THESEUS mission.

We expect strong synergies between the CTA science programs and THESEUS. One of the main science drivers for both observatories is the study of transient phenomena and especially GRBs. This field has recently seen tremendous breakthroughs with the detection of VHE emission from the GRBs detected by H.E.S.S. (GRB 180720B, [215], and GRB 190829A) and MAGIC (GRB 190114C, [216]). As an example, the detection of the nearby and very low luminosity burst GRB 190829A may indicate that the phase space of low luminosity events detectable in large numbers with THESEUS will enable many further joint CTA-THESEUS observations and studies. Access to this new phase space, combined with the high sensitivity of CTA and its fast reaction to multi-wavelength alerts within 30 s over the full sky, will enable detailed joint studies of GRB light-curves across many orders of magnitude in energy and covering long time ranges. These studies will naturally be extended into the multi-messenger domain through searches for VHE counterparts of GW events. The rapid and precise localisation of GW electromagnetic counterparts by THESEUS will enable to significantly increase the efficiency and performance of CTA observations of these high-priority targets.

3 Scientific requirements

3.1 High-level scientific goals of the mission

3.1.1 Exploring the early Universe with GRBs

"THESEUS shall achieve a complete census and characterization of GRBs in the first billion years of the Universe"

THESEUS aims at exploring the Early Universe (down to the cosmic dawn and reionization eras) by unveiling a complete census of the Gamma Ray Burst (GRB) population in the first billion years. In this context, a "complete census" is a sample that is representative of the parent population on a given redshift range within a certain confidence level. As a quantitative metric of the ultimate achievement of this scientific requirement, THESEUS shall be able to detect, to locate at the arc-second level with the IRT, and enable the determination of the host galaxy redshift for at least 40 long GRBs at $z \geq 6$ (corresponding to approximately the first billion years of the Universe in the standard ΛCDM cosmology) over the in-orbit nominal mission lifetime. The main drivers for this requirement are (cf. §2.2):

- Through these, the slope of the Star Formation Rate (SFR) can be constrained with an accuracy better than 1 magnitude on the cut-off magnitude of the galaxy luminosity function (cf. §2.2), a result that is completely out-of-reach even for JWST
- At least 30 GRBs with simultaneous determination of the galaxy SFR and of the escape fraction will allow to rule out at the 95% confidence level the hypothesis of reionization sustained by stars if low values of the escape fraction f_{esc} are consistently measured in the host galaxy of fully characterized GRBs detected by THESEUS

It shall be borne in mind that THESEUS will open a full new window in the exploration of GRBs with respect to what can be achieved by currently operational observatories such as *Swift* (in X-rays) or Fermi (in γ-rays), in particular at high redshift. This is discussed in details in §2.2 and shown in Figure 3-1, where the distribution of luminosity of the GRBs prospectively discovered by THESEUS as a function of redshift is compared to the sample currently available from *Swift* and *Ferm*i observations. THESEUS will be able to increase by at least one of magnitude the number of known GRB at z>6, as well as probing luminosities by over two orders of magnitude deeper than currently possible, reaching the average luminosity of the (estimated) underlying population at all redshifts.

3.1.2 Multi-messenger astrophysics

"THESEUS shall identify (i.e. detect and localize) and study the electromagnetic counterparts of GW and cosmic neutrino astrophysical sources through an unprecedented exploration of the time-domain Universe in near IR, X-rays and soft γ-rays."

As a quantitative metric of the achievement of this objective, THESEUS shall be able to detect at least 30 short GRBs over the in-orbit nominal mission time, in order to build a statistically interesting sample of Gravitational Wave (GW) and short GRB sources. A sample size of 30 events is enough to effectively test theoretical predictions on the nature of these objects and answer several questions such as: which is the fraction of Binary Neutron Stars (BNSs)/Neutron Star-Black Holes (NSBHs) capable to produce a relativistic jet? How are jets structured? Which are the properties of the electromagnetic emission from a possible massive NS remnant from BNSs and which is its formation efficiency?

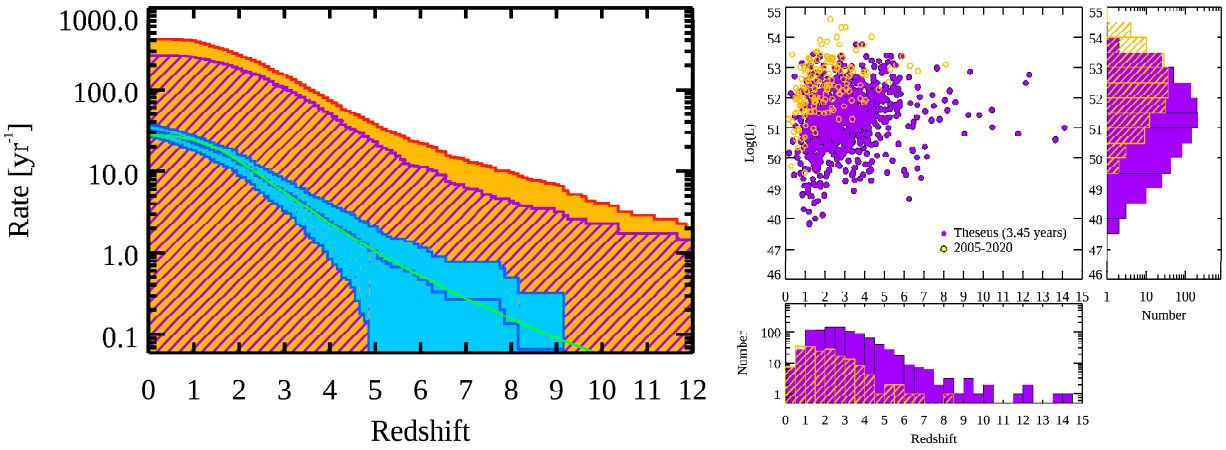

Figure 3-1 – Left Panel: expected detection rate of long GRBs by THESEUS (orange histogram) compared with those with measured redshift between 2005 and 2020. (blue area). The purple hatched histogram represents the GRBs for which a determination of the redshift by either THESEUS or ground-based facilities is expected. The green curve represents a model fitting the observed distribution on whose basis the THESEUS predictions are made (cf. §3.3.1). THESEUS will detect between one and two orders of magnitude more GRBs at any redshift, and most notably in the high-redshift regime (z>6). Right Panel: Distribution of long GRBs with redshift determination in the peak isotropic luminosity versus redshift plane now (yellow points and hatched histogram) and after the nominal operation life of THESEUS (purple points and full histogram).

Arcsecond precision localization can be achieved from follow-up observational campaigns on the ground within the XGIS localization area. Sky coordinates at the arcsecond precision are mandatory to activate deep monitoring of the electromagnetic counterpart using large facilities as VLT, ELT, etc. JWST will fully characterize for example the expected kilonova emission (too faint to be detected with IRT for most cases, i.e. at $z \geq 0.05$) through high-quality spectra and deep imaging, shedding light on the role of these sources to the cosmic chemical enrichment of r-process elements. A sample of about 30 will enable the accurate (≤1%) independent measure of the Hubble constant (H_0) by combining the luminosity distance obtained from the GW signal of BNS and the redshift from the electromagnetic counterpart, assuming the combination of ET+CE and THESEUS (cf. §2.3).

3.1.3 Transient and variable high-energy Universe

Additionally, THESEUS shall detect and characterize at least 300 transient and/or variable high-energy sources over the in-orbit mission lifetime, either on-board or in the off-line data processing, covering the whole range of astrophysical classes mentioned above. The current estimate of the rate of transients detected by the SXI largely exceed the science requirement, even not considering the most common classes of transient events (novae, stellar flares) that one could efficiently filter on-board to ensure that THESEUS has sufficient flexibility to follow-up less common classes such as GW counterparts, SN shock break-outs, TDEs, and magnetars.

3.2 Science performance requirements

The key science performance requirements of THESEUS described in this section are summarized in *Table 3-1*. These science goals are enabled by the synergetic working of the whole scientific payload. The high-level requirements described in §3.1.1 and 3.1.2 involve several complementary aspects that must be considered globally to make the best trade-off within the resources of a Medium-class mission. The conceptual relation between the highest-level (Level 0) scientific requirements and the Level 1 metric describing their achievement is shown in Figure 3-2.

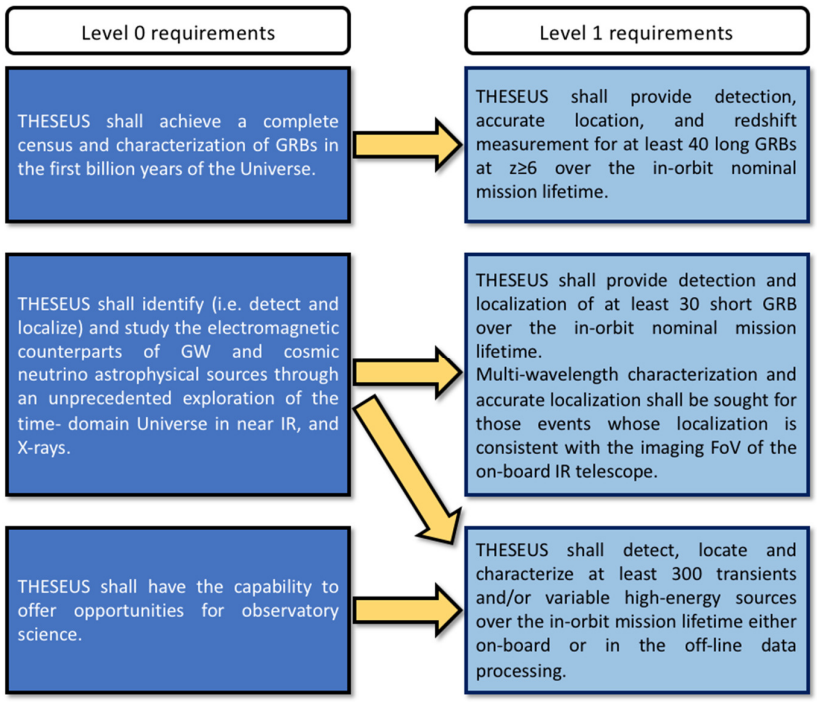

Figure 3-2 - Relation between Level 0 and Level 1 THESEUS scientific requirements.

The Phase A has successfully completed these trade-offs and identified a baseline mission profile that satisfies the scientific goals of the mission. The main performance requirements enabling the transformational THESEUS science and briefly justified in this section.

3.2.1 High-energy monitors sensitivity and grasp

Two high-energy monitoring instruments, with wide FoV and high sensitivity, are at the core of the THESEUS survey capabilities.

In Figure 3-3 we show the grasp (product of the effective area and the field-of-view) of the THESEUS SXI compared to that of the X-ray survey mission eROSITA (launched in 2019), and the large effective area ESA X-ray observatory XMM-Newton. The SXI grasp exceeds that of any existing or planned focusing X-ray telescope by over one order of magnitude. Above 4 keV, the nominal grasp of the Scanning Sky Monitor on board the Indian X-ray observatory ASTROSAT, and the Gas Slit Camera on board the JAXA X-ray experiment MAXI exceed that of the THESEUS SXI. However, these are collimated instruments without imaging capabilities. This implies that their sensitivity in the overlapping energy band is lower than that of the SXI by a factor of about 30.

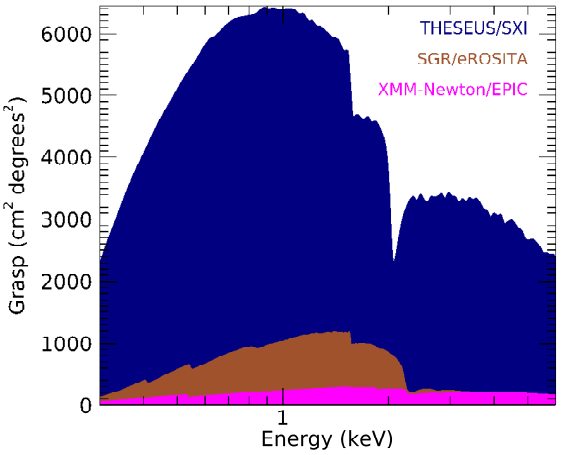

Figure 3-3 - SXI grasp (blue area) as a function of energy compared to that of the X-ray survey mission SRG/eROSITA (brown), and XMM-Newton/EPIC (European Photo-Imaging Camera; magenta). Credit for the XMM-Newton and eROSITA data: A. Merloni (MPE).

The Chinese observatory Einstein Probe (EP; launch date, end 2022; nominal operational life 4 years) will carry similar telescopes to THESEUS, with an even larger grasp. However, this does not invalidate the novelty of the THESEUS concept, which has a unique combination on a rapidly slewing platform of sensitive high-energy monitors covering a broad energy range, and a diffraction-limited IR telescope. Furthermore, the unpredictable variability of several classes of astrophysical sources leaves the discovery space of THESEUS highly attractive even after many years of successful EP operations. This is only strengthened by

the fact that THESEUS will be operated when several multi-wavelength ground-based and space-borne facilities having the transient Universe at the core of the science case will be fully operational.

Table 3-1 - Key science performance requirements of THESEUS. They shall be granted up to mission End-of-Life (EoL). The sensitivity requirements assume a power-law spectrum with a photon index of 1.8 and an absorbing column density of $5x10^{20}$ cm^{-2}.

SXI sensitivity (3σ)	$1.8x10^{-11}$ erg/cm^2/s (0.3-5 keV, 1500 s) 10^{-10} erg/cm^2/s (0.3-5 keV, 100 s)
XGIS sensitivity (1s, 3σ)	10^{-8} erg/cm^2/s (2-30 keV) $3x10^{-8}$ erg/cm^2/s (30-150 keV) $2.7x10^{-7}$ erg/cm^2/s (150 keV-1 MeV)
IRT sensitivity (imaging, SNR=5, 150 s)	20.9 (I), 20.7 (Z), 20.4 (Y), 20.7 (J), 20.8 (H)
SXI field-of-view	0.5 sr - 31x61 degrees^2
XGIS field-of-view (area corresponding to >20% efficiency)	2 sr (2-150 keV) – 117x77 degrees^2 4 sr (≥150 keV)
IRT field-of-view	15'x15'
Redshift accuracy (6≤z≤10)	≤10%
IRT resolving power	≥400
XGIS background stability	≤10% (over 10 minutes)
Field-of-Regard	≥50% of the sky
Trigger broadcasting delay to ground-based networks	≤30 seconds (65% of alerts) ≤20 minutes (95% of alerts)
SXI positional accuracy (0.3-5 keV, 99% c.l.)	≤2 arcminutes
XGIS positional accuracy (2-150 keV, 90% c.l.)	≤7 arcminutes (50% of the triggered sGRB) ≤15 arcminutes (90% of the triggered sGRB)
IRT positional accuracy (5σ detections)	≤5 arcsecond (real-time) ≤1 arcsecond (post-processing)

3.2.2 IRT imaging sensitivity and redshift measurement accuracy

The IRT sensitivity requirements and the overall requirement on the response time to a trigger (≤10 minutes for at least 50% of the triggered events) are coupled. They ensure that the requirement on the number of high-redshift long GRBs is fulfilled. This entails that THESEUS is able to start the cycle of photometric observations required to determine the redshift early enough, while the afterglow flux is above the IRT sensitivity threshold, on a sufficiently large number of high-energy triggers. The requirement has been determined based on a set of observed GRB NIR light curves converted to the expected signal if they would be located at at z=8 (Figure 3-4).

One of the key science goals of THESEUS is to measure the star formation rate densities in the early Universe as traced by GRBs. This is enabled by accurate redshift measurements. Redshifts are fundamental to derive the GRB number densities and, based on assumptions on initial mass functions, one can derive the corresponding star-formation rate histories in the early Universe beyond z>6.

To date the vast majority of redshift determinations of GRBs depend on optical to NIR afterglow spectra obtained from ground-based follow-up observations. Such facilities are not always available immediately or on a short timescale due to pointing limitations, weather constraints, etc. By being able to follow-up all

localised GRBs/ X-ray afterglows, THESEUS will detect with the IRT a large fraction of bright afterglows following the triggers on a short timescale. A redshift accuracy of 10% obtained from NIR spectroscopy measurements will ensure a clear distinction between a high-redshift event and a low redshift one.

Simulations show that the required accuracy in the determination of the photometric redshift can be achieved during the so-called, 12.5 minutes duration "Follow-up Mode" for 90% of the candidate GRB triggers above the IRT imaging sensitivity flux threshold (H-band magnitude of 20.8 for a 150 s exposure). For fainter sources, a sequence of deeper exposures, during the so-called 30-minutes duration "Characterization Mode", allows to recover the photometric redshift with the required accuracy in 90% of the remaining cases.

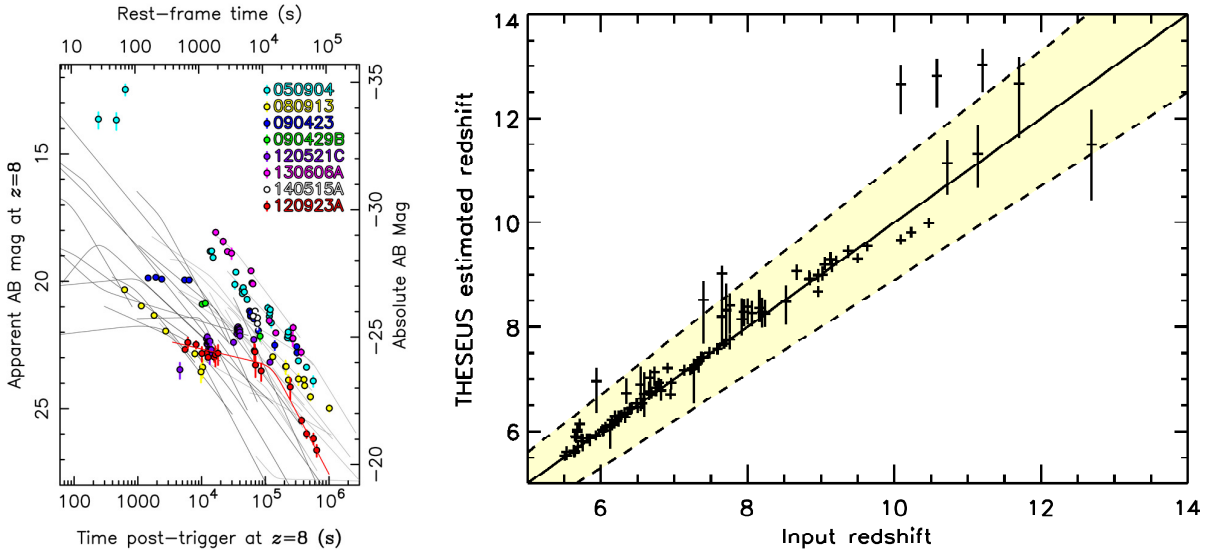

Figure 3-4 – Left panel: IR (H-band) light curves of a sample of known GRBs converted to the expected signal if they would be located at z=8. The grey lines represent on a sample of observed afterglows. The brightest ones after 1 day from the trigger are highlighted as filled dots (colour legend in the inset). Right panel: photometric redshift as a function of the source input according to Monte-Carlo simulations of the IRT observation sequence for a sample of 113 z>6 GRBs extracted from the sky model described in §3.3.1.

3.2.3 IRT High-Resolution Mode resolving power

IRT spectroscopy with resolving power of 400 allows an accurate redshift measurement, even with a S/N in the continuum of ~3 per pixel. Modelling of the Ly-α break profile for bursts at z>6 will provide information on the combined effect of the absorption from the neutral intergalactic medium and in the interstellar medium in the host galaxy [19]. Metal absorption line doublets, such as FeII 2374,2383, FeII 2586,2600, or SiIV 1393,1402, are all very common in long-duration GRB afterglow spectra. They are clearly resolved with the IRT resolution of R=400 and are identifiable even in low metallicity GRB environments provided that a S/N of ~10 per spectral pixel is achieved. This implies that THESEUS will be able to extend the range of redshifts for which an on-board redshift determination is possible to z=2.1- 6. At redshifts lower than z=2.1, absorption lines from CaII 3934,3969 become very weak, such that measuring redshifts within the IRT spectral range of 0.8-1.6 μm becomes impossible.

3.2.4 Background stability and orbit

As demonstrated by several past and present GRB experiments working in the 10-20 keV to a few MeV energy range operating onboard space missions like, *e.g.*, CGRO/BATSE, BeppoSAX/GRBM, Swift/BAT, Fermi/GBM, Konus-WIND, the stability of the background over a time scale of about 10 minutes is essential

to allow a very sensitive triggering capability. Indeed, even though at the peak and for the bulk of their emission typical GRBs tend to dominate the background, the weakest and often more interesting events (*e.g.*, GRB170817A, being associated to the GW event 170817) are background-dominated. In addition, a background as stable as possible is very important for optimizing the characterization of the transient, in particular the measurement of key physical parameters like fluence, duration, beginning and end of the phenomenon (when the transient source rises from, and faints down to be confused with the background.

The maximum time scale and amplitude of the variation of the background needed for getting the expected capability of detecting a sufficient number of long and short GRBs, as well as of measuring accurately key-observables while minimizing false triggers, come from the heritage, comparison and similarities with previous and past GRB experiments, as well as from specific simulations carried out for THESEUS.

3.2.5 Autonomous slewing capability

This requirement is at the core of the science profile of THESEUS. The autonomous slewing will allow THESEUS to rapidly observe with the IRT the error box of the transient, identify it with a IR source with the colours consistent with those expected from a high-redshift GRB afterglow, and measure its redshift. While other operational (*Swift*) and future (SVOM, EP) high-energy wide-field monitoring space mission feature rapid autonomous slewing capabilities, THESEUS is the only mission under study where slewing capabilities are coupled to a NIR telescope with the adequate combination of bandpass sensitivity and spectroscopic capabilities to measure GRB host galaxy redshifts in the early Universe ($z \geq 6$).

3.2.6 Alerts broadcasting

Broadcasting near real time data (event time and coordinates) of SXI and XGIS triggers to ground is mandatory in order to quickly activate multi-wavelength optical/IR/radio/mm facilities to catch the rapidly fading optical afterglow in its brightest phase.

In case of no IRT detection, near real time broadcast of the coordinates and time of the burst is mandatory to obtain arcsecond localization that is necessary to perform spectroscopic observations of the afterglow and/or the host galaxy that can provide the cosmological redshift. Faint optical afterglows (below IRT sensitivity) may reach R~22-24 mag already 5 hours after the burst, thus requiring very fast reaction. In case IRT successfully obtains imaging and spectra of the optical afterglow, near real time broadcast of the coordinates and time of the burst will enable to activate large telescopes (as e.g. VLT, ELT, etc.) that will greatly enhance the scientific output of both long and short GRB observations through high-quality spectra and deep monitoring (e.g. chemical abundance measures, kilonova characterization for short GRBs, etc.). In case of IRT detection in imaging mode but not in spectroscopic mode, then the underlying host galaxy localization is ensured. The burst time and coordinates at arcsecond precision level should still be broadcasted as soon as possible ($\leq$30 seconds for 65% of the triggers) to activate large telescopes to perform spectroscopic observations of the afterglow or the host galaxy and measure the redshift.

The experience with *Swift* (using NASA Tracking and Data Relay Satellite System, TDRSS) and the likely capability of the SVOM (whose VHF system, appropriately refurbished, THESEUS will inherit) has been used to gauge this requirement.

3.2.7 Positional accuracy

The IRT post-processing requirement is driven by the goal of identifying the host galaxy of a GRB in follow-up ground-based optical observations. Considering the Hubble XDF (extremely deep field) data, that span 2.3x2 arcmin, 5500 galaxies have been detected in 16560 sq. arcsec (down to a limiting magnitude of about 30). Hence for an error box of 1 arcsec radius, on average one expects 5000/16560*3.14~1 galaxy per error box, which allows for un-ambiguous identification of GRB host galaxies starting from IRT error boxes.

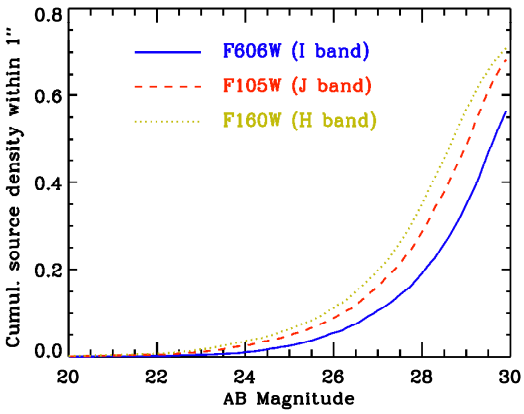

Figure 3-5 – Hubble UDF source density in a 1" error box as a function of AB limiting magnitude in various bands.

By analysing the Hubble UDF (Ultra Deep Field), we can construct galaxy spatial density curves as a function of magnitude. We need to recall that, following [6] and [18], GRB host galaxies at z>6 have H band magnitudes

that are typically fainter than ~28 (AB) and even ~30 in some cases. From Figure 3-5, one can see that for a limiting magnitude of 30 (and considering that the data are not complete at this depth) the number of objects contained in a region of 1 arcsec radius is close to 1 in the H band.

The positional accuracy of the monitors is primarily driven by the need of having a reasonable probability to locate a trigger within the IRT field-of-view. In the case of SXI, a 2 arcminutes positional accuracy serves three effects: (a) it allows for the source to be confidently placed within the IRT FoV; (b) it provides a source location accuracy comparable to that currently provided by the *Swift* BAT for immediate distribution via VHF; and (c) it helps eliminate false triggers by comparison with a list of known X-ray sources brighter than the THESEUS sensitivity requirements.

The definition of the XGIS requirement is based on the following considerations and analysis:

a) the requirement currently applies to short GRBs only, following the top-level requirement on multi-messenger astrophysics and on the number of short GRBs (as electro-magnetic counterparts of GW sources);
b) there is no requirement of following all short GRBs with IRT; thus, no strict requirement to localize them within a 7 arcmin radius (*i.e.*, half of the IRT field-of-view);
c) 15 arcmin localization accuracy is sufficient for reducing substantially the error region provided by GW detectors even in the '30s (the 2nd generation interferometers, with the 3rd generation possibly becoming operational later) and allowing identification of host galaxy with ground telescopes.

3.3 Verifying the core science of THESEUS through a realistic mission simulator

The core science requirements of THESEUS have been verified by simulating a number of observational scenarios. The main goal of these simulations was to ensure that a set of observation strategies exists enabling the core scientific requirements of THESEUS. These were then injected in the industrial study for their further validation and optimization. The simulations made use of a state-of-the-art GRB population model based on the original work by [217] that is described in §3.3.1. The validation results as well as the rationale of the selection of the baseline observational strategy are described in §3.3.2.

3.3.1 GRB population model

Our current knowledge of the population of (long and short) GRBs is based on samples (often thousands of bursts) detected by past and current detectors on different satellites. These samples, providing us a statistically rich view of the prompt emission properties of GRBs, depend on the sensitivity of the different detectors and are subject to varied and specific selection effects. In fact, given the prompt emission diversity in terms of temporal variability, duration and spectral shapes and spectral evolution, the GRB samples detected by a specific instrument are specifically biased by its instrumental properties (e.g. effective area as a function of energy, energy range and resolution, temporal resolution etc.). Over the last 20 years, with the discovery of GRB afterglows, our picture was further enriched by the measurement of redshifts (allowing us to access the

intrinsic properties of these sources). However, on average only ~30% of the GRBs triggered by Swift/BAT have their redshift measured.

If we aim to estimate the GRB detection rate of an instrument like none before, we cannot rely on these biased samples but rather construct a population of GRBs which eventually allows to extend the detection to any combination of source physical parameters beyond what has been explored so far.

A population of cosmic sources is fully described by two functions: the luminosity function (i.e. the number of sources as a function of their luminosity or energy) and their distribution in redshift or cosmic time. For GRBs, a direct measurement of these functions is hampered by (a) the many biases that affect currently observed samples [135] and (b) the paucity of GRBs with measured redshift.

To estimate the THESEUS expected performances we built a synthetic population of GRBs employing an indirect method [217]: we simulate the intrinsic distributions of GRBs in the sky under some motivated assumptions on the shape of the two functions and compare model results with the observed distribution of events as obtained by current satellites. In particular, we constrain the free parameters by reproducing the fluence, peak flux, observer-frame peak energy and observer-frame duration distribution of GRBs detected by Fermi and Swift. Moreover, we minimize the impact of observational biases by using a well selected, complete subsample of bright GRBs detected by Swift ([218], [219]), for which the measure of the redshift has been secured for the largest fraction of events.

In the literature ([218], [220]), the luminosity function of both long and short GRBs is usually parametrised as a double power-law with a faint end slope α_f, a bright end slope α_b and a break luminosity L_{break}. The luminosity function is extended to very low values (~10^{46} erg/s) so to include also low luminosity events. In virtue of the existence of a link between the luminosity and the peak energy, this also ensures that the population includes also very soft GRBs (also known as X-ray flashes, [133], [221]). The intrinsic redshift distribution will depend, in general, on the physical conditions that give rise to the GRB event and therefore its shape will be different for long and short GRBs.

Long GRBs are now firmly associated with the core collapse of massive stars by the detection of a type Ib,c supernova associated with almost all long GRB events in the low-redshift Universe where these studies are possible. This fact suggests that long GRBs can be a good tracer of star formation. However, both population studies [222] and the observed properties of the galaxies hosting the GRB event suggest that their rate increases with redshift more rapidly and peaks at higher redshift than that of stars. These evidence supports a scenario in which the GRB event requires a low-metal content in the progenitor star ([223], [224]) and, therefore, their formation is hampered in a metal-rich environment. We model this effect by convolving the cosmic SFR [225] by a factor $(1+z)^{\delta}$ ([222], [218], [217]).

Short GRBs instead are now recognized as the product of the merger of compact objects (NSs and possibly NSBH) binaries, as seen by the temporal and spatial association of GRB 170817A with the gravitational wave event GW 170817 due to the merger of two NSs ([50], [55]). Therefore, their intrinsic redshift distribution can be assumed to follow the cosmic SFR with a delay which is due to the time necessary for the progenitor binary to merge. Due to our poor knowledge of the merger delay time distribution, we assume that the intrinsic short GRB redshift distribution can be described by a Cole function [226] with all parameters free to vary and we constrain it on the basis of the observed samples.

3.3.1.1 Monte Carlo simulation of the GRB populations

We adopt a Monte Carlo approach to simulate the populations of long and short GRBs. In both cases, at each simulated event we assign randomly and independently a value of the peak energy and a redshift from the assumed distributions. Through the peak energy—isotropic luminosity [43] and the peak energy—isotropic energy [42] correlations (accounting also for their scatter) we assign L_{iso} and E_{iso}, respectively. The observer-frame fluence and peak flux of the bursts are obtained by assuming a Band spectral shape with typical low and high energy spectral slopes [227]. This procedure is iterated for 2 million bursts in order to avoid under-sampling issues when dealing with relatively steep input functions. The simulated population is then compared

with the observed distribution of bursts detected by Swift and Fermi accounting for their spectral sensitivity, field of view, mission duration and duty cycle.

The simulated populations are calibrated by the most updated observed distributions of Swift and Fermi/GBM detected bursts. In order to minimise observational biases, we consider only relatively bright bursts (selection is made on the peak flux) for which observed samples are complete. We consider the fluence, peak flux, observed peak energy and duration distribution of Fermi GRBs (selected sample contains ~800 long and ~200 short GRBs). For the long GRB population we also match the peak flux distribution of Swift GRBs. For both long and short GRBs we use as constraints the redshift, isotropic equivalent luminosity and energy distributions of the complete Swift samples (BAT6 for long – [218] and SBAT4 for short – [219]). The simulated populations are normalized to the detection rate of Fermi short and long GRBs. Our procedure produces a good fit of all observational constraints when the LF parameters are -1.2 and -2.5 (for the faint and bright end of the function and with a break at ~$2x10^{52}$ erg/s) for long GRBs. The redshift evolution parameter delta of long GRBs is found to be 1.7±0.5 ([218], [217]). For short GRBs we obtain a relatively flat faint end of the luminosity function with slope -0.5 and a steeper bright end (slope -3.4) and a break at $3x10^{52}$ erg/s. The intrinsic redshift distribution of short GRBs is consistent with a delay time distribution $P(\tau) \propto \tau^{-1}$ [228].

Owing to the softer energy band sampled (0.3-5 keV), THESEUS/SXI will access a softer population of GRBs where both soft, low luminosity events (mostly detected in the low redshift Universe) are present together with high redshift events. Compared to Swift and Fermi, THESEUS/SXI will contribute to the study of the population of low luminosity GRBs which could be characterized by different physical properties (e.g. opening angle and/or jet bulk velocities). The current knowledge of this population is limited by instruments which trigger on a considerably too large energy range compared to the typical soft peak energy of this part of the population.

3.3.1.2 Simulating the afterglow emission

To investigate the THESEUS capabilities of measuring the redshift of detected GRBs, we added to the simulated population of long and short GRBs an afterglow emission module. This is based on the emission produced by the deceleration of the fireball in a constant density external medium. We follow the prescription of [229]. The afterglow luminosity depends on the kinetic energy of the jet and on the shock efficiencies in amplifying the magnetic field and accelerating the emitting particles. These parameters are obtained by calibrating the simulated population of bright Swift GRBs with a complete sample of real bursts detected by Swift for which the optical afterglow emission has been sampled between 6 hours and 1 day. Through this code we produced a full prompt+ afterglow library of long and short GRBs to be used to compute the detection rates and the redshift measurements efficiency of THESEUS.

3.3.2 Mission Observation Simulator results

The top-level THESEUS scientific requirements described in §3.1 have been verified through mission analysis at ESOC (the Mission Observation Simulator, MOS). A realistic observational sequence of the THESEUS spacecraft according to the operational modes described in §6 was simulated considering all observational constraints (Earth occultations and eclipses, South Atlantic Anomaly passages) in response to a random set of short and long GRB triggers as per the GRB population model described in §3.3.1. External triggers (three per month as per science requirement) as well as estimated false alert rates (three and one per week for the SXI and XGIS, respectively, as per science requirements augmented in the case of the SXI, see later) were injected randomly in the simulations to estimate the associated inefficiencies. In order to achieve sufficient statistics, the results of 40 simulations of 4-years THESEUS nominal operations (corresponding to 3.45 years of science observations; cf. §6) were merged together.

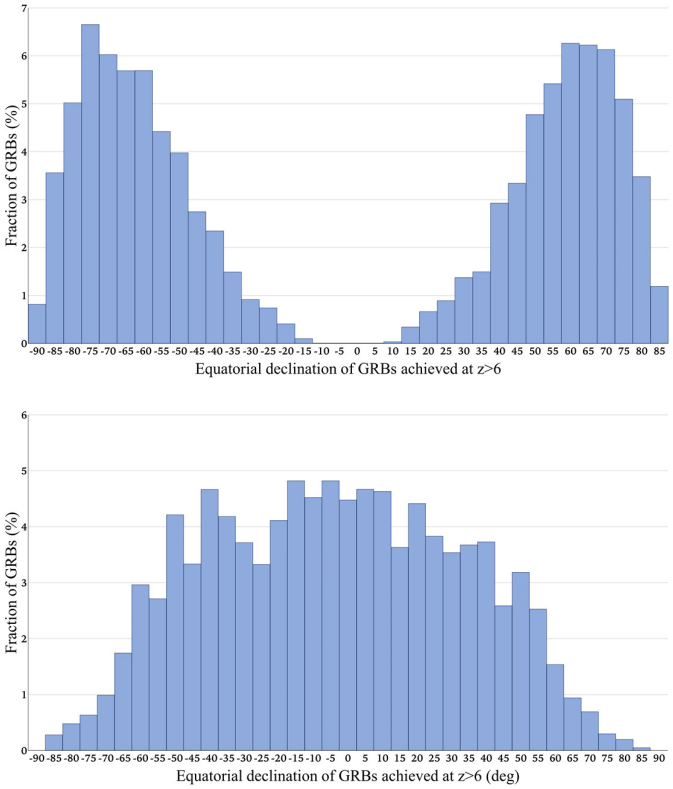

Figure 3-6 - Normalized z>6 GRB distributions for the ECP (upper panel) and the DYN (lower panel) pointing strategies.

Several possible pointing strategies have been evaluated, differing by the distribution of pointing directions during the Survey Mode. All pointing strategies must be compliant by design to a Solar Aspect Angle larger than 60 degrees. A trade-off was carried out during Phase A between a fixed Survey Mode pointing to the Ecliptic Poles (switching between the North and the South Pole every six months; "ECP" hereafter), and pointing strategies where two tilts per orbit by 30 or 60 degrees were allowed (the latter one will be identified as "DYN" hereafter). The former strategy maximizes the absolute rate of GRB triggers detected by the high-energy instruments; the latter strategies maximize the rate of THESEUS-detected triggers that can be follow-up by ground-based telescopes (typically located within ±30 degrees latitude). An example of the corresponding normalized distributions of triggers' latitudes is shown in Figure 3-6.

About 90% (50%) of the GRB triggers detected with the DYN strategy have a latitude lower than 55 (30) degrees, favourable to ground-based follow-up observations, against 30% (4%) for the EP strategy. The sky coverage of the survey with a DYN strategy is correspondingly more homogeneous than with the ECP strategy (Figure 3-7). The mission analysis confirmed that the basic science objectives of the mission can be achieved with all pointing strategies. The ECP yields more than 45 long GRBs at z>6 and at least 40 short GRBs during the 4-year nominal operations. The baseline DYN strategy yields about 15% less short GRBs, and about 5% more long GRBs. The combination of more homogeneous survey sky coverage, higher probability of ground-based follow-up observations of THESEUS-detected triggers, and comparable trigger detection efficiencies leads to the DYN pointing scenario to be chosen as the baseline during Phase A.

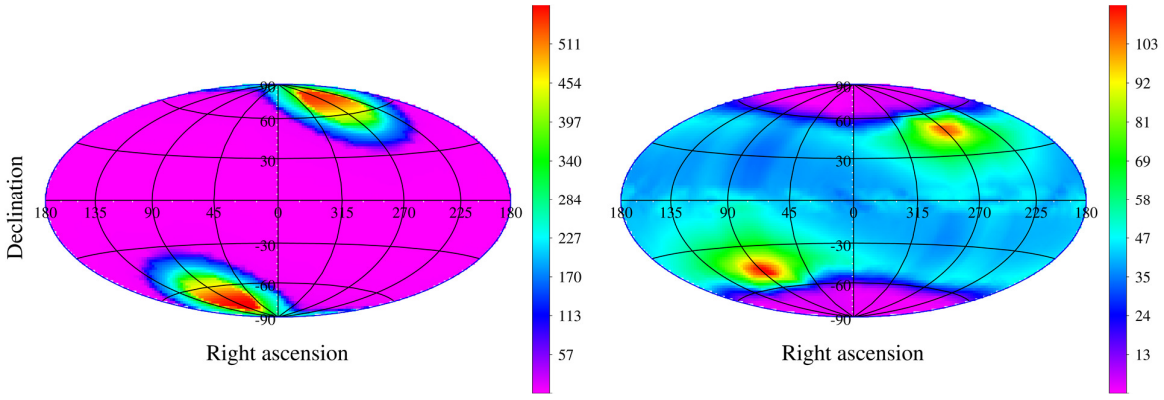

Figure 3-7 - SXI Exposure maps for the ECP (left panel) and DYN (right panel) pointing strategies. The units are days over the nominal mission duration [credit: A. Rocchi and V. Doroshenko].

4 Payload

4.1 SXI

The Soft X-ray Imager instrument on the THESEUS mission will revolutionize transient astronomy by using Lobster eye wide-field (~0.5sr) focusing optics to increase the sensitivity to fast transients by several orders of magnitude [230]. The use of such optics provides uniform sensitivity across a very large field of view while maintaining arcminute localisation accuracy. Working in combination with the XGIS and IRT, the SXI will: (a) enable the discovery of many hundreds of X-ray transients per year, particularly enhancing sensitivity to high redshift GRBs thereby facilitating an exploration of the earliest phase of star formation; (b) will search for X-ray transients associated with multi-messenger sources at a time when a new window is opening on the Universe; and (c) will monitor the X-ray sky on a wide variety of timescales, while simultaneously providing important targets for future observing facilities, such as ATHENA and the 30m class ground-based telescopes.

4.1.1 Instrument description

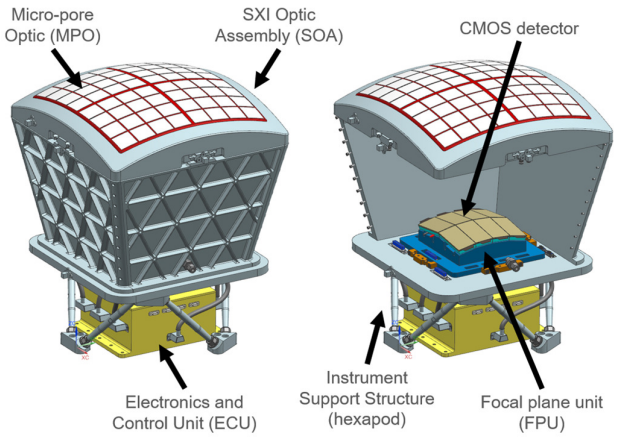

Figure 4-1: left panel shows the SXI module exterior view; right panel cut-away shows the focal plane assembly located below the optics assembly. The electronics box is shown here below the focal plane within the structure which mounts to the spacecraft.

The SXI instrument comprises 2 identical modules (see Figure 4-1 and Table 4-1). Each module is a wide-field, "Lobster eye" X-ray telescope, using the X-ray imaging principle first described by [231]. This configuration provides for a wide FoV, focussing X-ray imaging system with an effective area maintained across the entire FoV. The optics aperture for the SXI modules is formed by an array of 8x8 square micro pore optics (MPOs) mounted on a spherical frame with a radius of curvature of 600 mm. Figure 2 shows an MPO and the point spread function. X-rays which reflect off the square pore sides form a central focus (even number of reflections) or a line focus (odd number), giving a cross-arm PSF. In this configuration some 75% of the incident X-rays are focused, with detailed simulations showing the optics provide the required <2 arc-minutes transient location accuracy. The angle at which the cross arms first go to zero is determined by the L/d ratio of the pores, where L is the MPO thickness and d the pore width. For optimum performance (combination of sensitivity and imaging quality) at 1 keV we require L/d=60 and use L=2.4mm and d=40 µm. Mounted directly onto the frame, behind the optics, are a set of magnets forming an electron diverter. Optics heaters are also mounted on the frame, and together these components comprise the optics assembly, which provides a FoV of ~0.25 steradians (31^ox31^o) per module. The 2 modules will be aligned on the sky, with a 1^o wide overlap on one side, coaligned with the IRT FoV to provide redundancy.

The SXI modules comprise an optics assembly focussing light onto a focal plane assembly comprising 8 CMOS detectors. A dedicated instrument structure comprising of an Aluminium Optic Assembly Frame, a tapered Aluminium Telescope tube and Aluminium/Titanium Instrument support structure maintain the focal length between the optics and the detectors and provide the interface with the spacecraft platform. The SXI module is enclosed in MLI in order to maintain thermal control.

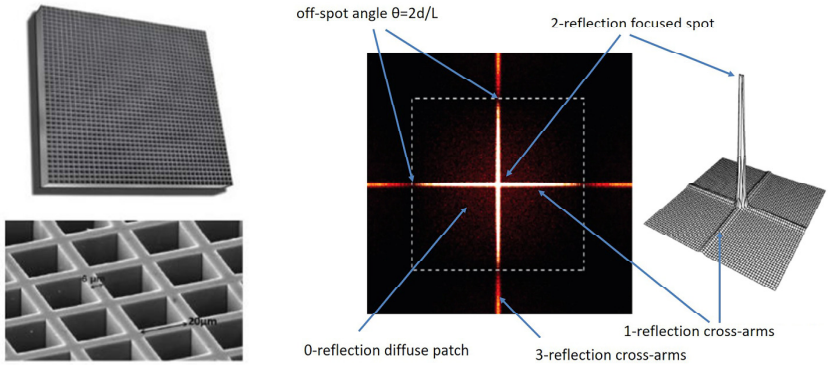

Figure 4-2 Left panel – a bare MPO and a micrograph of the square-pore glass structure. Flight MPOs are covered with a sky-facing, thin Al layer. Right panel – the MPO point spread function. The inner dotted square shows where the cross-arms first go to zero.

The MPOs and detectors both have sky-facing thin Aluminium layers acting as a light block. The MPO Al layer also efficiently rejects Earth light to aid thermal control. The SXI module has two key thermal control challenges: maintaining the MPOs within the optimum temperature range (20°C to 30°C) and gradient and maintaining the CMOS detectors at their optimum temperature (<=-30°C) and stability (±1.5°C).

Table 4-1 SXI module physical characteristics

Energy band (keV)	0.3-5
Optics configuration	8x8 square pore MPOs
MPO size (mm^2)	40x40
Focal length (mm)	300
Focal plane detectors	CMOS array
CMOS size (mm^2)	80x40
CMOS pixel size (µm)	40
CMOS pixel Number	2000x1000
Number of CMOS	8
Module Field of View (sr)	0.25
Centroiding accuracy (best, worst) (arcsec)	(<30, 180)
Mass	35.9 kg (includes EBox and margins)
Power	44.2 W (includes margin)

The former is achieved through Proportional-Integral-Derivative controlled heaters installed on the Optic Frame; the latter is achieved via a spacecraft provided Cold Finger (CF), the use of thermoelectric coolers (TECs), and good thermal coupling between the focal plane array (FPA) support (cold base) and the warm base which is part of the instrument support structure (Figure 4-3). The Phase A mechanical analysis performed with a simple finite element (FE) model demonstrates a first mode (Figure 4-3) within the anticipated launch specification and material limits. A functional block diagram of the SXI is shown in Figure 4-4. The SXI modules utilise front-end electronics (FEE) for focal plane control/data acquisition, and back-end electronics (BEE) for thermal control and housekeeping. The FEE provides local power conditioning for the detector bias lines and clocks and routes the digital data output from the detectors to a small processor for event list generation – data is transferred between the FEE and DHU via SpaceWire interface.

There are 4 detector pairs (per instrument module), and 1 FEE board will be required to drive 2 of these detector pairs. The 2 FEE PCBs and a power board are housed within an Electronics Control Unit (ECU) for each module that is placed near the focal plane. The BEE are located inside the SXI DHU box (which can be placed up to 3m away from the modules) and provide overall thermal control for both SXI modules (i.e. TEC drive/control for the focal plane and heater drive/control for the optics structure) as well as handling of the housekeeping data (thermal sensors on the optics structure, focal plane, and ECU box). The SXI DHU provides the data interface to the spacecraft platform and controls (switches) the spacecraft power to the SXI ECU.

4.1.2 Interfaces and resource requirements

Each SXI module has an estimated mass of 35.9kg (Table 4-1). The mechanical and thermal interfaces with the spacecraft are via CAM CF (for SC thermal strap) and via ECU and Instrument Support Structure mechanical interfaces with the PLM, see Figure 4-5.

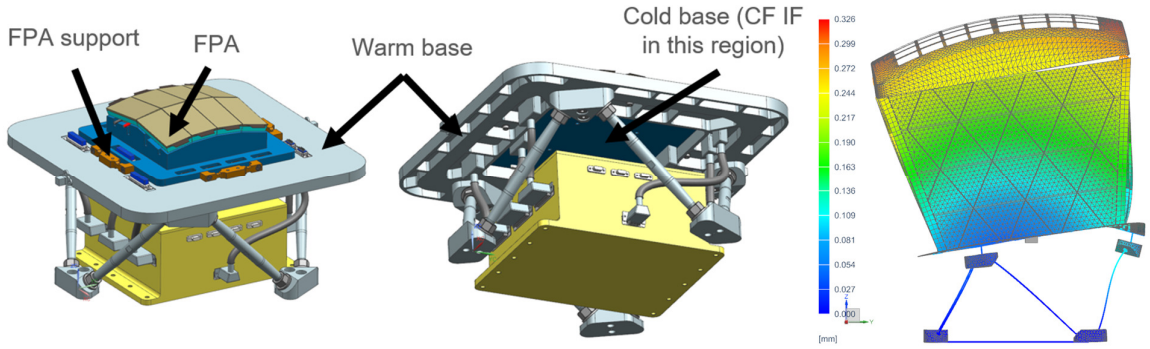

Figure 4-3 Left & middle: Focal Plane Assembly Cold Base and Warm Base. Right: Example of the mechanical analysis (first mode) performed on 1 SXI module.

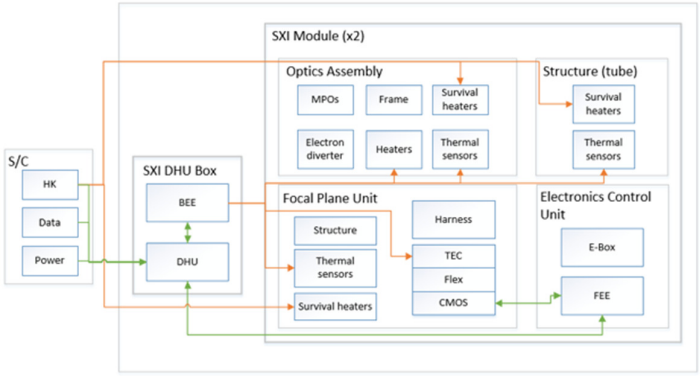

Figure 4-4 SXI block diagram.

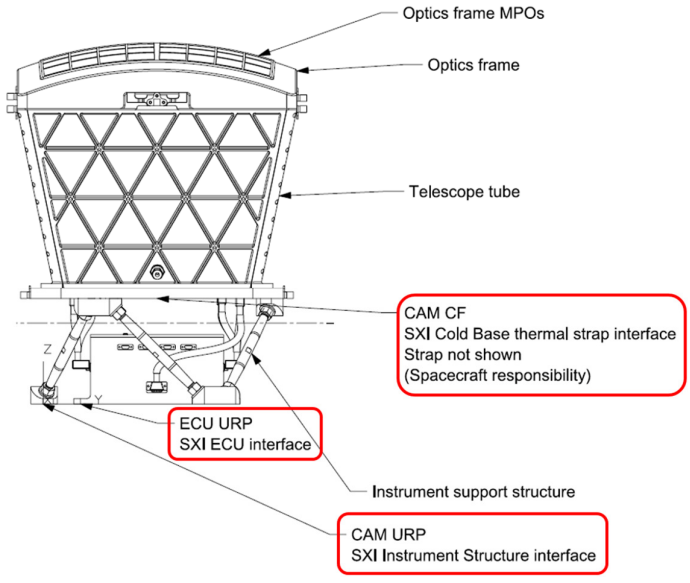

Figure 4-5 SXI Module Thermal Interfaces.

Each module will also require a purge interface with the spacecraft. The total power for each SXI module is ~45W. The SXI DHU requires ~12W of power and hence the total power requirement for the full SXI instrument (i.e. 2x modules and the DHU) is <110W (Table 4-1). Concerning the telemetry: for the science mode, the SXI average rate is 50kbit/s (calculated assuming on average 320 X-rays per second at the SXI instrument, equating to ~2k pixel/second across both modules); for HK it is 12.8kbit/s.

4.1.3 Operation requirements

The instrument operates almost always in the same observing mode, except when performing calibration, which is performed in parallel across the module detectors. The detectors are clocked out every 100ms, photons are graded in the electronics and the photon stream (with grade, energy and pixel locations) are passed to the DHU within which runs the trigger system. All photons are telemetered to ground to conduct the X-ray sky survey. Event list processing (e.g. trigger algorithms) occur in the DHU which also provides event list and housekeeping data storage.

4.1.4 Heritage and technology development

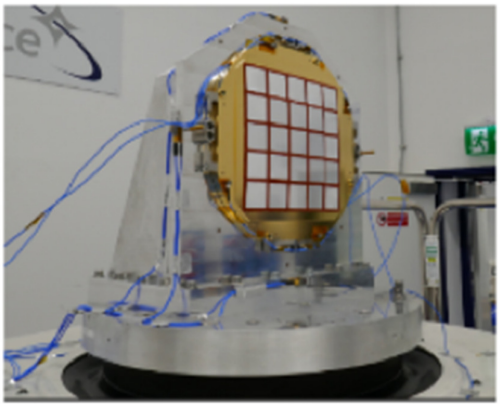

Figure 4-6 SVOM FM Vibration Test.

The THESEUS SXI optics are based on those developed for the recently launched ESA BepiColombo mission, and also those under construction for the China-France SVOM and ESA-China SMILE missions. The SXI optic is a larger version of the SVOM MXT optic, the flight model for which has been assembled and has undergone thermal and vibration testing (see Figure 4-6 and Figure 4-7). The SVOM and SMILE optics assemblies use the same materials as baselined for the THESEUS SXI, and these missions share a common MPO bonding, testing and alignment process. These missions all make use of MPOs supplied by the French Photonis company, but during Phase A the possible use of an alternative MPO supplier – the Chinese North Night Vision Technology (NNVT) company, which is presently supplying MPOs for the Chinese Einstein Probe mission – has been investigated. An ESA funded Technology Devlopment Activity (TDA) compares the MPOs from both potential suppliers and enables MPO development at Photonis to further improve optics quality, hence reducing risk and cost for MPO provision.

There are two ongoing detector technology development studies involving large-format CMOS X-ray that are relevant to the SXI (i.e. an ESA funded Technology Development Exercise (TDE) activity and an ESA funded TDA activity). The TDE activity involves the development of a large area CMOS detector that is suitable for X-ray spectroscopy applications, i.e. a CMOS device with: large, deep depleted pixels (~35-40µm square, to optimally match X-ray event size) and appropriate on-chip optical blocking filters (e.g. Al, to ensure suitable rejection of straylight whilst maintaining soft X-ray detection efficiency). A detailed study of the X-ray performance of the CMOS devices developed during the TDE activity will be performed during the SXI detector TDA. The scope of the TDA also includes the top level design of the SXI camera system (including thermal and mechanical analysis, top level design of the FEE and BEE, and development of an autonomous event detection algorithm) and a full, end-to-end demonstration of the SXI system level performance (including representative FEE and BEE systems, and representative optics).

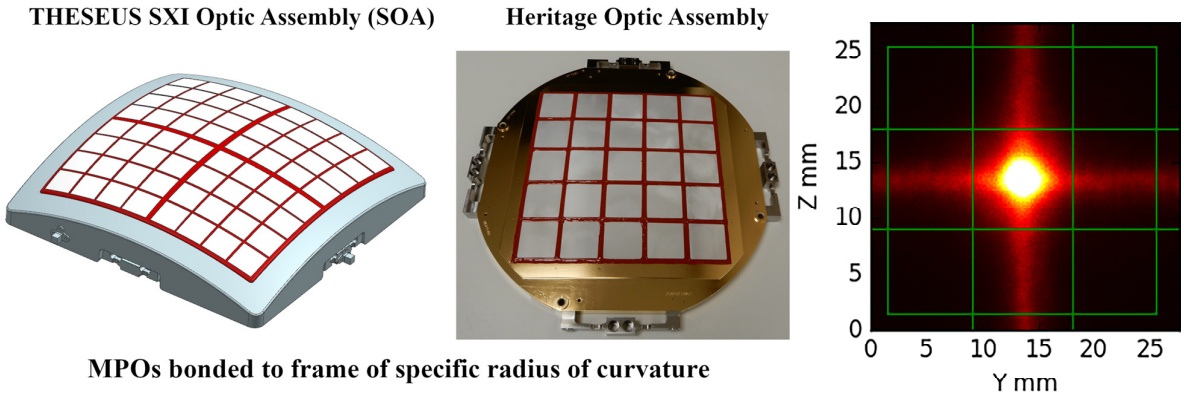

Figure 4-7 SXI optics assembly (left) compared to the SVOM MXT optics assembly (centre). Right: X-ray verification image for the SVOM FM optic demonstrating excellent alignment accuracy for multiple MPO [credit: UL, CNES, SVOM].

4.1.5 Performance

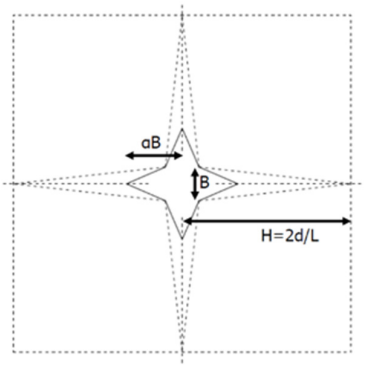

Figure 4-8 A schematic of the lobster eye cross-beam shape.

The SXI optics PSF is characterized by a central spot and four extended cross-arms (Figure 4-8). An optimised event detection algorithm which uses different fractions of the detailed shape of the PSF as a function of trigger time will be used to ensure that as many of the X-ray sources as possible (i.e. that are located within the FoV of the instrument) activate the instrument trigger system. The X-ray events associated with the detected source will then be stored in the instrument's DHU. Ideally, the onboard algorithm would perform matched filtering on the full PSF but in order to reduce computation time and in order to minimise the effects of the sky and detector backgrounds (i.e. maximise the source to background flux ratio of the instrument), the algorithm utilises a cross-beam region of interest (ROI) shape that is limited to a fraction of the overall source counts (i.e. the event extraction region is limited to specific regions around the central core and arms).

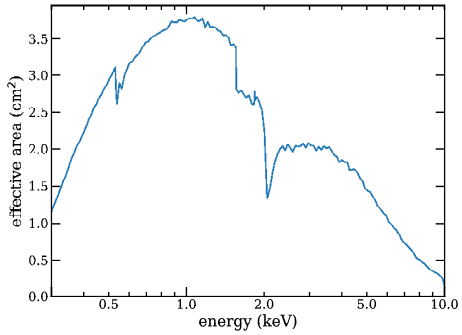

Figure 4-9 SXI total effective area.

A schematic of a typical lobster eye cross-beam is shown in Figure 4-8. The parameters B and a depend on the quality of the optics, and can be optimised with exposure time such that the cross-beam contains as high a fraction of source counts as possible while limiting the contributions from the background. If the parameters are set such that the source flux is limited to 50% of the total, B is a robust measure of the half energy width of the PSF. An accurate and rapid source position is determined by implementing a multi-stage centroiding process. Initially, a centre of gravity calculation is performed for all events found within rectangular zones on the detector image (created by stacking many individual frames together). In the second stage, the centroid position is further refined by performing sequential, single axis binning and weighted centroiding (based on the known profile of the PSF). In the final stage of the process, the parameterised PSF ROI described above is used to obtain a final determination for the source position. Ray tracing simulations across the 0.3-5keV energy range show that the SXI effective area peaks at 1 keV (see Figure 4-9) and that the optics exhibit a FWHM of ~6 arcmins at the peak energy. The curve in Figure 4-9 shows the SXI total effective area, accounting for the 80nm aluminium filter on the optics and 100nm aluminium coating on the detector and the quantum efficiency of the CMOS device. For triggers we use a tuneable fraction of the PSF; for example, when using the 50% cross beam extraction algorithm source

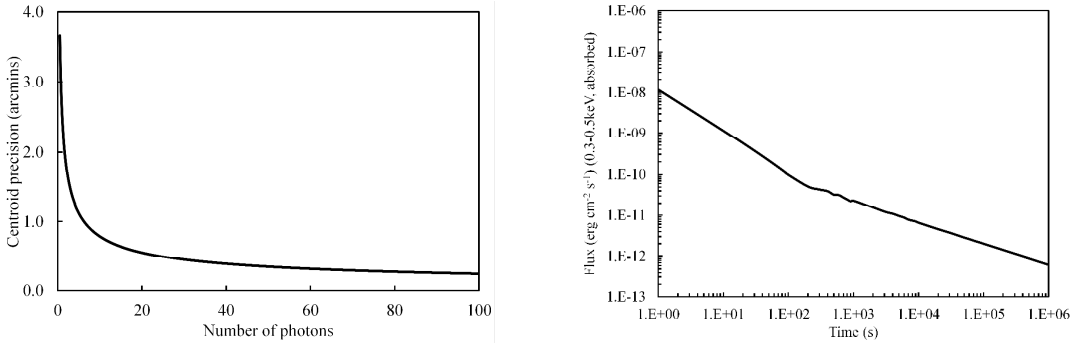

Figure 4-10 Left: the typical accuracy of a weighted centroid as a function of photon events. Right: minimum detectable flux level achieved by the SXI as a function of time.

in simulations, counts are collected across a total area of 675 square arcmins (i.e. equivalent to a circular beam of radius 14.7 arcmin).

Table 4-2 SXI simulation parameter.

Parameter	Value
N_H (absorbing column)	$5x10^{20}$ cm^{-2}
Index	1.8
Sky background	$1.14x10^{-5}$ c s^{-1} arcmin^{-2}
Detector background	$9.75x10^{-7}$ c s^{-1} arcmin^{-2}
Total background	$1.24x10^{-5}$ c s^{-1} arcmin^{-2}

To demonstrate the localisation accuracy achievable with the SXI instrument as a function of time a Monte Carlo simulation of this approach was generated to model the interactions of the photons imaged by the SXI instrument (i.e. by modelling the expected SXI PSF shape and interactions with the detector, and applying the cross-beam analysis method for centroiding). Through this model the minimum number of counts required to achieve the localisation accuracy at a subpixel level was determined. Figure 4-10 shows the centroiding accuracy as a function of photon counts for a weighted centroiding method. Through the analysis, it has been demonstrated that when using a standard weighted centroiding method, the position of a source can be determined from 50 counts to an accuracy of less than 1 pixel. These simulations were configured with 30μm pixels and the background levels given in Table 4-2 The background is dominated by the sky, where in Table 4-2 we give the median sky background level derived from the ROSAT All Sky Survey. The minimum detectable flux level achieved as a function of time is shown in Figure 4-10.

4.2 XGIS

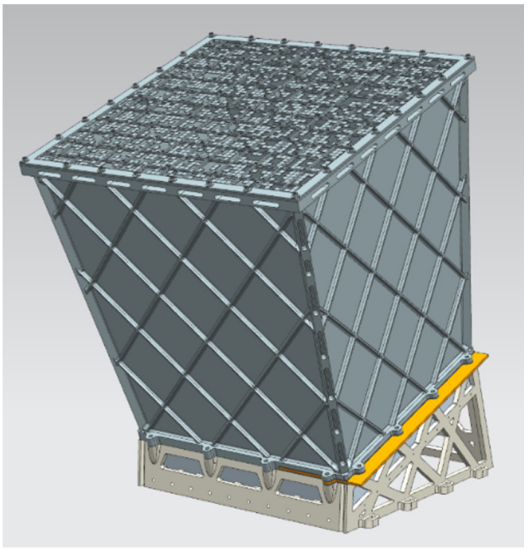

Figure 4-11 Sketch of an XGIS camera.

The inclusion in the payload of a broad field of view hard X/soft gamma-ray detection system, covering a >2sr FoV (that includes that of the SXI) and extending the energy band from few keV up to several MeV with at least a few hundred cm^2 effective area over the whole range is fundamental for: a) detecting and localizing short GRBs, which are a key phenomenon for multi-messenger astrophysics, being up to now the most likely and only one detected EM counterparts of GW signals (specifically, from NS-NS and NS-BH mergers), and determining the hard spectrum of these events, which makes them mostly undetectable with the SXI; b) complementing the SXI capabilities for the detection and localization of high-z GRBs, thanks to the large effective area at <10 keV with respect to past/current GRB detectors; c) providing unique clues to the physics and geometry of the emission of GRBs and other bright X-ray transients through sensitive timing and spectroscopy over an unprecedentedly wide energy band; d) detecting possible absorption features in the low-energy spectra of GRBs that may be used for investigating the circum-burst environment, and hence the nature of the progenitor star, as well as inferring the redshift. In addition, as the SXI lobster-eye telescopes can be triggered by several classes of transient phenomena (e.g., flare stars, X-ray bursts, etc), the detection in hard X-rays with the XGIS provides an efficient tool of identifying *bona fide* GRBs) [232].

4.2.1 Instrument Description

XGIS system is composed by two coded-mask X/gamma-ray cameras (sketched in Figure 4-11), two power supply boxes (XSU), a Data Handling Unit (DHU) and harness ([233], [234], [235], [236]) . The XGIS system has imaging capabilities up to 150 keV, in a FoV overlapping the SXI one, and is a spectrometer covering a wide energy range from keV to MeV, partially overlapping the SXI one. As an imager XGIS is based on the

coded mask principle with the mask *shadowgram* being recorded by a position sensitive detector, that can then be deconvolved into a sky image. The size of the point spread function in the sky image is determined by the ratio of the mask pixel size and the mask-to-detector distance. The mask pixel size must always be larger than the corresponding detector resolution. The XGIS detector plane contains 10×10 modules arranged side by side. A Module contains 8x8 pixels. A passive space, one pixel wide, is interleaved between one Module and the adjacent ones. In this way there are 9 "dead" rows and 9 "dead" columns. Above 150 keV the FoV of a XGIS camera is not delimited. The two XGIS cameras have a partially-coded imaging FoV of 77x77 degrees^2 (15-150 keV) and are misaligned by ±20 degrees with respect to SXI and IRT, thus providing a full FoV of 117x77 degrees^2.

The architecture of the XGIS system is shown schematically in Figure 4-12. DHU is the interface of XGIS with the S/C for power, commands and data; on the other sides it interfaces the rest of XGIS system. The burst trigger functionality is implemented as a part of the DHU that contains also mass memory and operates as instrument control unit (ICU).

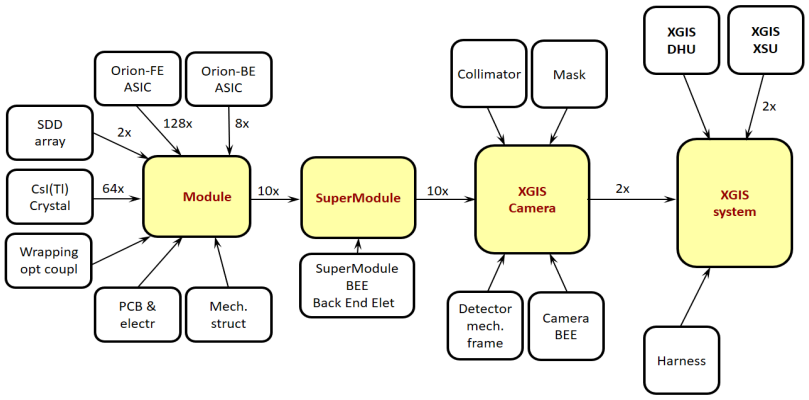

Figure 4-12 Block diagram of the XGIS system.

Figure 4-12 shows the functional block diagram of XGIS system whose component are from right to left: the **Data Handling Unit** (DHU) and two **XGIS Supply Units** (XSUs) that manage the Cameras power supply; two **XGIS cameras** each one made of a **Collimator** and **Mask** assemblies, a **detector mechanical frame and camera support** including the Cold-Finger for the detector thermal control, Camera **Back End Electronics** (BEE) that provides provide mass memory, common services and interfaces to the DHU and the XSU, and 10 **Super-Modules**. A **Super-Module** assembles 10 **Modules**, providing a mechanical structure to hold and align the Modules and an electrical BEE-Board with common services the Modules as power supply, command and control logic, mass memory for data and I/Fs with the Camera-BEE.

A **Module** is the basic element of the detector plane, it is made of 64 pixels The Module contains all active detection elements, the electronics circuits for full signal analysis and the mechanical frames for detector and electronics components. In detail, a Module consists of an array of 8x8 individual pixels. The linear size of each pixel is roughly half the size of a single mask element. Figure 4-14 gives a representation of the Module: two sets of Silicon Drift Detector SDDs (top and bottom) are optically coupled through transparent silicone layers to the scintillator crystals. The crystal wrapping optically insulates one crystal to the others so that the scintillation light of one crystal can reach only its two coupled SDDs. The SDDs are mounted on a Processing Control Board (PCB) where also the first stages of the electronic chain, the preamplifiers Front End Application Specific Integrated Circuit (FE-ASIC), and the Orion-FE, one for each SDD, are mounted. A third PCB contains the Orion-BE ASICs that elaborate the pre-amplified SDD signals. The front face of the 'top PCB' is exposed to the incoming radiation, while the SDDs are glued on its back face; the PCB has large openings so that the low energy radiation can pass through and reach the SDD.

Figure 4-13 shows the pixel operation concept. Two SDD are placed at the two opposite sides of a scintillator CsI(Tl) crystal. Low energy radiation (roughly with E < 25–30 keV) is detected in the SDD on the top surface of the Module, while radiation with higher energy reaches the scintillator placed under the SDD. The scintillation light produced by a photon interaction in the crystal is then collected in both SDDs. The crystal is

wrapped with a light diffusive foil to enhance light collection and optically coupled to the SDDs by a silicone pad transparent and flexible, less than 1 mm thick. In XGIS the SDD have a square cross section 5x5 mm^2 while the scintillator crystal has the form of a small bar 4.5x4.5x30 mm^3 in size. The CsI(Tl) scintillator emits light peaking at about 560 nm. While the electron-hole pair creation from X-ray interaction in Silicon generates a fast signal (about 100 ns rise time), the scintillation light collection is dominated by the CsI(Tl) fluorescent states de-excitation time 0.68 μs (64%) and 3.34 μs (36%) therefore a few μs shaping time is needed to avoid a significant ballistic deficit. The discrimination between energy losses in Si (top SDD) and CsI(Tl) is done in the electronic FE. For interactions in Si, the pixel size determines the position resolution in the detector plane.

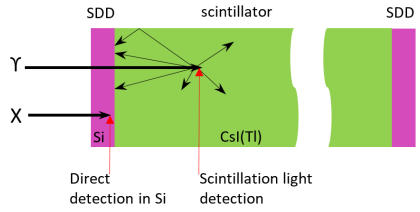

Figure 4-13 Pixel detector operation concept.

In the CsI, the scintillation light is diffused/reflected on the crystal walls before reaching the SDD; the larger is the scintillation distance from the SDD, the greater is its attenuation. By weighing the two SDD signals (top and bottom) the scintillation depth in the CsI bar can be evaluated producing a 3-D position detector. The signals from an SDD is collected and processed by the Orion family ASICs.

A single channel Orion-FE ASIC is placed near the SDD anode, in order to maintain the stray capacitance as low as possible. The Orion-FE ASIC collects the SDD charge signal and performs a pre-amplification and buffering of the signal that is sent to the Orion-BE ASICs placed a few cm away. The signal processing in the Orion-BE (8 pixel) assumes that:

- An X-ray (2–30 keV) will be detected only in the top SDD, with a signal having a fast rise time (a few hundreds of ns), so that the best signal/noise ratio will be achieved with a short shaping time (typically 1 μs). The signal discrimination will operate only on the top SDD signal that will be AD converted, and the time marking of the signal will be related to this discriminator trigger. As the X-ray detection is (almost) point-like in the SDD, the arrival time of the signal at SDD anodes will be eventually delayed up to 1 μs with respect to the event occurrence due to the charge drift time in the SDD; the time marking of the event is then affected both by the uncertainly due to jitter of the trigger and by the unknown position of the photon interaction in the Si.
- A Γ-ray (>20 keV) will be detected in time coincidence in both top and bottom SDD, in this case the signal rise time will be of the order of few μs, due to the scintillation light characteristic timescale. The best signal/noise ratio will be achieved with a shaping time of the order of 3 μs (typical); the best signal/noise discrimination will be achieved by operating on the sum of top and bottom SDD signals. The time marking of the event will be related to this discriminator trigger, that will command the AD conversion of both signals. In total each pixel will have three Analog-Digital Converter (ADC) inside the ASI: one for X-ray shaped signal, and two for γ-ray shaped signals.

The digital signals from the ASICs are stored at different levels in the Super-Module and in the Camera BEE, and then sent to the DHU where the data will be pre-processed in order to distinguish X and γ-events, cleaned from particles events on the basis of the number of time coincident triggered pixels, their topology and their energy deposited, sorted in time, calibrated in energy also recognizing Compton events. The GRB trigger search uses essentially two methods based on rate and/or on images variations:

- The *rate trigger method*, which operates on the whole XGIS energy range, will compare variation of count rate on different energy bands, different integration times and different detector areas. Each estimated rate will be compared with the background rate evaluated dynamically around the orbit.
- The *image analysis* operating up to 150 keV will compare images integrated on long time intervals (e.g. 20, 100, 500 s), and one or two energy ranges, with background images evaluated dynamically around the

orbit with the same parameters. For each rate trigger event, the image analysis will be performed in order to get, in addition to the light curve, also the celestial direction of the event.

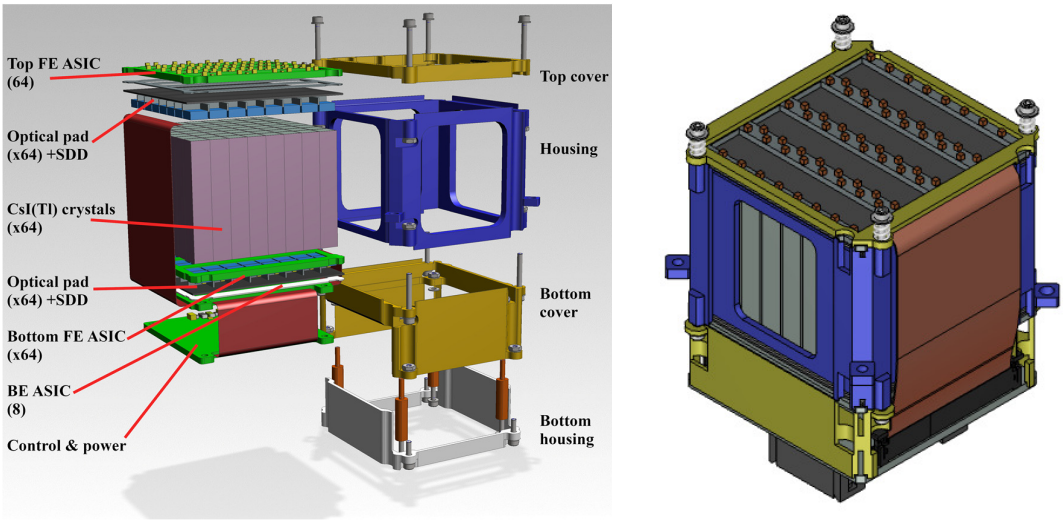

Figure 4-14 XGIS detector Module design.

Table 4-3 Main characteristics of a XGIS camera.

Energy band	2 keV -10 MeV
# detection plane modules	100
# of detector pixel/module	8x8
pixel size (= mask element size)	4.5x4.5 mm^2
Low energy detector (2-30 keV)	Silicon drift Detector (450 µm thick)
High energy detector (>30 keV)	CsI(Tl) (3 cm thick)
Discrimination Si/CsI(Tl)	Pulse shape analysis
Dimension (cm)	49x49x74
Power (W)	123.0
Mass (kg)	72.0

Table 4-4 XGIS data load foreseen for the different THESEUS modes.

	Imaging	**Gamma ph by ph**	**Total**
Survey mode	0.2+	2.5 *	2.7
Follow up mode	-	0.3**	0.3
Burst mode	-	3.6 **	3.6

4.2.2 Interfaces and resources

The body envelope of an XGIS Camera is 600x600 mm at the mask level and 566x566 mm at the basis of the Camera support structure. The two Cameras have an inclination of +20° and -20° with respect to the S/C X-axis. The height of the Camera is 910,8 mm (mask to farthest point of the support). The body envelope of an XSU box is 337x236x116 mm. The weight of one camera and one XSU including contingency are 78.1 kg and 9.5 kg respectively, the harness is 4.8 kg. The main thermal interfaces with the S/C are a Cold Finger flange visible in Figure 4-11 connecting the top PCB-SDD layer to the heat pipes coming from the spacecraft radiator dedicated to XGIS and the base of the Titanium support frame bolted to the payload platform. To maintain the temperature of the top PCB around 10 °C so ensuring the best performances of the SDD, and having the S/C platform at 20 °C the Cold Finger should be maintained at 5 °C. Overall one camera must dissipate via radiative and conductive means about 50 W (without contingency). The main thermal interface of XSU box is its baseplate, the thermal load to dissipate is 29.3 W. As shown in Figure 4-12, the XGIS DHU provides instrument control for the two XGIS Camera units, as well as data processing, time management, instrument calibration, housekeeping (HK), and the switching of unregulated power. In more detail:

- Data Interfaces: The XGIS DHU interfaces with the XGIS Camera units via the two BEE units. Data, telecommands, and HK data are communicated between the DHU Digital Processing Board and the BEE via a single (cold-redundant) SpaceWire connection. The XGIS DHU interfaces with the S/C On-Board Digital Unit and Memory Management Unit (MMU) through a SVM-mounted SpaceWire Routing Switch (described in §4.4.1). The DHU also receives PPS signals from the S/C through dedicated low-jitter lines. As the nominal Master DHU, the XGIS DHU also interfaces with the other I-DHUs. This is achieved by SpaceWire connections through the SpaceWire Router. The data load in Gbit/orbit in one orbit for both XGIS cameras is shown in Table 4-4. It assumes an average background rate of about 6 events/cm^2/sec, a burst average count rate of 10 events/cm^2/sec, a burst lasting 1000 seconds with a follow up lasting 420 seconds, and 1 burst/orbit.
- Power Interfaces: The XGIS DHU's PSB receives an unregulated 28 V (TBC) from the S/C primary power line. The PSB passes the unregulated power to the two XSUs and is responsible for ON/OFF switching of the power. The PSB also conditions the unregulated power, generating the required voltages for each board of the DHU. Overall, the max power dissipation, with contingency are: two Cameras, 119 W; two XSU, 70 W; and the DHU 22 W, respectively.

Table 4-5 XGIS system main characteristics.

Energy range	**2–150 keV**	**> 150 keV (up to 10 MeV)**
Partially coded FoV (PCFoV)	77 × 77 deg^2	
FoV		2π sr
Peak eff. area	~500 cm^2	~1000 cm^2
XGIS sensitivity (two combined cameras)	End-of-life >10^{-8} cgs over 2–30 keV in 1 s, and > 3x10^{-8} cgs over the 30–150 keV range in 1 s	> 3x10^{-7} cgs over the 150 keV–1 MeV energy range in 1 s
Angular resolution	< 120 arcmin	
Source location accuracy	≤ 15 arcmin 90% confidence level in the 2-150 keV energy band for a source with SNR > 7	
Energy resolution (EoL)	≤ 1200 eV FWHM @ 6 keV	≤ 6 % FWHM @ 500 keV
Relative timing accuracy	7 μs	

4.2.3 Operation

Figure 4-15 shows the controllable operational modes managed by the DHU. In Observation Mode, the XGIS will fulfil the THESEUS science-driven modes that are reported in the following:

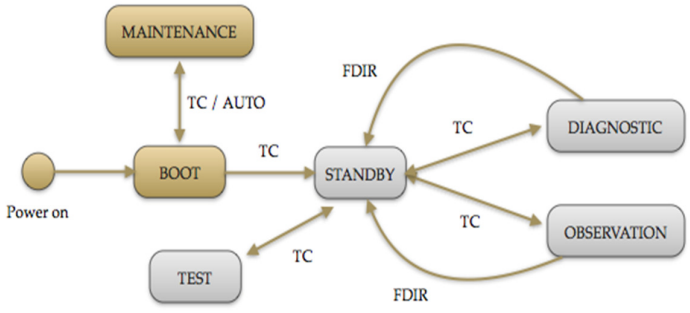

Figure 4-15 Overview of the XGIS operation modes and transitions.

- Survey ("burst hunting") Mode: monitoring and looking, with different methods for GRBs within the FoV.
- Burst Mode: in case a detected GRB, XGIS switch to the photon-by-photon mode.
- IRT Follow-up Mode: XGIS operates as in Survey Mode.
- External Trigger Mode: with a GRB observation triggered externally to THESEUS, trigger, XGIS will operate as in survey mode.
- IRT Observatory Mode: XGIS will operate as in Survey Mode.

4.2.4 Heritage and key technologies

SDD, ASIC and detector assembly are the key technologies for XGIS. SDD has been used in many experiments on ground and proposed for space mission as for example the Large Observatory for X-ray Timing (LOFT) ESA M3 candidate mission, and eXTP as well for the nano-satellite constellation High-Energy Rapid Modular Ensemble of Satellites (HERMES). A strong heritage came from the research program ReDSoX financed by INFN (Istituto Nazionale di Fisica Nucleare) and co-financed jointly by the "*Fondazione Bruno Kessler*" for the part related to the SDD technology, within this program a first version of the full SDD detector array (composed of 64 elements) has been simulation, designed and manufactured at FBK. The parametric and functional verification phases are ongoing. The availability of high-performance detectors is not enough to achieve a high-performance instrument. A read-out ASIC capable of exploiting the detector performance is also required. The ASIC development team within the THESEUS consortium, consisting of Polytechnic of Milan and University of Pavia, acquired know-how and expertise over the last 20 years, successfully developing several mixed-signal ASICs, specific for X- and γ-ray detectors, which represent the technological background on which the ***ORION*** ASICs for THESEUS are based. The previously developed devices are:

- The ***StarX32*** ASIC has been developed for an ESA tender. The ASIC is designed to be connected via bump-bonding to a silicon or GaAs detector, consisting of 32x32 pixels with 300x300 μm pitch.
- The ***VEGA*** ASIC has been specifically developed for the LOFT mission and is presently been exploited also in the eXTP.
- The ***LYRA*** ASIC chipset has been specifically developed for the HERMES mission, which aims to the detection and localization of GRBs through a constellation of more than one hundred nano-satellites. It will be tested in-flight in the next two years

CsI(Tl) scintillators with solid state readout is a well proven technology already flown in several space missions (INTEGRAL, AGILE, Fermi). In all these instruments the scintillators readout was achieved using Si-Photodiodes made with PIN-technology. PIN and SDD have the same Quantum Efficiency, but SDD has a much smaller capacitance its electronic noise figure is is between 50 and 100 times less that in PIN. The IBIS-PICsIT instrument on board INTEGRAL is an example detector plane composed of scintillator detectors tightly packaged to form a position-sensitive instrument with a concept similar to the XGIS one.

4.2.5 Expected performances

The main expected performance of each XGIS camera is summarized in Table 4-5. Figure 4-16 shows the effective area as a function of photon energy and off axis angle, while Figure 4-17 shows the sensitivity as a function of exposure as well as an example of source location accuracy (both figures refer to the combination of the two cameras). The XGIS response as a function of photon energy and off-axis angle were derived from Monte-Carlo simulations making use of instrument and spacecraft GEANT4 mass models. The particle-induced background level, spectrum and orbital modulation (outside the SAA) were evaluated by combining these models with the predictions of the ESA-validated trapped proton radiation models for the foreseen altitude and inclination of the THESEUS orbit.

4.3 IRT

The main goal of the Infra-Red Telescope (IRT) on board the THESEUS mission is to detect, identify and measure the redshift of GRB afterglows detected by SXI and XGIS, especially those at high redshift (z>6). This task has to be accomplished on board and in real time. In addition, IRT will be used to characterize the afterglows, through spectroscopy for a part of them (spectroscopic redshift, neutral hydrogen absorption, presence of metals), and it can be used as a multi-purpose agile NIR observatory in space through the implementation of a dedicated GO programme, and a ToO programme, with special emphasis on multi-messenger and time-domain astrophysics. The IRT responsibility is shared among ESA (telescope, thermal

control, detector procurement) and a consortium, led by France in collaboration with Switzerland and Germany, that will deliver the IRT instrument.

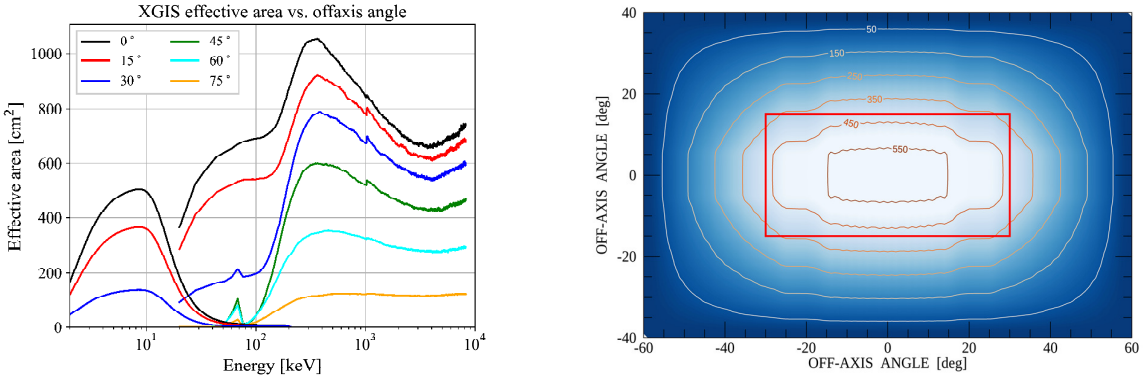

Figure 4-16 Left: off-axis effective area as a function of energy, for different off-axis angles. Right: XGIS effective area at 10 keV as a function of off-axis angle for the combination of two units. The rectangle at the centre corresponds to the SXI FoV.

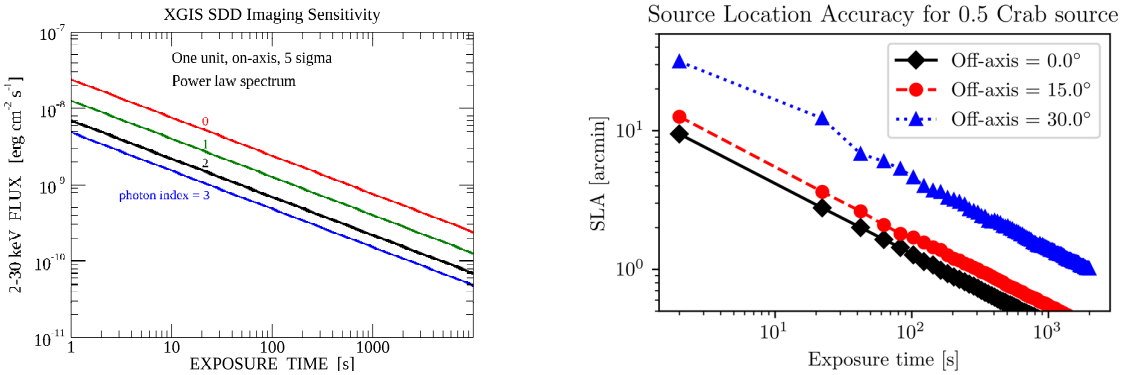

Figure 4-17 Left: XGIS imaging sensitivity (5σ confidence level) as a function of exposure time provided by the SDDs in the 2-30 keV range for a single XGIS unit and sources in the fully coded field of view (the central 10x10 deg² of each unit's FoV). The different lines refer to sources with a power law spectrum with the indicated photon index. By combining the two units, the sensitivity plotted here is achieved over a 60x30 deg², similar to that of the SXI. Right: XGIS Source Location Accuracy (SLA) as a function of exposure for a 500 mCrab source detected at different offset angles.

4.3.1 Instrument description

The IRT is a 70 cm Korsch telescope, optimized for an off-axis line of sight (LoS) of 0.884° (for a description of the IRT telescope see §4.3.6). The optical scheme of the telescope is sketched in Figure 4-18. The optical design will implement two separated fields of view, one for photometry with a minimal size of 15 x 15 arcmin (potentially extendable to 17 x 20 arcmin), and one for spectroscopy of 2 x 2 arcmin. On the photometric field of view the IRT will be able to acquire images using five different filters (I, Z, Y, J and H) and on the spectroscopic field of view the IRT will provide moderate resolution (R~400) slit-less spectroscopy in the 0.8-1.6 μm range. The different observation modes will be implemented through the design of the IRT Camera (IRT-CAM) that includes a filter wheel, carrying the different optical filter, as well as a grism, which will allow for spectroscopy, see Figure 4-19. The IRT-CAM will consist mainly in a structure (IRT-STR), an isostatic

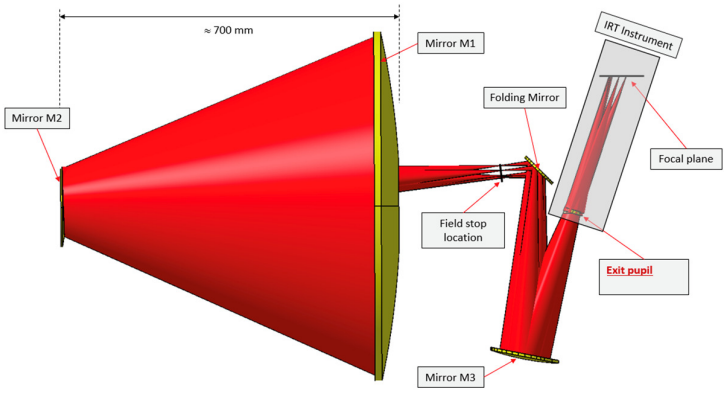

Figure 4-18: IRT Optical scheme. M1, M2, M3 are under ESA/Prime responsibility. The exit pupil represents the optical interface with the IRT-CAM provided by the consortium.

mount (IRT-ISM), a filter wheel assembly (IRT-WA), a calibration unit assembly (IRT-CUA), and a focal plane assembly (IRT-FPA), hosting the detector and its associated cold electronics.

The whole structure will be covered with thermal isolating blankets. The detector currently envisaged for the IRT FPA is a Teledyne H2RG, sensitive in the 0.7-2.5 µm wavelength range.

4.3.2 Interfaces and resources

The optical interface of the IRT-CAM and the telescope is at the telescope exit pupil corresponding to the filter positions in Figure 4-19. The IRT instrument consists of the IRT-CAM and of the IRT Data Handling Unit (IRT-DHU). Both the IRT-CAM and the IRT DHU will be provided by the Instrument Consortium to the Prime Contractor through ESA as Customer Furnished Items. The integration of the IRT-CAM and IRT-DHU with the IRT telescope onto the spacecraft will be the responsibility of the Prime contractor. The IRT-CAM is accommodated onto the IRT Main Bench that also supports the telescope. The cooling of the IRT Camera is ensured thanks to two Cold Fingers (CF1 and CF2) connected to a cryo-cooling system (the cryo-cooler(s) will be provided by the Prime Contractor and the thermal interface to the instrument consists in the cold fingers). Figure 4-20 shows the intended position for CF1 and CF2: CF2 will be on the IRT-WA and CF1 on the IRT-FPA. Taking into account the scientific requirements in terms of thermal background, we defined the following temperatures for the IRT-CAM: the ISA (the support structure) and the WA shall be kept at 160K (CF2), while the detector assembly (DA) and the FPA shall be kept at 120K (CF1), thanks to the cryo-cooler(s). To maintain the temperature stability of the camera (at IRT-FEE, IRT-FPA, and IRT-WA levels), we will consider, at instrument level, to use temperature probes as well as heaters that shall be controlled by a dedicated electronic (function within the Detector Control Electronics IRT-DCU and Filter Wheel control electronics IRT-WCU (TBC)). As a baseline, we consider that the cryocooler will provide the specified temperature and thermal power at the cold finger (CF1 and CF2) and that the fine control of the instrument temperature is ensured by the IRT using heaters (opened or closed loop).

Table 4-6 IRT resources.

Element	Mass (kg)	Average Power (W)	Maximum/Average Required Telemetry (Gb/day)
IRT-CAM	32.5	36.2	
IRT DHU	11.0	30.1	
IRT instrument total	**43.5**	**66.3**	**40/13.5**

Concerning the power dissipation at CF1 and CF2, it is expected to be in the range1.9-2.8 W, and 2.8-6.7 W, respectively. Figure 4-20 depicts the overall electrical architecture of the IRT Instrument. It includes a warm electrical sub-assembly (DHU) and cold electrical sub-systems: the IRT-FPA, the IRT-WA and the IRT-CUA. The IRT DHU will have digital interfaces with the S/C and the IRT FPA, and analogue interfaces with the FPA (bias and signals), with the WA (motor control) and with the CUA. A primary power interface with the S/C will complete the electrical interfaces. The main dimensions of the IRT Camera are shown in Figure 4-21. The mechanical interface to the optical bench is a hexapod, each of its six feet is bolted with three screws. The IRT-DHU main dimensions are 210 mm x 228 mm x 220 mm (not shown). Given the design and interfaces presented above the total mass and power budget for the IRT, excluding harnesses, and including typical phase A margins is reported in Table 4-6, where we also report the telemetry budget. The latter is based on the fact, that a series of images in different

filters are needed to acquire the GRB afterglow position and the photometric redshift (see later). For a complete sequence up to the photometric redshift we estimate that at least 252 Mbytes of data need to be transmitted to ground. If we include the GRB Characterization Mode between 25 Mbytes and 1.2 GBytes per GRB are needed. For the GO mode, about 80 kbits/s are needed.

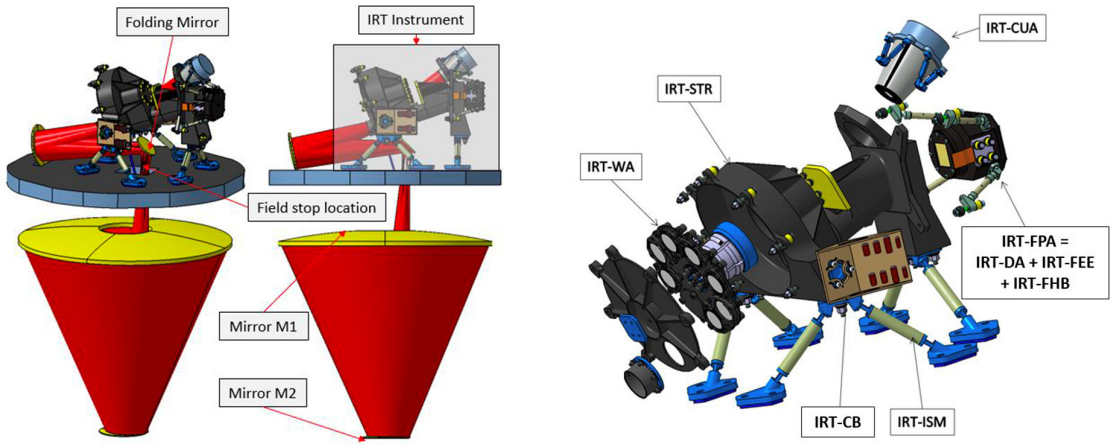

Figure 4-19: Left: Full optical scheme of the IRT, including IRT-CAM and optical bench. Right: exploded view of the IRT-CAM and its subsystems (without insulating blankets).

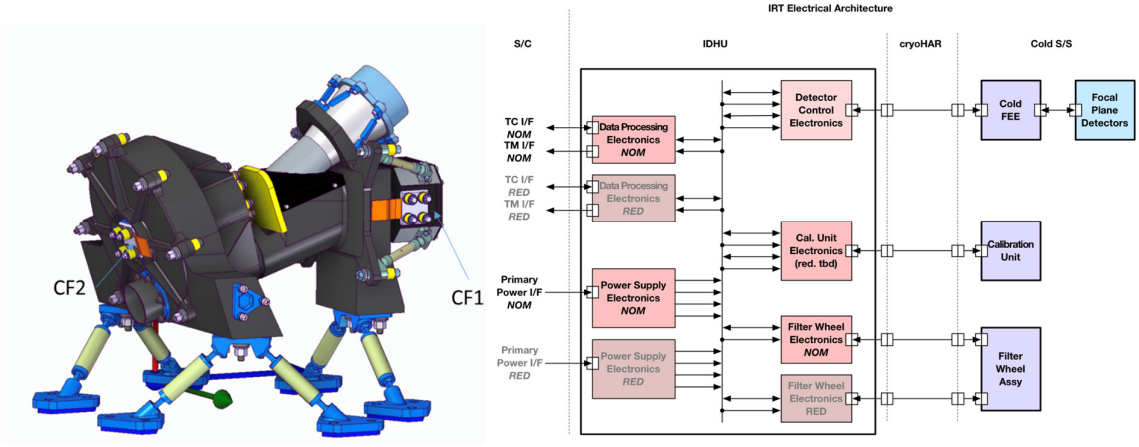

Figure 4-20: Representation of the IRT instrument cold fingers (orange colour, left) and electrical architecture (right).

4.3.3 Operations

The IRT operation sequence after a GRB trigger is summarized in Figure 4-22. Once a GRB is detected by the SXI and/or the XGIS, a slew is requested to the platform in order to place the GRB error box within the IRT photometric FoV. Then, when the S/C is stabilized, the IRT enters *the Follow-up* Mode, where a 150 s exposure for each of the available filters (I, Z, Y, J and H) is acquired; the depth of each image shall exceed 20.4 mag (AB). Thanks to these images and an on-board catalogue (based on Gaia and Euclid surveys), the IRT shall be able to autonomously identify the GRB afterglow candidate, compute its coordinates (to a better than 5 arcsec

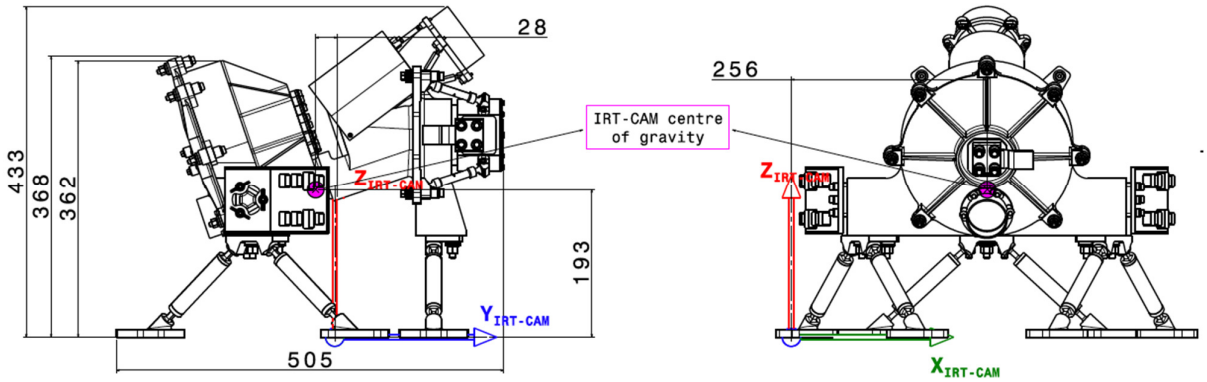

Figure 4-21: IRT Instrument main dimensions.

accuracy) and its photometric redshift (expected accuracy better than 10%) and send this information to ground via the VHF system. Then, as a function of the source flux, the IRT enters either the *characterization mode*, which includes spectroscopy mode for 1800 s (if the source is brighter than 17.5 mag (H, AB)) followed by 1800 of deep imaging, or directly the Deep Imaging Mode for 3600 s. In order to activate the spectroscopic mode, the satellite needs to perform a small slew to put the afterglow positions within the 2x2 arcmin spectroscopic FoV.

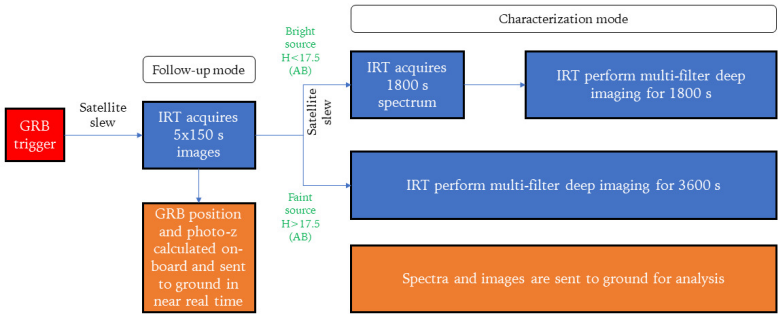

Figure 4-22: IRT science operations after a GRB trigger.

Except from GRB follow-up, the IRT can be operated in GO mode: in this mode, in order to cope with the allocated telemetry resources, only three windows of 200 x 200 pixels centred on three sources (one is the target, the other two astrometric and photometric references) will be transmitted to ground. IRT can also be operated in calibration mode.

4.3.4 Heritage and key technologies

The detector chosen for the IRT is the Teledyne Hawaii 2RG with a 2.5 µm cut-off (although due to cooling restrictions it will be used only up to 1.8 µm). It is the same detector type that is currently used in the Hubble WFC3, and that will be flown in the Euclid NISP instrument. It has, hence, a very high TRL level. Another key technology that is inspired from the NISP, is the use of SiC for the IRT-CAM structure. The latter allows for excellent mechanical and thermal stability, minimizing thermo-elastic deformations, which are a major source of astrometric uncertainties in low-Earth orbits, due to the rapidly evolving thermal environment. Globally, IRT-CAM benefits greatly from the experience acquired on the Euclid NISP instrument.

4.3.5 Expected performance

The main IRT characteristics in terms of expected scientific performances are summarized in §3.2.2 and §3.2.3. In order to precisely estimate the photometric capabilities of the IRT, we have developed a simulation tool, that takes into account the detector performance (readout noise, dark current, pixel size, …), the operating conditions (temperature, photometric aperture), the satellite planned pointing (expected zodiacal light background and out of field straylight), the observation conditions (source characteristics, exposure and individual frame duration), the filter characteristics, and the optical imperfections of the system. The latter

include the satellite jitter and drift, which together with the detector readout noise are the main limitations to the instrument sensitivity.

Table 4-7 IRT main characteristics.

IRT characteristic	Value
Photometric wavelength range	0.7-1.8 μm
Spectroscopic wavelength range	0.8-1.6 μm
Photometric field of view	15 x 15 arcmin (goal: 17' x 20')
Pixel size/scale	18 μm / 0.6 arcsec
Required Photometric sensitivity (AB, in150 s, SNR=5) for each implemented filter	I: 20.9 (goal: 21.3) Z: 20.7 (goal 21.2) Y: 20.4 (goal: 20.8) J: 20.7 (goal: 21.1) H: 20.8 (goal: 21.1)
Expected photo-z accuracy	< 10%
Astrometric accuracy	< 5 arcsec in near-real time < 1 arcsec after ground processing
Spectroscopic field of view	2 x 2 arcmin
Resolving Power at 1.1 μm	> 400
Required Spectroscopic sensitivity (AB, H filter, 1800 s, SNR=3 for each spectral bin)	17.5 (goal: 19)

Taking all these effects into account, we estimate both the expected limiting sensitivity with and without astrometric correction due to the satellite drift. In fact, in order to simplify the on-board processing, no drift correction will be applied for the near-real time on-board processing. Our simulations indicate that we are always compliant with the requirements. In addition, some extra margin can be gained by the optimization of the filters bandpass. With these sensitivities we expect to be able to determine the photometric redshift (through the determination of the Lyman-alpha break wavelength) to an accuracy of better than 10% in more than 90% of the observed GRBs, cf. §3.2.2 and Figure 4-23. Due to the detector passband we are limited to redshifts in the range 5.5-12. Detailed simulations have been performed also for the IRT spectroscopic mode. In this case, given the longer exposure of 1800 s (with individual frames of 60 s), the satellite drift plays an even stronger role. In order to assess the IRT spectroscopic performance in the most realistic way, we used several S/C simulated drift patterns, expected for the THESEUS orbital conditions and the expected attitude control system performances. We also weighted our results in terms of expected zodiacal background over the foreseen THESEUS sky pointings (see §3.3.2). The source and background signals have been estimated for each detector pixel, and some margin has been taken for imperfect stacking of the single frames (note that in order to stack the individual 60 s frames we used the "0th" spectral order as a guide). We could in this way estimate the expected SNR of each spectral bin (summed over three detector lines), and this as a function of the resolving power for each wavelength. With this performance we

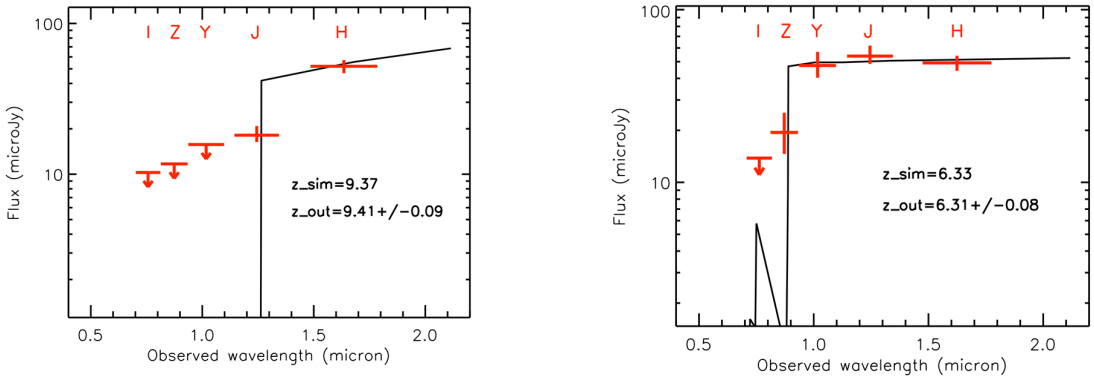

Figure 4-23: Two examples of simulated photometric data and model fitting.

expect to be able to determine the spectroscopic redshift of GRBs (also for those at z < 5.5; cf. §3.2.2), and, for the brightest ones, to determine the neutral absorption column density and to detect the presence of metals (cf. §3.2.3).

4.3.6 IRT telescope

The IRT payload element consists of an infrared telescope to be procured and developed by a Prime industrial contractor under ESA contract and of the IRT instrument to be delivered to the Prime through ESA by the THESEUS consortium as a Customer Furnished Item. The telescope optical concept is under responsibility of ESA to guarantee any optical, thermal, and mechanical concepts developed by the different prime contractors can interface with the single design of the IRT instrument. This section describes the current telescope optical design (Figure 4-24,) but does not cover the different implementations of the primes, e.g. the mirror support structure materials, the mirror coating type, the use or not of a refocusing mechanism and its type, the baffle design, and the telescope support structure geometry, the thermal concept etc.

*Table 4-8 IRT telescope key figures. Note: *Thermal emission being part of the telescope straylight requirement, the temperature is actualy a free parameter. **Telescope and interface contribution only.*

Type	Focusing off-axis Korsch
Entrance pupil	700 mm
M1-M2 distance	675 mm
Exit pupil	36 mm
Collecting area	> 0.34 m^2
Wavelength range	700-1800 nm
Throughput	> 80%
Focal length	6188 mm
Temperature*	240 K
LoS (photometric)	0.884° from M1-M2 axis of symmetry
Straylight requirement**	70 photon/m^2/arcsec^2/s
Image quality requirement (at 1800 nm wavelength)**	50% of the encircled energy diameter < 1.28 arcsec 80% of the encircled energy diameter < 2.29 arcsec

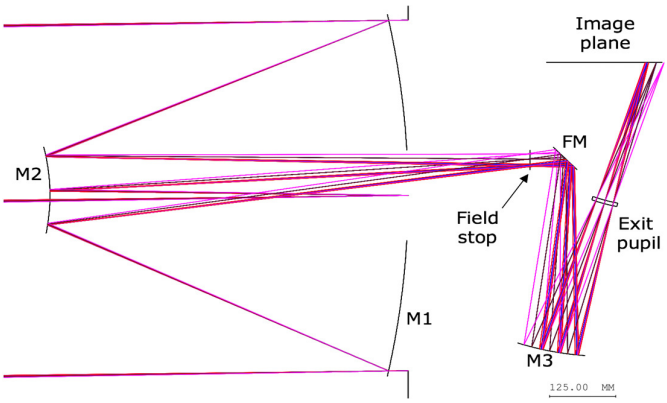

Figure 4-24: IRT telescope optical concept.

The IRT telescope is a focusing three-mirror Korsch configuration with an off-axis field. Between the secondary and the tertiary mirrors of the Korsch, there are two additional optical components: a field stop at the intermediate focus to reduce stray light and a flat folding mirror (FM in the figure) to facilitate accommodation in the SC. Note that in the absence of the folding mirror, the three powered mirrors of the Korsch (M1, M2 and M3) are coaxial, the common axis being coincident with the axis of radial symmetry of each mirror. The mirror shapes are conics of revolution. The aperture stop is at the primary mirror. Its image, the exit pupil, in the converging output beam is the interface with the IRT instrument.

5 Mission design

5.1 Mission Analysis

5.1.1 Launch vehicle Characteristic

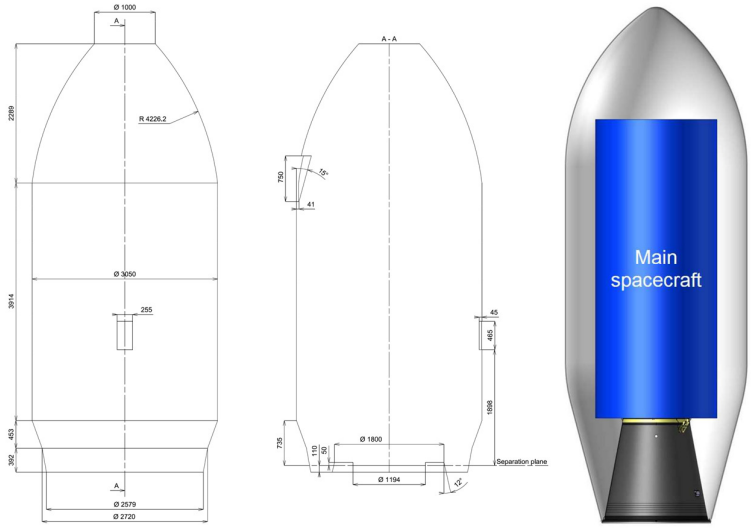

Figure 5-1 the usable volume inside Vega C fairing for single launch configuration (from the VEGA C User's Manual, Issue 0, Version 0, May 2018).

The mission and systems are designed for launch with a VEGA-C vehicle (and Ariane 62 as back-up, Figure 5-1). The launcher performance into THESEUS nominal orbit is above 2,500 kg including adapter and ESA launch margins. This capability allows for very comfortable mission margins over the SC maximum wet mass. The usable volume inside VEGA-C fairing drives the spacecraft configuration design and payload accommodation as explained in the dedicated §5.2.3.

5.1.2 Orbit

The THESEUS space segment will be placed directly into an equatorial Low Earth orbit (LEO) with an inclination of 5.4° and nominal altitude from 550 km to 640 km. There are no seasonal constraints on the launch date. The Right Ascension of the Ascending Node (RAAN) is left unconstrained; due to the Earth's oblateness, precession of the line of nodes will take place during the mission: a 360° rotation of the RAAN, assuming the reference orbit, will take place every 49.5 days. The orbital period at nominal reference altitude of 600 km is 96.7 min (decreasing to 95.6 min for an altitude of 550 km and increasing to 97.5 for an altitude of 640 km)

This orbit provides near-complete shielding of the spacecraft by the geomagnetic field against damaging solar particle events and Galactic cosmic rays. Moreover, the spacecraft is designed to maintain the nominal altitude within a 10 km corridor driven by controlled spacecraft orbital decay constraints, and that also ensures a low and stable background as required by the XGIS non-cosmic X-ray background threshold (i.e. stable within 10% over timescales of ≤10 min over the mission in-orbit life time and outside the South Atlantic Anomaly region; cf. the scientific justification for this requirement in §3).

The nominal inclination value is almost the lowest that can be reached by a Launch from Kourou without requiring the Launch Vehicle to perform an orbit plane change (dog-leg manoeuvre).

This inclination together with the nominal operational altitude choice depends on several factors which are discussed in the following sections, but none are especially driving and the suitability of the environment of this orbit for the THESEUS performance has been demonstrated in previous missions such as BeppoSAX and AGILE.

5.1.3 Eclipses

The spacecraft design allows operations of the payload during eclipses. The eclipses, occurring at every orbital revolution around the Earth, last between 33.7 and 35.7 minutes for the nominal reference orbit parameters with duration variations by only ~10 s per 50 km altitude change.

5.1.4 Orbit decay

The mission shall comply with ESA debris avoidance regulations which require that the Spacecraft re-enters into the Earth atmosphere within 25 years from end of operations. Under this criterion, any altitude between 550 km and 640 km may be selected, trading maintenance delta-V vs mission extension capabilities.

5.1.5 Ground station coverage

The ground stations considered for the THESEUS mission belong to two subgroups:

- the mission operations ground station (baseline nominal, plus backup) used for telemetry, tracking and command (TT&C);
- the very high frequency (VHF) ground stations used for the burst/transient alert system.

The nominal ground station for TT&C is ASI Malindi MLD-2B (13-m) with the ESA Tracking station network (ESTRACK) Kourou-1 (15-m) as backup; the coverage data for both stations is reported in Table 5-1 for the reference orbit. Concerning the VHF ground stations, coverage information is provided in §6.

Table 5-1 Mission operations ground station coverage data (5° minimum elevation assumed).

Station	Average contact time per mass (min)	Minimum contact time per pass (min)	Average contact time per day (min)
Malindi	10.7	9.9	149.2
Kourou	10.4	9.1	145.1

5.1.6 South Atlantic Anomaly pass

The low altitude and inclination serve to minimise the van Allen trapped charged particles seen by the SC, avoiding especially the South Atlantic Anomaly (Figure 5-3). A study of the populations and effects of these sources of trapped protons has been conducted during the assessment phase (by ESA) using PSB97 trapped proton model (SAA defined as region of space where flux for particles with energy >20MeV is above threshold of 1 p+/cm^2/s) and including comparison with previous missions in LEO, e.g. BeppoSAX.

Present simulations show that for an altitude of 600 km, the fraction of the orbit exposed to >20 MeV protons is about 15% of the orbital time. This increases by a few percentage points at 640 km. However, there is a significant spread in results depending on the model used (PSB97 vs AP8/AP9). ESA is currently concluding a technology development activity where results from actual spacecraft measurements in the Van Allen belt regions crossed by THESEUS will be used to tune the existing model, potentially reducing uncertainties.

5.1.7 Mission phases

The operational phase of the mission has been scoped for Launch and Early Orbit Phase (LEOP) of ~7 days, a S/C (satellite and payload) commissioning lasting for 3 months. It is proposed to execute a Calibration and Performance Verification phase which includes an initial Science Demonstration, lasting 2 months. A total Operational Phase of 4 years includes a final deorbit phase (disposal) of about 1 month. Assuming nominal allocation for safe modes, calibration, collisional avoidance during mission lifetime, the net time for nominal science observations is therefore estimated to be about 3.45 years. For the disposal, if an uncontrolled re-entry is baselined at end of mission, the casualty risk on ground due to remaining spacecraft fragments is close to the

mandatory limit of 10^{-4}. Therefore, the Spacecraft is designed conservatively for a controlled de-orbit. This can be achieved by a sequence of propulsive manoeuvres lowering progressively the orbit perigee.

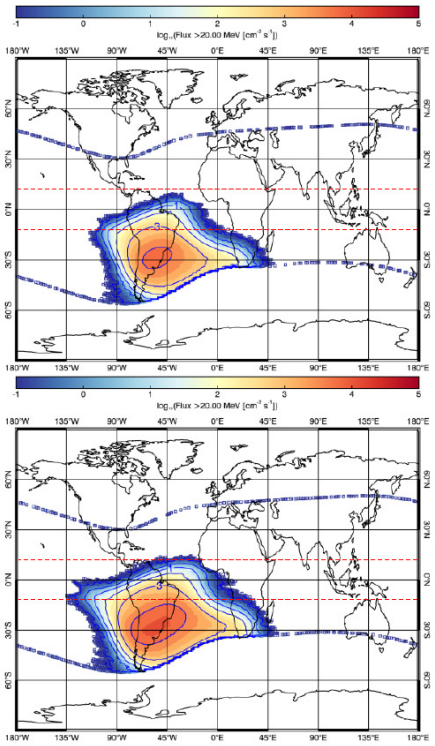

*Figure **5-2** (left) shows the flux maps for proton integral flux >20 MeV for all latitudes at 530 km (top) and 650 km (bottom). Note: ±6 degrees latitude range is indicated by dashed red lines (obtained form from ESA RELLENA contract).*

The perigee of the last full orbit cannot be too low because the spacecraft needs to be fully controlled and quite large aerodynamic torques will be experienced at altitudes below 200. For a strategy where the total deorbiting is split in 4 burns, the starting altitude is 640 km (worst case) and average thrust of ~60N is available on-board, the required ΔV is ~215 m/s. This totally dominates the propellant budget.

For the THESEUS mission, a collision probability level of $2x10^{-5}$ (which implies a risk reduction of 90% as common practice for ESA missions) is required. This implies ~3 manoeuvres per year, at a cost of 0.22 m/s delta-V per year. This would lead to a total delta-V of 0.9 m/s for the 4-year nominal mission duration, plus an additional 0.2 m/s for the possible mission extension. A total delta-V of ~1.1 m/s is sufficient for collision avoidance manoeuvres for 5 years independently of the orbit altitude.

5.1.8 Concept of operations

Overall, the THESEUS nominal mission concept of operation consists in a predefined mission timeline (MTL base) uploaded by MOC on a weekly basis which contains the nominal mission observation plan. The MTL base contains the science observation plan based on SC attitude pointing law for the Survey Mode together with all the required SC operational and planning aspects (e.g. start / stop, downtimes, maintenance manoeuvres, collision avoidance, etc.). The objective of the MTL base is the autonomous detection (on-board by the 2x SXI and 2x XGIS wide field monitors) of a candidate gamma-ray source (short or long GRBs), X-ray variable or transient source, any of them a.k.a. target source or trigger. Details of the spacecraft operations modes are given in §6.

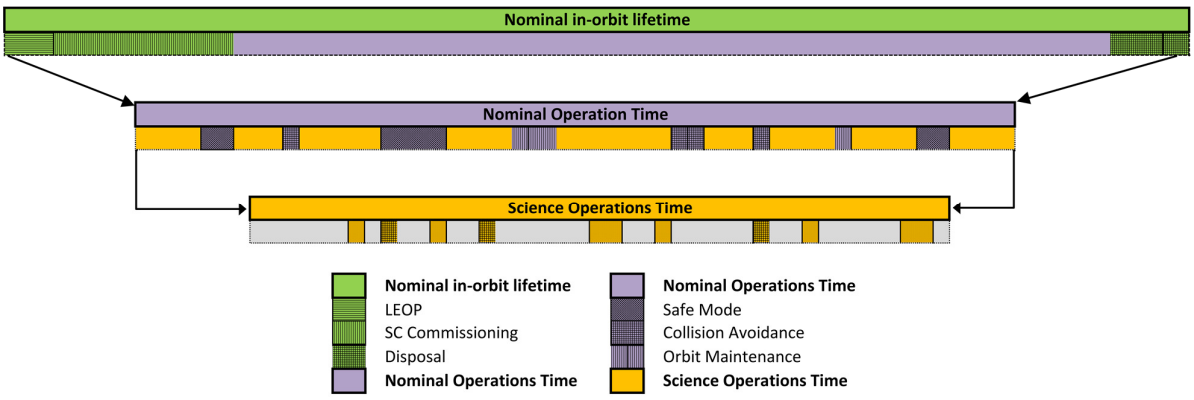

Figure 5-3 - schematic representation of the time definitions adopted for THESEUS Phase A. Note allocations are not to scale. They are provided only for conceptual reference.

5.2 Spacecraft design

5.2.1 Spacecraft overview

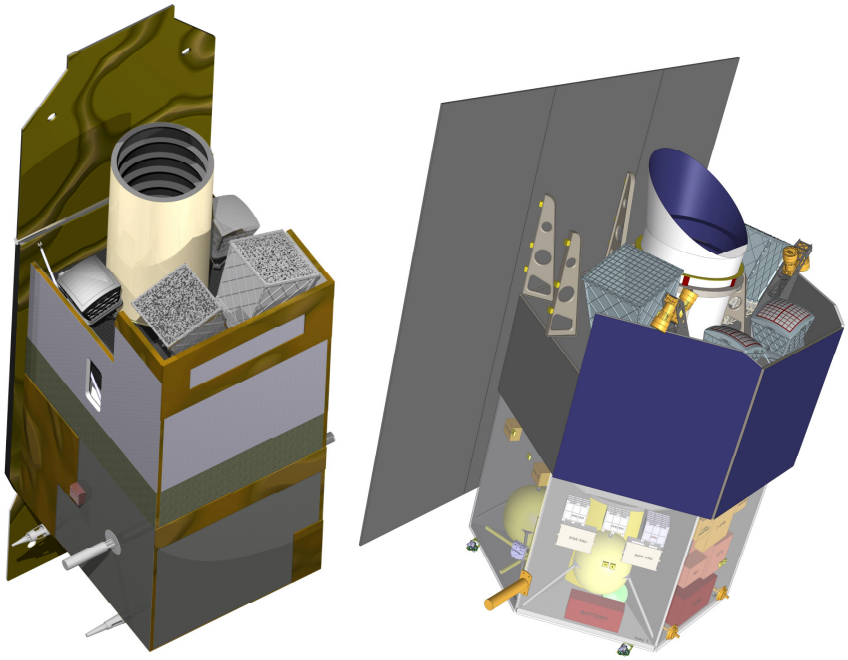

Figure 5-4 - Schematic view of the spacecraft design for the Phase A ADS (left) and TAS (right) Studies.

The key aspects of the design of the THESEUS spacecraft (SC) are driven by the requirements of the three different instruments and the on-board autonomous (i.e. without ground intervention) capabilities. More specifically, as far as the payload is concerned, the drivers are accommodation and the operational requirements for the instruments thermal control in a low Earth orbit considering the field of regards requirement (≥50%) and the associated thermo-elastic stability to comply with the required pointing performance. Both factors contribute to the achievement of sensitivity and astrometric requirements of the instruments to enable the THESEUS science objectives.

The implementation of the autonomous on-board capabilities does not call for novelty HW&SW design. Autonomy needs to be developed carefully for satellite applications. Today, FDIR as well as sub-mode transitions are handled typically up to a certain level in an autonomous manner. On some missions, also the main mode transitions are handled autonomously, but with care and corresponding parameter flags which allow to switch these transitions on and off. The main concern with respect to more advanced autonomous spacecraft capabilities is related to their difficult pre-launch verification.

During the current assessment Phase, two SC designs have been derived by industrial teams, leading to similar concepts of the bus design based on 3-axis stabilised spacecrafts with box shaped structure, essentially with similar modular architecture based on a SC configuration divided into a Payload and a Service Module (PLM and SVM) with a 1194-mm launcher I/F. From both Primes' spacecraft concepts, a generic subsystem design can be extracted and the main highlights are provided in Table 5-1. Overall, the avionics, attitude control, and electrical systems aim to be based on a Low Earth Orbit (LEO) platforms developed for Earth Observation and for commercial programmes which enables cost savings in hardware procurement and AIV/AIT.

Both industrial designs preliminary satisfy all key spacecraft requirements, and there is very good confidence that a mission profile satisfying the overall science and mission requirements will be achieved at the end of Phase A. A schematic view of the corresponding designs is shown in Figure 5-4.

5.2.2 Spacecraft subsystems

The table below summarizes the main highlights of the spacecraft subsystems design (IRT telescope is addressed in §4.3.6).

Table 5-2 Main highlights of spacecraft system design.

THESEUS – Subsystems design Summary	
AOCS	- Based on 4 star trackers optical heads configuration with 2 always in tracking, coarse rate sensor and sun sensors. - (3N+1R) Reaction Wheels to provide the required SC agility and magnetic torquers for quasi-continuous desaturation.
Data Handling	- Standard Data Handling System architecture with Spacewire router for I/F with the payload - High heritage OBC that offers the required autonomy and FDIR capabilities. - MMFU (Mass Memory and Formatting Unit) of ~2Tbit that will provide sufficient data storage for Science and HK with 100% to prevent data loss through up to 7-day Ground outages. - Remote Terminal Unit for providing dedicated discrete and serial interfaces for all satellite equipment units. - On-board Global Navigation Satellite System (GNSS) to provide an additional PPS (Pulse Per Second) line to transfer the synchronisation signal from platform OBC to instruments.
TT&C Communications	- Based on off-the-shelf hardware. - S-band transponder with 2 low gain antennas (LGA) to provide omni-spherical coverage and nominal TM/TC. - X-band transponder and 2xLGAs with a TWTA (Travelling Wave Tube Amplifier) of 35W radio frequency output power is required to downlink the observation data at 8.3 Mbps and the baseline ground station.
Propulsion	- Monopropellant thrusters for de-tumbling at separation, for Safe Mode, collision avoidance, orbit maintenance and de-orbiting functions. - 4x96 l hydrazine tanks to provide the required 270 m/s (plus margins) propellant load for the mission.
Power	- Standard elements from LEO platforms developed for Earth Observation and for commercial programmes as PCDU (Power Control and Distribution Unit), battery and fixed and partly deployable solar array and Sun shield provided a total area of 13-16 m^2. - Maximum Power Point Tracking (MPPT) to cope with varying sun incidence angle and 28V unregulated bus for the payload I/F and to avoid losses in efficiency.
Structures	- Primary structure based on Aluminium honeycomb and carbon fibre reinforced polymer skins. - PLM carrying the IRT telescope and optical bench with additional tripods/balconies to support the monitors.
Thermal	- Cryo-coolers with compressors & Control Drive Electronics for the active cooling of the IRT instrument (filter wheel and detector) - East-west radiator coupling needed to provide lower sink temperature for instruments heat rejection demands. - Radiator area 10-12 m^2: SVM thermal control is fully passive and presents no critical issues; see in §4 more details of the payload thermal design details.

5.2.3 Payload accommodation

The main constraints driving the accommodation of THESEUS three main instruments can be summarised as follow:

- accommodating two XGIS units, two SXI units, the IRT instrument and the IRT telescope in a configuration fitting the Vega C rocket fairing, while
- avoiding direct sun illumination for SAA < 30 degrees, and
- preserving each of the unit's FoV unobstructed.

Both primes payload accommodation concepts are compliant. They are both organised in a similar fashion with a central IRT telescope surrounded by the wide-field monitors units. The exact location of these units is imposed by the choice of S/C configuration. Hereafter are detailed additional challenges that have shaped the payload accommodation.

The IRT telescope baffle height of more than 2 meters above the primary mirror - to avoid direct Earth impingement on M1 for pointings down to 20 degree away from the Earth limb - drives the SC sunshield height, the payload module height and to a certain extent the overall SC height and configuration. Both concepts show as a result an IRT instrument located deep in the SC surrounded by the SC SVM, and a structure

called IRT optical main bench interfacing between the IRT instrument and telescope and serving also as the main supporting structure for the other instruments.

As shown in §4.3, the IRT instrument accommodation is particularly complex; parts of the telescope optical elements are located within the instrument volume as well as the IRT cryocooling system.

The payload module should also provide enough radiating area to meet the instrument thermal needs summarized in the following section.

The payload structure should be rigid enough to fulfil pointing and coalignment requirements. For this reason, the payload module also accommodates in both concepts (TBC) the star trackers.

Three instrument DHUs, and the XGIS separate power supply units must be accommodated such that the harness length between the instrument and its DHU is less than 3 m. Note that each of the SXI units has a separate e-box located right underneath the SXI focal plane assembly between instrument bipods.

Last but not least the SC configuration concepts have been designed such as to allow for independent integration of the instruments to remain flexible with respect to the exact order in which instruments will be delivered.

THESEUS fourth payload element, the TBU is facing different accommodation constraints: it should be located such that the two antennae will be pointing towards Earth most of the time, and with a 1.6π sr unobstructed field of view. Both primes have thus chosen to locate the TBU antennae at the bottom of the SC within the SVM.

5.2.4 Payload thermal control

The payload thermal design is key to satisfy THESEUS science requirements. The thermal control design main drivers are: the instrument heat dissipations to be evacuated, the instrument temperature ranges and stabilities as defined in §4, and to be achieved in the challenging environment of the THESEUS baseline orbit and SC attitude pointing within the required FoR.

The payload thermal requirements throughout all mission phases are achieved by a combination of conventional passive and active thermal control techniques:

- The IRT telescope (optics and baffle) is passively cooled down to about 240 K. The different zones are thermally decoupled from each other using MLI and other insulating materials.
- The IRT camera unit requires heat rejection of 2W at118 K and 2.3W at 152 K at the thermal interfaces of the Focal Plane Assembly (FPA) and filter wheel, respectively. Active cooling by Pulse-Tube (PT) cryo-coolers is foreseen and several PT coolers options have been traded during Phase A. The proposed baseline is based on cryo-coolers in cold redundancy architecture, which provide the 50% cooling margin capabilities required at this stage of the study. These cryo-coolers, together with its compressors and control-drive electronics relay on European technology with flown heritage and demonstrated lifetime of more than 5 years and extrapolated lifetime over more than 10 years
- The SXI camera units require a focal plane cooled down to -30° C. This cannot be achieved using just a purely passive approach due to the continuous variation of the thermal environment, which in turn means that no surface with a constant view of deep space will be available as a radiator. The adopted solution is the use of Coupled Radiators East-West. This is a common solution in telecom satellites as demonstrated in Hispasat 1E. It consists of two aluminium radiators, coupled using two loop heat pipes with pressure regulation valves. This enhances the heat rejection capability of the spacecraft by using the radiator with the most favourable conditions at any point in time, i.e. while one of them faces Earth (hot radiator), with maximum absorbed heat fluxes (albedo and infrared), the other has direct view of deep space (cold radiator).
- The high-power dissipation of the XGIS camera units (70 W each if working at a detector cold finger interface goal temperature of -10° C) require radiator area of more than 3 m^2 , which is coupled via heat pipes in order to evenly distribute the heat through the radiator and minimise the temperature gradient.

5.2.5 Spacecraft pointing performance

The pointing requirements of THESEUS are directly flown down from each of the instrument performance needs. In particular the instrument sensitivities and required on-board astrometric accuracies drive the main requirements on the attitude control system and the thermo-elastic behaviour of the SC including the IRT telescope. The latter is especially challenging in the THESEUS orbit with a required field of FoR of 50%.

The main pointing control performance indicators driven the system are:

- provide Absolute Pointing Error (APE) <30 arcsec at 3σ to ensure the source falls into the IRT FoV after monitors' triggering;
- provide Relative Pointing Error (RPE) <1 arcsec at 3σ over 25 s to satisfy the IRT sensitivity (photometric SNR) requirement which limits the jitter of a source in the IRT field of view during follow-up mode;
- provide Mean Knowledge Error (MKE) over windows of 150 sec <18 arcsec at 3σ to comply with on-board astrometric requirement for the positional accuracy of 30 arcsec to be delivered on-ground by the burst alert data after IRT follow-up;
- provide Performance Drift Error (PDE) <1 arcsec at 3σ over 60 s to satisfy the IRT sensitivity (spectroscopy SNR) requirement which can be particularly sensitive to drift-induced point spread function smearing during spectroscopy characterization mode;

The above main drivers are relevant to the IRT Line of Sight over different phases of the mission. A rather good accuracy star tracker (i.e. few arcsec) can support a star tracker-based configuration for the baseline of the THESEUS attitude sensors, however the compliance could only still be guaranteed if it would be possible to have a good knowledge of the IRT LoS to star trackers misalignment over the entire environment boundaries imposed by the THESEUS orbit and FoR. Typically, on-ground alignment knowledge could be in the order of 10-20 arcsec, but it would be fundamental to limit the thermo-mechanical deformation over the mission otherwise such deformation would be in the order of 1-2 arcmin without taking particular means, meaning that none of the knowledge requirements would be fulfilled. Therefore, the activity effort from the Primes has aimed to find these particular means or solutions to overcome the thermo-elastic error contribution without additional cost or complexity such as the implementation of Fine Guidance Sensor in the loop.

5.2.6 Autonomy, FDIR and operations

Based on the THESEUS concept of operations which is built upon the science driven modes (cf. Sect.6), the spacecraft demands a substantially higher autonomy level than other flown ESA science missions to fulfil its science objectives. However, such an increase of system complexity has to be traded against the associated mission risk and programmatic envelope that, unavoidably, goes along with it. Moreover, the spacecraft will operate fully autonomously without real-time surveillance from the mission control centre.

The selection and definition of a suitable Fault Detection Isolation and Recovery (FDIR) framework altogether with the related definition of interfaces and responsibilities between SC and instruments will also contribute to enhance the autonomy capabilities while limiting the mission risk. THESEUS will implement an FDIR layered framework based on a hierarchical scheme defined by levels (from unit up to spacecraft and mission control centre) which aims at minimizing the impact of all kinds of failures on the system performance and system availability. The key to achieving this goal is to detect, isolate and recover failures at the lowest level possible. Each higher FDIR level will implement more complex and more powerful recovery actions, while subsequent lower FDIR levels will implement more transparent actions, with lesser availability impact on the system operations. All in all, this approach is a good trade-off to manage risk while promoting the concept of Autonomous Fail Operation (AFO) for the sake of increasing the THESEUS SC autonomy.

The current implementation of the operations approach (still under assessment with the Primes during Phase A), aims at introducing the minimum required autonomy level that allows the mission to be successful, and to rely on well-proven and deterministic solutions wherever possible (heritage, re-usage, and design-to-cost). This mainly means the generation and maintenance of the single MTL "updated" where only trigger sequences (either on-board detection by the monitors or provided to the SC from Ground with the boundaries of THESEUS "external triggers") are added into a pre-defined MTL "core".

5.2.7 Budgets

Table 5-3 - Preliminary mass budget (synthesised from parallel studies) to be consolidated at the end of Phase A.

Mass budget	CBE with DM [kg]	Mass fraction (dry) [%]
Payload	**340**	**21%**
SXI instrument	75.8	5%
IRT	38.4	2%
XGIS	186.1	12%
TBU	8.4	1%
Payload level system margin (10%)	30.9	2%
IRT telescope	**221**	**14%**
Platform	**1022**	**65%**
NGRM (Next Generation Radiation Monitor)	3.8	0%
Structure (SVM and PLM)	505.4	32%
Thermal control incl. instruments TCS	122.6	8%
Data handling	20.3	1%
Communications	28.3	2%
Propulsion	71.0	4%
Power	112.2	7%
AOCS	61.5	4%
Harness	97.3	6%
THESEUS (dry mass)	**1583**	**100%**
System margin (20%)	**316.7**	
Satellite (dry mass incl. system margin)	**1900**	
Propellant (incl. 2% residuals)	**290.0**	
Satellite (wet mass)	**2190**	

Table 5-4 - Preliminary power budget (synthesised from parallel studies) to be consolidated at the end of Phase A.

Power budget	CBE (Sci+TTC) [W]	Fraction [%]
Instruments	426.8	34%
Cryo-coolers	150.0	12%
IRT telescope TCS	80.0	6%
Sub-system Thermal (SVM and PLM)	70.0	6%
Communications	138.0	11%
Data handling	82.0	7%
Propulsion	1.0	0%
Data handling	82.0	7%
Power (incl. losses)	100.0	8%
AOCS	126.0	10%
Consumed power including DMM	**1256**	**100%**
System margin (30%)	376.7	
Consumed power including SM	**1633**	

6 Mission operations and ground segment

6.1 Scientific observational modes and pointing strategy

THESEUS is mainly designed to catch high-energy transients and provide transmission to the ground the most important information (e.g., trigger time, position, and redshift) within few tens of seconds and full resolution data within a few hours.

Most of the mission lifetime will be spent in the so-called "Survey Mode", where the two wide field X-ray monitors (the XGIS and the SXI) observe the accessible portions of the sky searching for X-ray transients. Once an on-board trigger occurs due to the on-set of an impulsive X- and/or gamma-ray event, the spacecraft will switch to the "Burst Mode" and an automatic slew is initiated in order to place the transient, localized by either the XGSI or the SXI (or both), within the field of view of the IRT. The narrow field IR instrument will first acquire during the "Follow-up Mode" a sequence of images in different filters (lasting about 12 minutes) aimed at: (i) identifying the counterpart of the high-energy source, (ii) narrow down its localization to the arcsec accuracy, (iii) provide a first indication of a possible high redshift event ($z \geq 6$). The spacecraft will then enter either the "Characterization Mode", during which the IRT will acquire a sequence of deeper images in different filters and spectra or the "Deep Imaging Mode" during which only images in different filters will be acquired (depending mainly on the IR brightness of the identified counterpart). The main goal of the observational sequence carried out in the Characterization Mode and the Deep Imaging Mode is to determine on-board the redshift of the transient source. If the counterpart identified by the IRT is a known transient or variable source not associated with a GRB, the spacecraft will go back to the Survey Mode. The Survey Mode is anyway restored after the Characterization or Deep Imaging Mode is completed. Note that only a specific portion of the IRT FoV can be used for IR spectroscopy. Therefore, a further small satellite slew to place the identified GRB counterpart in this portion of the IRT FoV is required, if and when the Characterization Mode is initiated. During the Follow-up, Characterization, and Deep Imaging modes, the monitors will continue collect data.

Two main trigger search algorithms will be implemented in the XGIS-DHU: the so called 'rate-search' and 'image-search'. The first one looks for statistically significant excesses by monitoring the rate of events in different time intervals, energy ranges and detector sections and it performs imaging analysis only when an excess is found in the event rates. This can be implemented in different ways, i.e., either running in parallel several instances of the same program with different setting parameters, or by combining different searches (e.g., multiple time scales) within the same instance. The second one performs a continuous imaging analysis to search for new point like sources. This image-based triggering method is more sensitive to the detection of long and/or slowly rising GRBs than the rate-search algorithm. In addition, the image-search can also detect new sources during conditions of highly time variable background. As for the rate-search, several instances of the image-search can run in parallel, using different time scales and energy ranges. The XGIS DHU will also have the capability of implementing more advanced GRB search algorithms based on rate-search, e.g., screening of multiple timescales through a set of excess masks already calibrated on GRB profiles (MEPSA; [237]) or Bayesian Blocks analysis. The residual XGIS false alarm rate estimate is 1 per week. This is based on the chance probability that a statistical fluctuation of the background in a given energy band on a given time scale exceeds the threshold set in the trigger algorithms. Triggers from known celestial sources will be identified through on-board catalogues. For off-line analysis, solar flares will be also identified through the coincidence with publicly available information on solar activity.

The SXI trigger system will search for sources using 'image search' on a variety of timescales and will provide a source location known to better than 2, and usually better than 1, arcminute (radius). This is sufficient to filter out known bright X-ray sources by comparison with an on-board catalogue (also used for XGIS), a process previously used on other missions. Data on known sources can be simultaneously monitored for unusually bright outbursts, information which can be sent to ground as a known-source flagged alert. Some previously unknown transients will be flare stars, but these can be efficiently filtered out by a multi-stage process: (a) comparison with an on-board catalogue of those stars of spectral type, brightness (optical and X-ray) and proper motion in the optical/IR sufficient that they may give rare X-ray flares. The large majority of stars will not produce X-ray flares bright enough to trigger the SXI over short trigger durations, where GRBs are the brightest cosmic sources, but a location cross-check will flag those for longer duration triggers where

this may be possible. (b) The IRT images will reveal no new optical/IR source not already in the stellar catalogue. We estimate a residual SXI false alarm rate of 2 per week.

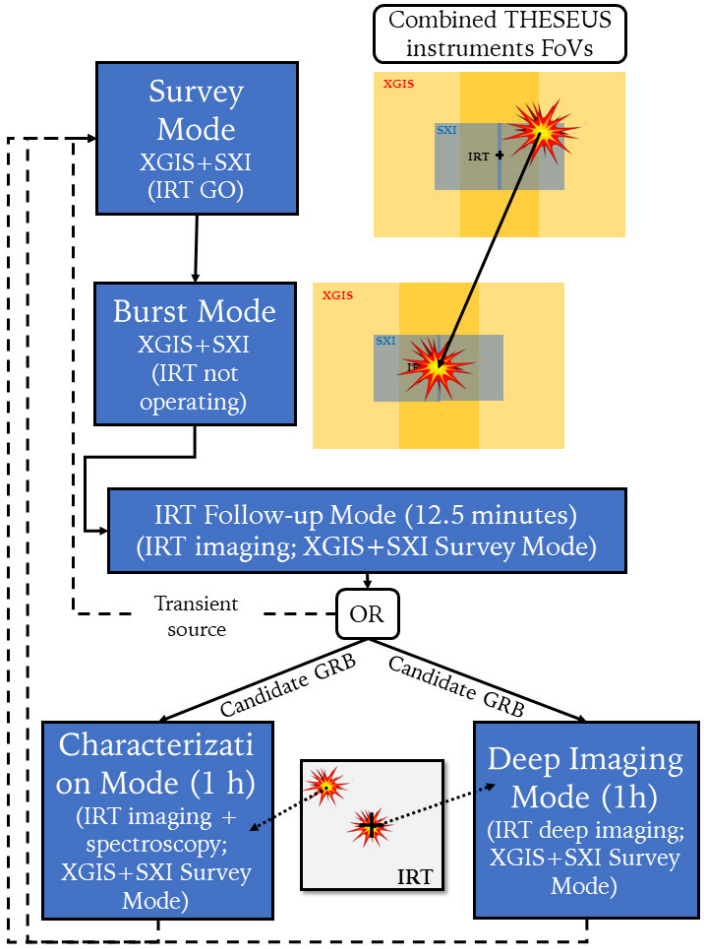

Figure 6-1: THESEUS observational modes and strategy during the detection, follow-up and characterization of an internal trigger (i.e. an event detected by either the XGIS or the SXI, or both).

While the SXI has a single data collection mode comprising full frame images with full energy and timing resolution, the XGIS collects only binned data in both the energy and time domain during the Survey Mode in the softer energy range (below 30 keV) and switches to the full resolution mode (photon-by-photon) exclusively when a trigger occurs (i.e., during the Burst Mode). The full resolution XGIS data are stored continuously on-board and binned before the transmission to the ground only if no impulsive event is detected. XGIS data in the higher energy range (above 30 keV) are always collected in photon-by-photon mode. This strategy has been implemented mainly to reduce the XGIS telemetry needs and the availability of continuous photon by photon XGIS data is possible in case the bandwidth of the telemetry downlink is increased (e.g., by the addition of multiple ground stations). During the Survey Mode, the THESEUS pointing direction will be slightly adjusted in order to allow the IRT to perform observations of interesting IR sources and maximize the science return of the mission.

THESEUS is also designed to rapidly respond to triggers that are provided by other facilities. In this "External Trigger Mode", it is foreseen that the coordinates of an interesting source are provided from the ground to the on-board computer and a custom version of the IRT characterization mode is initiated depending on the specific nature of the event to be observed with all THESEUS instruments (including the SXI and XGIS in Survey or Burst Mode). The time required to re-point the S/C toward a specific direction can be as short as 4 hours after the trigger, if the trigger occurs during favourable working hours for the ESA-led institutions in the mission ground segment (see §6.2) and in an accessible portion of the sky.

As extensively illustrated in §3.3, despite all largely conservative assumptions on the spacecraft, instruments, and operational limitations, the MOS has definitively proven that THESEUS will be able to fulfil its core science objectives at the end of the nominal 4 years mission lifetime with margins. The most efficient pointing strategy, achieving the largest number of fully characterized events at large redshifts ($z \geq 6$), is the one where THESEUS is prevalently observing the Ecliptic poles while in Survey Mode. Pointing toward these regions are characterized by the lowest down-time of the SXI and XGIS, due to the reduced obscuration of the instruments field of views by the Earth, and thus provide the largest time available to hunt for GRBs. Alternative pointing strategies have been investigated to optimize the THESEUS science return under different aspects. The current baseline is a pointing strategy assuming a maximum of two slews, of 60° each, during one orbital revolution. This strategy allows an efficient minimization of the Earth occultation and maximizes the number of high-redshift GRBs detected at low equatorial declinations, which are the most favourable for the follow-up with the ground-based telescopes. In this configuration, the MOS predicts (with very conservative assumptions) a total number of 17 GRBs detected per year at redshifts $z \geq 6$ (out of a total detected number of

over 500 GRBs per year). Out of these, about 52 % are located at equatorial declinations in the range (-30°, 30°). The MOS exercise has demonstrated that there is no need to limit *a priori* different possibilities for the THESEUS pointing strategy, as the mission is robustly designed to safely achieve its science goals. Optimization of the baseline pointing strategy can be considered later during the study, depending also on specific science return optimizations that will be traded-off by the THESEUS science teams.

6.2 Ground segment overview

The Ground Segment (GS) provides the means and resources with which to manage and control the mission via telecommands, to receive and process the telemetry from the satellite, and to produce, disseminate and archive the generated products.

The responsibility for and provision of the GS is split between ESA and a nationally funded Consortium SGS (CSGS). ESA will be responsible for the following GS elements:

- The ESA tracking station network (ground stations),
- The Mission Operations Centre (MOC),
- The Science Operations Centre (SOC),

while the THESEUS Consortium is responsible for the Consortium Science Ground Segment (CSGS), including the Science Data Center (SDC), the Instrument Operation Centers (IOCs), and the THESEUS Burst Alert Ground Segment (TBAGS).

The ground stations together with the MOC constitute the Operations Ground Segment (OGS), while the SOC and the CSGS comprise the Science Ground Segment (SGS).

A schematic view of the THESEUS ground segment organization is provided in Figure 6-2. The following preliminary definition of the data products for THESEUS is considered:

- Raw telemetry (TM): this is the telemetry stream received from the spacecraft and downlinked through the THESEUS ground station. It comprises the science telemetry and the preliminary auxiliary files generated on-board.
- Level 0 data (L0): these data are obtained from the TM that is de-commutated and split into functionally independent parallel streams per instrument. L0 data will be in FITS format, such that they can be conveniently handled by any scientist in the community through the THESEUS distributed software, as well as other standard tools. Conversion to physical units is applied for each instrument to L0 data.
- Level 1 data (L1): these data are obtained once all corrections (such as aspect correction, time calibration, barycentric corrections) and instrument-specific calibrations (such as detector gains and good-timing information) are applied to level 0 data. The L1 data can thus be considered as cleaned event files.
- Level 2 data (L2): these are obtained from L1 data by applying pipelines and algorithms leading to the extraction of a set of standard scientific products per observed source and/or per observation. L2 data are provided to different partners in the THESEUS SGS to perform quick-look analysis activities, as well as to the community for quick inspection of the outcomes of an observation.
- Level 3 data (L3): these data are obtained from L2 data by applying higher level processing pipelines. At these stage, L3 data are not yet fully defined, but in the usual approach they are defined as longer term products that can enhance the scientific return of the mission. They can include historical measurements of the properties of the celestial sources over the mission lifetime, catalogues of the detected sources, large scale mosaics of the high energy and IR sky, as well as cross-matches and associations with sources in catalogues derived from different energy domains.

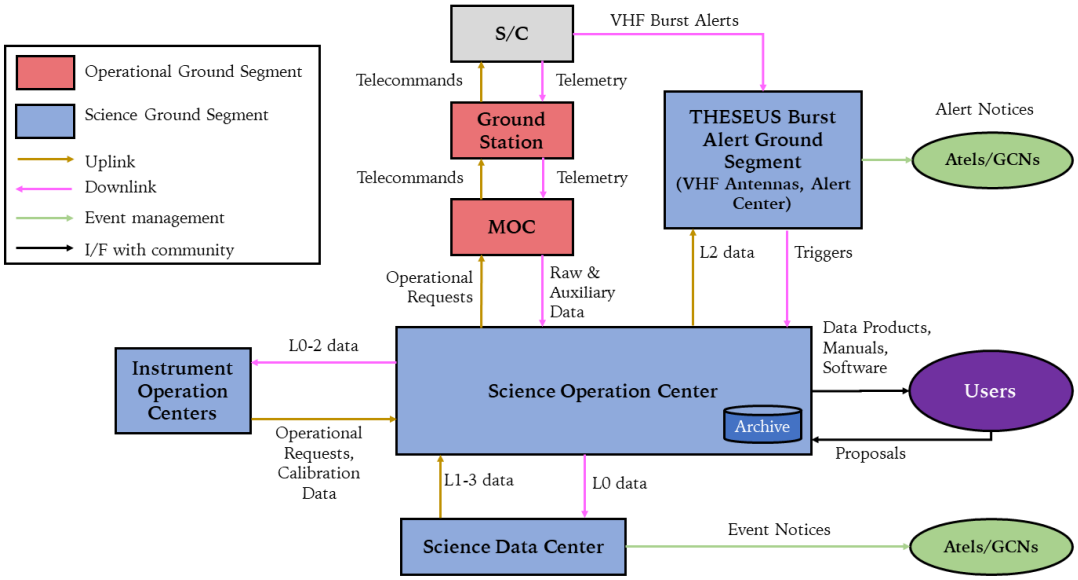

Figure 6-2: Overview of the THESEUS ground segment organization and data flow.

6.3 Mission operations

6.3.1 Mission Operations Centre (MOC)

The MOC is responsible for the operations of the spacecraft, for monitoring and ensuring the spacecraft safety and health, for provision of flight dynamics support, including determination and control of the satellite's orbit and attitude, and intervention in case of anomalies.

The MOC is responsible for the handling of telemetry/telecommands for both the spacecraft and payload. The telemetry, tracking and command subsystem of the mission must be compatible with the ESA ground segment and the ESA tracking station network.

The MOC is responsible for the ground station bookings, for collecting the raw telemetry science and auxiliary data and for making it available to the SOC for further processing.

The responsibility for the design, implementation, and operation of the MOC rests with ESA/ESOC.

6.3.2 Ground stations

For THESEUS, it is foreseen that a single ground station located at Malindi and operated in the X-band will be used for TM downlink and telecommands uplink. This ground station is provided as an in-kind contribution by the Italian Space Agency (ASI). A number of VHF receivers will be located around the Earth equator to receive and further distribute on the ground the on-board alerts produced by the detection of gamma-ray bursts and other impulsive events through the TBU. This is described in more details in §6.4.2.3.

6.4 Science operations and data handling

6.4.1 Science Operations Centre (SOC)

The SOC is responsible for the science operations of the ESA-funded part of the Science Ground Segment (SGS), and the system engineering aspects of the complete SGS.

The SOC will be the main interface with the MOC and with the science community. It will host the central THESEUS archive, containing all data levels, the calibration files, all software, and all relevant user manuals that allow scientists in the community to process, extract, and handle the THESEUS scientific products. The SOC will also take care of the daily processing of the TM into level 0 data exploiting the software made available by the SDC. Processing of the TM to level 0 data at SOC will ensure at any time of the mission

lifetime the availability of the lowest data level accessible by the community to scientifically exploit the observations performed by THESEUS.

The responsibility for the design, implementation, and operation of the SOC rests with ESA/ESAC. To fulfil its mandate the SOC at ESAC benefits from common and/or re-usable tools and cross-mission support in the Science and Operations Department of ESA's Science Directorate. ESAC provides the data archives for all ESA scientific missions, and a dedicated team, the ESAC Science Data Centre (ESDC) ensures the same level of quality and tailoring to the mission needs for the archives together with added value tools for the general scientific community.

6.4.2 Consortium SGS

6.4.2.1 The Science Data Center (SDC)

The THESEUS Science Data Center (SDC) will be fully funded and provided by the THESEUS consortium.

The SDC will be responsible for delivering to ESA the software needed for the processing of all mission data from TM to Level 3, interfacing with the instrument teams that will provide the instrument-specific algorithms for their instrument.

The SDC will process Level 0 data to produce higher Level data products (1, 2, and 3), and be responsible for the inspection and quality assurance of these products (with validation reports). The SDC will also be responsible for the quick look analysis of the data, and for providing alerts to the community. The SDC will support the SOC in handling the helpdesk and in organizing scientific events related to THESEUS, as well as data analysis and exploitation workshops.

6.4.2.2 The Instrument Operation Centers (IOCs)

The Instrument Operation Centers (IOCs) will be fully funded and provided by the THESEUS consortium. There will be one IOC per instrument and each IOC is where the instrument expertise will be maintained all along the mission lifetime.

The IOCs are responsible for providing instrument-specific support to the SOC, MOC, and SDC. This includes providing calibration files for the analysis software, inputs for and reports on calibration observations, support for handling both regular instrument operations and anomalies when needed by the MOC/SOC, and support to the community through the participation to the mission helpdesk. The IOCs will also provide the instrument-specific analysis software components required for the processing pipelines.

6.4.2.3 The THESEUS Burst Alert Ground Segment (TBAGS)

The THESEUS Burst Alert Ground Segment (TBAGS) is entirely funded by the members of the THESEUS consortium, and will comprise the ground VHF receivers and the Alert Center (AC). The ground-based VHF receiver network will be a subset of that used by the SVOM mission, and the current baseline is that they are provided as in-kind contribution from CNES.

The VHF alerts generated by the on-board instruments will only go through the VHF ground receivers and are not part of the nominal telemetry: they are not downlinked to the MOC/SOC. The VHF alerts will contain only the basic information of triggers (e.g. the GRB position and onset time) and will be distributed automatically to the scientific community through the ground VHF receivers.

The AC will comprise personnel on shift from the THESEUS consortium in charge of verifying the validity of the alerts (especially during the initial phases of the mission) and providing any other relevant follow-up information on these alerts to the community. The AC personnel will have access to all THESEUS data in order to perform necessary checks and refinements on the information distributed to the community by the VHF ground receivers. The main scientific objectives of THESEUS do not require any specific mission planning activities: the spacecraft will be designed to be fully autonomous in the detection of high-energy transient sources, the validation of the corresponding on-board triggers, the slew to place a validated trigger within the field-of-view of the IRT, and the rapid transmission of trigger data to the ground via the TBU.

The outcomes of the THESEUS Phase A study have shown that it is reasonable to assume that the spacecraft will be endowed with a large degree of automation not only in response to triggers generated onboard by the

XGIS and SXI, but also to external triggers provided by other facilities operating in the early 2030s (including the gravitational wave detectors, neutrino telescopes, as well as other facilities across the entire electromagnetic spectrum) and leading to requests for ToO observations. The foreseen level of automation implies that THESEUS will be able to determine the technical feasibility of a given change of observational plan associated to a ToO observation based only on the provision of a simple list of target coordinates, observation durations, and instrument configurations. Such a level of automation would significantly reduce the need for SOC/MOC support for both scientific mission planning and observation scheduling, as long as the number of ToO requests is kept within a reasonable balance versus the nominal (surveying) mode operations. It is foreseen that a board chaired by the ESA mission Project Scientist supported by elected members of the consortium will perform a preliminary screening of the ToO requests submitted by the community to ensure at the same time an optimal balance of the observational modes and the fulfilling of the THESEUS core science objectives. An alternative possibility, featuring an even higher level of automation, is that there will be a system in place endowed with the required artificial intelligence to provide the largest screening of the alerts such that these could even be handled by the sole Project Scientist. A lot of intelligence can be introduced into a machine learning decision tree approach to filtering and handling requests for observations. There is an effort in this direction that has started in 2019 at ESOC, and it could very well be foreseen that more than a decade from now it will be mature in terms of its level of sophistication and reliability.

In order to maximize the science return of the mission, it is however still assumed that there will be a limited GO program also for THESEUS (as it is commonly done for all observatory-type missions). During the assessment phase study, it was baselined to allow small positional adjustments (a few degrees at the most) of the satellite during the nominal Survey Mode observations in order to permit the collection of IRT data for a pre-defined list of scientifically interesting targets. The SOC will be in charge of issuing a yearly announcement of opportunity (AO) to the community, providing also all the required public AO-related software, managing the proposal reception, and handling the time-allocation committee (TAC). The SOC will be in charge of preparing the observation plan and communicate to the principal investigators (PIs) of the accepted proposals when the selected targets are observed (assuming a best effort basis, regulated by the on-going surveying pointings). The IRT GO program requires the SOC to prepare spacecraft pointing and payload (instrument) operations requests, which will then be passed to the MOC and converted into telecommands via defined procedures for transmission to the spacecraft.

All the activities associated to the IRT GO programme will benefit from a significant restructuring and simplification of the proposal handling system at ESA for the 2030s scenario. In this time frame, it is planned that for all observatory-type missions there will be TACs in place covering different themes of research. Each TAC will comprise a network of self-organized selected scientists who evaluate the proposals and formulate a recommended observing programme. The ESA infrastructure for the proposal submission will be made such that all aspects of their technical evaluation is automated, and thus requiring minimal human inspection or intervention. Instrument teams are planned to be responsible for the delivery of tested instrument simulators to be used in the technical evaluation of the proposals. All TAC activities would also be directed, recorded, and overseen by ESA from the centralised proposal handling system for simplicity and traceability. Overseeing and managing the entire AO process could then be handled by very few people, and possibly even the Project Scientist on their own.

6.4.3 Instrument Operations and Calibration

The primary responsibility for instrument health and performance monitoring lies with the instrument teams and specifically it is handled by the IOCs. Nevertheless, the MOC/SOC will also be required to perform instrument monitoring with the goal of maximising science output by minimising response time to anomalies and implementation of corrective actions. Instrument monitoring is foreseen to be automated based on machine learning. Technical instrument expertise within the SOC is essential. This is therefore foreseen.

All instrument operations requests, including for calibration observations, will be submitted through a centralised Operational Change Request (OCR) system (as currently available in SOCCI-Jira at ESAC) that will be maintained and administered by the SOC/MOC, and to which all instrument teams and other mission-related technical experts will have access. The OCR system will allow for the definition of workflows including multistep approval by those identified to hold specific responsibilities (e.g., Mission Manager, Operations Manager, Project Scientist, Instrument PI, etc).

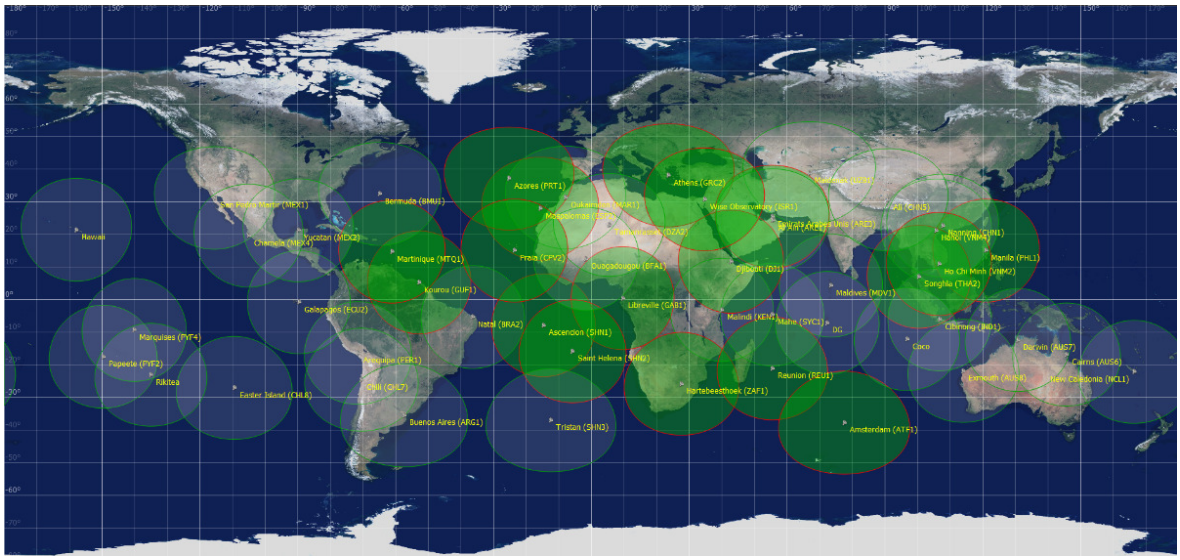

Figure 6-3: the VHF ground receivers planned for SVOM. Those in green are already operational. The others are either being installed or the agreement with the hosting site is not yet finalized. Only a sub-set of these stations will be used for THESEUS, as its orbit is less inclined compared to that of SVOM (30°) and thus coverage at the higher and lower declinations is not required

Operations will be carried out by the MOC with the support of the SOC and instrument teams. Calibrations are foreseen to take place roughly every six months and will require minimal attention given the restricted range of operating modes of the instruments. Most of the calibrations for the large FoV instruments will occur automatically through the acquisition of the Survey Mode data, further reducing the effort of the periodic activities. In-flight specific calibration strategies for the three THESEUS instruments are detailed in the following sub-sections.

6.4.3.1 XGIS in-flight calibrations

XGIS in-flight calibrations will mainly concern the flux and spectral response at different off-axis positions and the boresight of the two cameras. These calibrations will be performed taking advantage of celestial sources in three ways:

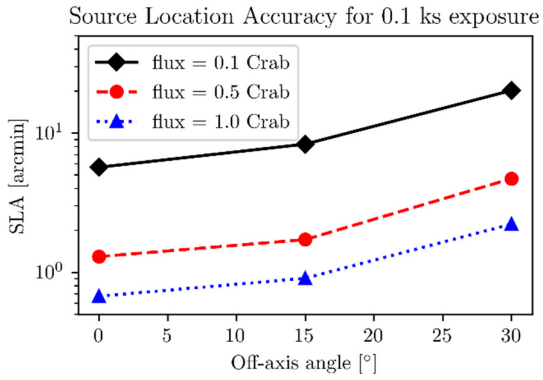

Figure 6-4: XGIS SLA as a function of off-axis angle for three source fluxes.

a) through pointed observations during the initial commissioning and verification phases of selected bright persistent X- and gamma-ray sources;
b) exploiting the observations during Survey Mode of bright persistent X- and gamma-ray sources serendipitously included in the XGIS FoV;
c) exploiting observations of the best localized GRBs by the SXI and those localized to an accuracy of few arcsec by the IRT.

Detailed simulations have been carried out to determine the achievable XGIS SLA as a function of the exposure time for different fluxes of the detected source and for different values of the off-axis angle. Figure 6-4 shows an overview of the changes expected in the SLA as a function of the off-axis angle assuming a fixed exposure time of 100 s and three different flux levels (a flux of 1 Crab corresponds to 2.15×10^{-9} cgs in the 2-10 keV energy range). The basic conclusion is that, concerning the methods (a) and (b) illustrated above, the boresight calibration can be straightforwardly performed by using exposure times as short as a few hundreds of seconds taking advantage of the presence of many well-known bright persistent high energy

sources in the sky. Concerning method (c), about 220 GRBs per year will be detected and localized by the IRT with an accuracy as goods as few arcseconds, providing rich datasets to perform additional XGIS boresight corrections (if needed).

6.4.3.2 SXI in-flight calibrations

The SXI in-flight calibration are aimed at obtaining initial functionality tests followed by boresight alignment, plate scale determination, and spectral response verification (including gain, effective area, and PSF crossbeam verifications).

Initial boresight can use a bright point source. As for the case of the XGIS, there are sufficient bright, known, persistent X-ray sources on the sky (with count-rates of several tenths per second), to have several per SXI module FoV enabling boresight verification at <30 arcsecond level in a 15-20-minute exposure. Combining data from a few tens of FoV will determine the plate scale. The SXI alignment can be monitored continuously using X-ray survey data obtained during normal operations.

The initial spectral performance can be verified using observations of a few standard known, bright X-ray calibration sources, which are distributed around the sky, combining data to accumulate a few tens of ksec exposures per source. SNRs Cas A and Tycho can be used for the initial gain verification: simulations suggest a Si-K (1.865 keV) line centroid uncertainty of 10 eV (90%) will be achievable in 2 ks for Cas A (Tycho and Pup A observations are also planned in the pointing verification phase). The detector gain can be later monitored by regularly combining data obtained during normal operations. The optimum source to use for this verification is Cas A, however, this may require a dedicated pointing due to its location in the sky. Pup A (0.65 keV) is also considered for the detector gain verification due to its optimum location in the sky – for example, the instrument will be able to obtain ~30ks of exposure a day for a fortnight a year, at off-axis angles of ~11-15 degrees.

The effective area will be modelled and verified first on the ground at PANTER pre-launch. During flight, the effective area verification will be performed following the alignment and plate scale determination. The optimum source for this verification is the Crab, which will then be used to measure the in-flight effective area (through the conversion of photons per pixel into sky flux) and will be compared to the model verified at PANTER. The source will be rastered across the two modules' FoV at different angles to verify the level of vignetting at each module.

For verifying the crossbeam PSF, sources in the Galactic centre will be observed at different off-axis angles.

The calibration process is estimated to require of the order of 4 weeks of exposure time over the entire mission.

6.4.3.3 IRT in-flight calibrations

Calibration observations for the IRT will be performed at regular intervals (the frequency depends on the nature of the information required) to obtain the data needed to produce the calibration files and to monitor the good health of the instrument. To monitor the detector health (bad pixels, flat field, linearity) an on-board calibration unit (CUA) will be used. On the other hand, in order to be compliant with the photometric accuracy requirements (<5%), every roughly 6 months calibration observations of known stars will be required. The same is valid for spectrophotometry, where known stars need to be observed over the entire (spectroscopic) FoV. Concerning the wavelength calibration, planetary nebulae with clear emission lines will be observed at different positions on the detector for adjustment and verification of the line centroids. On the launch date of THESEUS, it will be possible to use the catalogue produced for Euclid's NISP instrument, thus optimizing the chosen targets for the calibration observations and minimizing the requested exposure time.

6.4.4 Data Processing

According to the presently planned data flow scheme (see Figure 6-2), all TM will be collected at MOC from the ground station and then transmitted to the SOC. Expected TM data volumes are around 60 GBits/day. The TM will be stored and automatically processed by the SOC to produce L0 data. Higher data products are generated by the SDC accessing the L0 data from the THESEUS central archive at SOC and performing an automated processing leading to L1, L2, and L3 data. All data products are stored in the THESEUS archive and made available to the community accordingly to the data policy and rights. The SOC will maintain the

ability to replicate the entire processing chain in case of needs. This is essential to ensure the real-time service to the scientific community, and to provide the means to cross-check the outputs while ensuring redundancy.

The quality control of the pipeline products will be responsibility of the ESDC, with support from the instrument teams, Consortium, the SOC, and CSGS. The strategy for assessing quality will be agreed to by the SOC and ESDC in collaboration with these entities. The scientific validation of the data products will be performed by the SDC before data are distributed to the community.

The software components for every part of the data processing from level 0 to level 3 will be the responsibility of the SDC, with support from the IOCs. All software will be delivered to the SOC, and integration and acceptance-testing of the components into the various processing pipelines will be the responsibility of the SOC in collaboration with the CSGS, the IOCs, and other relevant consortium members. ESA (the SOC) will be the custodian of the software components and processing pipelines, managing also all along the mission lifetime the configuration control.

It is currently assumed that the source code of the THESEUS data analysis software will be made available to the community, but no support will be given for local installations. At the time when THESEUS will be operational, the centralized cloud ESA system, DataLabs, will be fully operational and it is expected that scientists will use this system to run their customized processing and scientific product extraction from the THESEUS data. This is compliant with the long-term ESA view of the handling of data from observatory-like scientific missions. This approach would also require a substantially reduced effort from SOC and SDC to make software releases compatible with many different platforms and operating systems. Rather, a solid and robust analysis environment will be provided to the community at large.

6.4.5 Archive

The data processing pipeline products will automatically populate both the Mission Database (operational part of the archive) and the Science Data Archive, which after completion of the post-operations phase will be the basis for the Legacy Archive. These will provide the unique / only official repository of the THESEUS data, and will be hosted and maintained at ESAC by the SOC and ESDC. All mission and pipeline data products will be accessed through these interfaces.

Optimised and streamlined data access will be provided to the IOCs, SDC, and AC in order to allow them to promptly fulfil the task of the data processing, validation and quick-looking.

Data releases and data rights will be captured in the Science Management Plan and at the end of the assessment phase study only a preliminary proposal is put forward for later discussion. This is summarized in §7.

6.4.6 Quick-look activities

Beside repointing automatically bright impulsive events detected by the XGIS and SXI (as GRBs) or crucial events for the THESEUS core science objectives provided by external facilities (as gravitational wave sources), THESEUS will also be able to monitor hundreds of variable and/or transient X-ray sources on a daily base. This is ensured by the combination of sensitivity and large field of view of the XGIS and SXI, as well as by the nature of the spacecraft pointing strategy during the Survey Mode.

Many variable and/or transient sources in the Milky Way, as well as in other Galaxies, might not get bright enough to trigger the on-board system and request a slew of the spacecraft. However, beyond these events there are large community investigating a wide range of different high energy phenomena and for which the report of the discovery of new episodes of enhanced X-ray emissions from these sources, as well as the discovery of variability, is a key information that can be used to eventually trigger multi-wavelength observations and advance our understanding of the involved fundamental physics. Examples of variable/transient sources at reach for THESEUS have been discussed in §2.6.

The THESEUS Consortium has thus planned to include among the tasks of the SDC personnel that of the “sky monitoring”: scientists on duty at the SDC, providing coverage 24/7, will be using the L2 data and inspect the outcomes of the surveying observations carried out with the XGIS and SXI and alert the community in case a relevant astrophysical event is discovered. Contrary to the on-board search for bright impulsive events in X- and gamma-rays, the searches carried out on the ground can exploit also much longer exposure times by combining different observations or merging together different parts of one observation performed at different

times. Pending the final agreement on the data rights and distribution policy, all allowed products of the SDC scientists on duty analyses will be made available to the community through proper online interfaces (or directly through the centralized archive). Given the large number of rich datasets that the THESEUS instrument will produce per day, the direct involvement of the community is mandatory to ensure that all scientific products are exploited at best.

6.4.7 Community Support

Traditionally, the SOC takes on the responsibility to provide to the community not only the observation proposal preparation and handling tools, but also all other relevant documentation (users handbook, data processing guides, archive guide, etc), that are needed for the exploitation of the THESEUS data (with the support of the SDC and IOCs). Furthermore, data exploitation is promoted in the community through the organization of data analysis workshops and focused science conferences.

The SOC will also hold the responsibility of the helpdesk. It is foreseen that the helpdesk will be a shared effort using a centralized system hosted at ESA and maintained by the SOC in which the mission's different subsystems will be mandatory fields in the ticket submission such that they reach different subsets of instrument team and consortium experts that will be automatically notified. Oversight of the process of interaction between the community and the SGS partners will be the responsibility of the SOC.

7 Management

7.1 Project management

THESEUS is an ESA mission with contributions from ESA Member States; the project management approach will follow the current practices of ESA science missions.

ESA management: The overarching responsibility for all aspects of the THESEUS mission rests with ESA's Directorate of Science. During the development phase, ESA will appoint a Project Manager, responsible for implementing and managing ESA's activities during this phase. This work will cover all industrial activities (procurement of the spacecraft & IRT telescope, integration of spacecraft and instruments, testing, launch campaign and early in-orbit phase). After commissioning, the ESA Mission Manager assumes responsibility for operations of the spacecraft, its payload, and the ground segment.

Payload management: Different teams within the THESEUS consortium will provide the payload elements to the mission (XGIS, SXI, IRT, TBU, and DHUs), each team being responsible for their own delivery to ESA. All members of the THESEUS Consortium feature a long track record of relevant expertise in these fields, having provided in the past instruments for successful high-energy missions (e.g. *EXOSAT*, *XMM-Newton*, *BeppoSAX*, *INTEGRAL*, *AGILE*, *Swift*, *ASTROSAT).* During the early stage of spacecraft operations, the instrument teams will provide ESA with all the required support to operate and monitor the instrument behaviour and performance. A Multi-Lateral Agreement (MLA) will be established between ESA and the Consortium funding agencies to formalize the commitments and deliverables of all parties by the time of mission adoption.

A *Science Data Centre* (SDC) is included in the consortium contribution to the mission. The SDC is responsible for: (i) ensuring suitable pipeline processing tools for the science data, (ii) producing validated scientific products for ingestion into the archive, (iii) developing all software tools required for the interactive handing and customized scientific product extractions from the THESEUS data.

7.2 Share of responsibilities

THESEUS is an ESA mission. The payload and the contribution to the Science Ground Segment of the mission will be provided by the *THESEUS* Consortium, supported by the ESA Member States, with the exception of the IRT instrument cooling system and detectors, as well as the SXI detectors which are procured by ESA. The IRT telescope is developed by the Prime under ESA responsibility. Figure 7-1 shows the split of responsibilities between ESA and the THESEUS consortium for all elements.

7.3 Organization of the THESEUS consortium

The THESEUS consortium (Figure 7-2) is an entity coordinated by five main contributors, with Italy acting as consortium lead and United Kingdom, France, Switzerland, and Germany as co-leads. Members of the coordination team are supplying the payload and science ground segment elements of the mission. Through this coordinating team, the THESEUS consortium:

- represents the THESEUS international collaboration and interfaces with both ESA and the scientific community;
- grants the maximum interaction and discussions among the payload contributors on the scientific and operational (including the ground segment) aspects that are of general interest ad strategic for the mission as a whole;
- provides fundamental services for optimizing the communication among the payload contributors and the feedback to ESA (payload system engineering support, management of the Mission Observation Simulator), PA/QA support, documentation support, management and coordination of the scientific activities from the THESEUS community (mostly through scientific Working Groups), as well as coordinated efforts for mission advertising (conferences, papers, etc.) and outreaching.

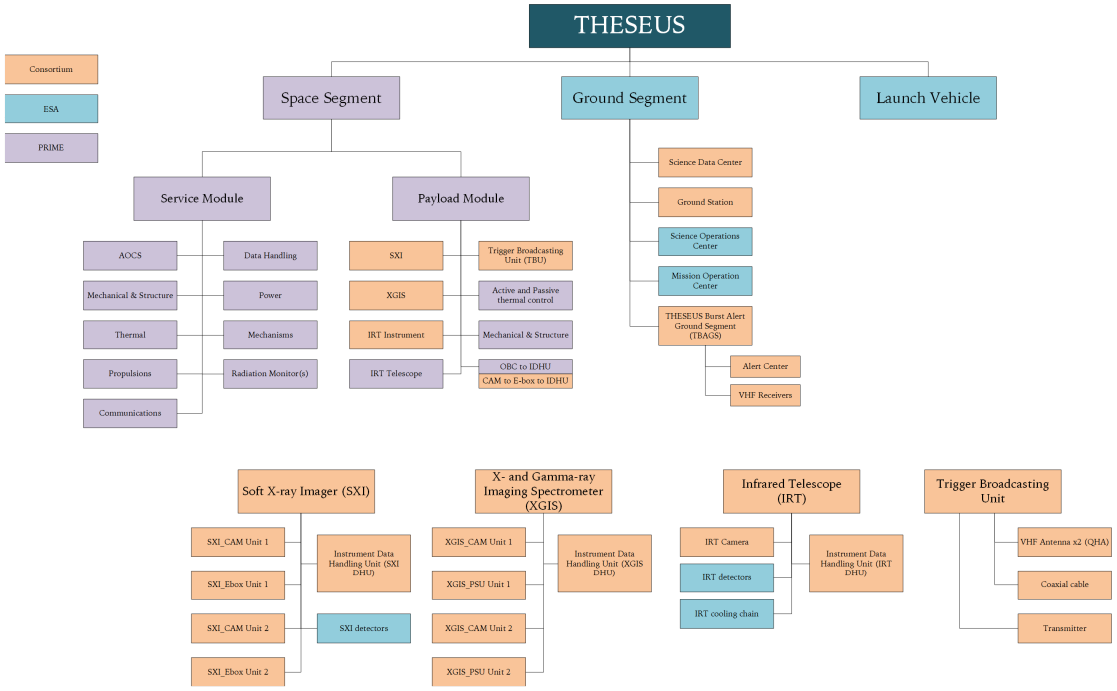

Figure 7-1 THESEUS top-level system product tree. While separated for clarity, it shall be reminded that Primes are also under the responsibility of ESA.

A Consortium Project Office is put in place with the prime responsibility of facilitating the coordination of the payload and ground segment element developments. It is foreseen that the Consortium Project Office team (including the project documentation support, the payload system engineering support, and the PA/QA support) provides support to the activities of all THESEUS teams, maintaining a tight collaboration with the corresponding project managers, system engineers, and PA/QA managers, as well as maintaining a direct link with the consortium lead.

The science team, within the THESEUS consortium, has the prime responsibility to perform all science trade-offs and monitor the evolution of the scientific requirements over time. This science team is divided into 5 main working groups (exploring the early Universe with GRBs, multi-messenger Astrophysics, time-domain Astronomy, populations & GRB science, synergies with future facilities, additional and GO science), each including a number of sub-working groups. There is an additional "coordination working group" which is responsible for the coordination of all other working groups and is the points of contact between the consortium lead/co-leads and the science team.

7.4 Schedule

The THESEUS schedule (Table 7-2) is consistent with a launch date at 2032 with the appropriate margins. Given the currently high TRL of the different payload components, no item is currently expected to be on the critical path. The THESEUS mission schedule is derived from the programmatic requirements and mission phases and duration. Main reviews dates and payload delivery need dates will be confirmed at the end of Phase A with the Primes inputs and iteration with the instrument's providers. Table 7-1 summarizes the breakdown of the different ESA member states responsibilities within the THESEUS consortium.

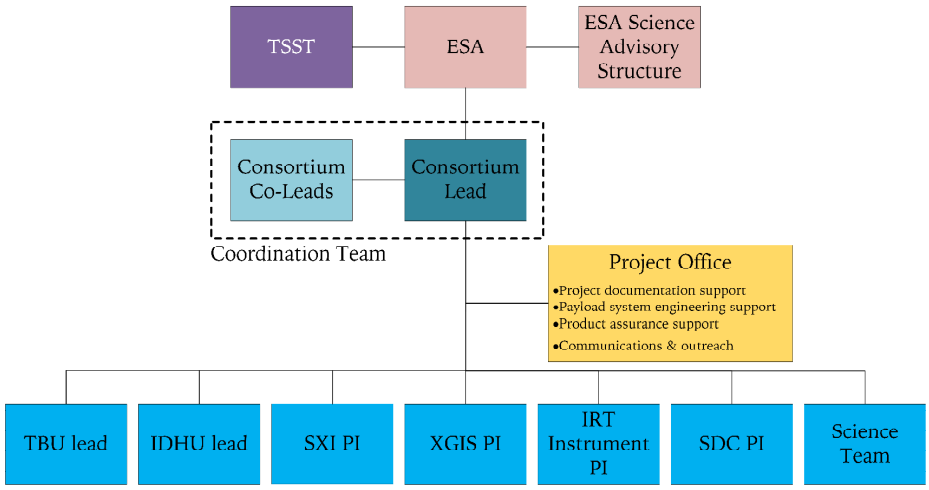

Figure 7-2 Top level organization of the THESEUS consortium

Table 7-1 Overview of member state contributions within the THESEUS consortium.

Italy	• THESEUS consortium lead • XGIS instrument PI • TBU PI • Consortium Project Office • XGIS instrument design, detection plane procurements and assembly, electronics, integration, testing, simulations, and calibrations. • Malindi ground station provision (ASI in-kind). • XGIS instrument operation centre lead • Contribution to the SDC
France	• THESEUS consortium co-lead • IRT instrument PI & IRT science lead • IRT instrument design, detection plane assembly, electronics, integration, testing, simulations, calibrations, filter wheel grism • IRT Telescope optical requirements • IRT instrument operation centre lead • Contribution to the SDC • Theseus Burst Alert Ground Segment (CNES VHF Network of ground receivers and the Burst Alert Centre)
Germany	• THESEUS consortium co-lead • SXI and IRT DHU design, electronics, integration, testing, and software development • Overviewing of the XGIS DHU development • Contribution to the consortium project office • SDC contribution
Denmark	• XGIS DHU design, electronics, integration, testing, and software development
Belgium	• Contribution to the SXI instrument integration, characterization, and tests
Slovenia	• Investigation of possible mobile round station additional antennas (for telemetry downlink) • Contribution to the SDC
Netherlands	• Contribution to the SDC
United Kingdom	• THESEUS consortium co-lead • SXI instrument PI • SXI instrument design, detection plane characterization, optics assembly, electronics, integration, testing, simulations, and calibrations • SXI instrument operation centre lead • Contribution to the SDC
Switzerland	• *THESEUS* consortium co-lead • SDC PI • Contribution to the consortium project office • SDC engineering, software development, data processing, quick-look, data scientific validation, sky monitoring, community alert broadcasting • IRT filter wheel mechanism and optical elements (filters)
Spain	• XGIS coded mask and collimator • Contribution to SXI focal plane assembly and mechanical structure
Poland	• XGIS power supply units
Czech Republic	• Contribution to the SXI instrument mechanical structures and thermal control
Ireland	• Contribution to the SDC

7.5 Science Management

In Phase A and B1, the overview of all THESEUS-related science activities is provided by the mission ESA Study Scientist in synergy with the ESA-appointed TSST, chaired by the Lead Scientist and including key scientists of the Consortium, as well as external experts. In these phases, the TSST is the formal ESA's interface with the scientific community for all scientific matters and is responsible for the assessment and consolidation of the scientific requirements and to advise ESA on scientific trade-offs. After mission adoption, the science coordination role will be taken by an ESA Project Scientist (PS), supported by an ESA-nominated THESEUS Science Working Team (TSWT). The PS, supported by the TSWT, will monitor the evolution of the science requirements, advise the Project Manager (during the development phase) and the Mission Manager (during the operation phase) on all issues that affect the scientific performance and output of the mission. Though the THESEUS coordination team, the PS and the TSWT will receive support for their tasks from the Consortium science working groups, who, as for Phases A and B1, will provide expertise and perform specific investigations.

In preparation to the formal adoption of THESEUS in the ESA Science Program, the ESA Coordination Office, in coordination with the PS and after consultation with the TSST, will elaborate the Science Management Plan (SMP). The prime goal of the SMP is to ensure the best possible scientific return for the mission, promoting the largest possible involvement from the international scientific community and guaranteeing a fair return to the member states that have funded the payload and ground segment elements.

Table 7-2 - THESEUS schedule

Milestone	Milestone Schedule
Mission Adoption	June 2024
Start of the Launch Campaign (L)	Q1 2032
Launch Campaign duration	3 months
LEOP	7 days
Satellite and Payload Commissioning which ends at In-Orbit Commissioning Review (IOCR)	3 months
Nominal in-orbit lifetime (From launch to end-of mission disposal)	4 years
Disposal duration	1 month

At present, the THESEUS Consortium has provided the following suggestions toward the definition of an optimal SMP for the next phase:

- During nominal scientific operations of the mission, data will be made public as quickly and extensively as possible (which will be an advantage also for the management of the scientific ground segment). The consortium will release regular XGIS and SXI survey products, and near real-time on-line data products will be available for monitoring many known transients and for alerting the community to new transients found during survey data processing (i.e. the so-called quick look and sky monitoring activities performed by the SDC).
- Some limited reserved access to GRB data will be granted to the THESEUS consortium and instrument teams, either identified as the products derived from a specific phase of the mission, or those corresponding to a certain fraction of GRB with a redshift higher than a given threshold. It could be planned that:
    - all mission data are reserved to the instrument teams until and including the Early Orbit Phase (LEOP);
    - data rights are extended to scientists in the whole THESEUS Consortium during the Performance Verification Phase;
    - GRB data at $z > 6$ will be reserved for the THESEUS Consortium for a period of 6 months during the first 6 months of nominal operations;
    - alerts on GRBs and other transient sources, reporting basic information (e.g., trigger time, sky coordinates, flux, redshift) transmitted by the TBU will be made public during any phase of the mission after LEOP
    - all other data taken during the nominal mission will be public as soon as they are processed.
- There will be an IRT GO program. It will be managed by ESA exploiting the share of tools and resources with other (operating and past) missions. The community will be asked periodically by the ESA for

proposals to use the IRT during Survey Mode, pointing interesting targets that allow no major deviations (a few degrees) from the baseline survey pointing strategy. The corresponding plan will be produced by the SOC and delivered to the MOC for upload to the spacecraft. A GO program involving also the high-energy monitoring instruments, supplying additional data to those already collected during the survey program and exploiting pointings substantially deviating from the baseline survey strategy, could be implemented later along in the mission lifetime if some observational time remains available after the main THESEUS core science goals are achieved. GO program data will be subjected to a proprietary period of 3 months for the proposer and will become public afterwards.

The presence of a dedicated alert center within the TBAGS, featuring scientific personnel on shift to verify (especially during the earlier phases of the mission operations) the automatic alerts generated on-board for bright impulsive events in X- and gamma-ray will also secure the strong scientific involvement of the THESEUS Consortium over the mission lifetime. This commitment is further strengthened by the presence within the THESEUS alert center team of "burst advocates", i.e. scientists in charge of following-up the TBAGS alerts and disseminating further information to the community.

The THESEUS SDC will also host a service with scientific personnel on shift (working remotely from their home institution through the tools made available by the SDC PI) to monitor sources as detected in the large field-of-view XGIS and SXI instruments, hunting for transient celestial objects, changes of states of known sources and other interesting events to be rapidly disseminated to the international community via the on-line data products noted above.

Finally, a "ToO screening team", chaired by the ESA Project Scientist and composed by appointed SDC Consortium members, will screen triggers coming from the community and guarantee the achievement of the mission core science objectives in the field of multi-messenger and multi-wavelength astronomy. ToO data products will have no proprietary period to maximise scientific return to the whole community.

The above science management policies, together with the synergies of THESEUS with the next generation large facilities in both the multi-wavelength and multi-messenger domain, will maximize the participation and interest of the international scientific community in the mission.

8 Communications and Outreach

ESA will be responsible for planning and coordinating education and outreach activities related to THESEUS, with the support of the THESEUS Consortium. An outreach and education plan will be developed and executed jointly by ESA and the Consortium. The following guidelines will apply:

- ESA leads and coordinates the execution of all education and outreach activities within the data rights framework of the mission;
- For the purpose of public relation activities, the consortium will provide to ESA unlimited access to all processed and analysed data, even during their proprietary period (if applicable); this material will anyway follow the data rights policy for matters concerning scientific publication purposes;
- Members of the Consortium have a duty to support ESA with regards to education and outreach;
- ESA gives credit to members of the Consortium regarding scientific and technical results, when applicable.
- The Consortium has the duty to exploit the outreach and educational potential of THESEUS. The contributions from national funding agencies to the science exploitation phase will include resources to develop plans and produce education and outreach material, such as high-quality websites, children booklets, secondary school material, press releases, popular science-level material, animations and simulations, audio-visual kits, etc. As appropriate, the Consortium members will develop locally targeted educational material, and cultivate local contact points to broaden the Europe-wide network of outlets for the public relations activities.

The SDC plans to develop additional tools to facilitate the access of the science community to THESEUS legacy data products, as well as simplified tools to allow citizens to visualize the variable X-ray sky, explore source behaviours and flag interesting events, provide target advocacy and participation, connect with public robotic telescope networks etc.

During the mission implementation phase the Consortium will gather feedback from existing citizen science projects to better understand the lessons learned on engagement, tools, interfaces and data production. This will be used to inform the THESEUS outreach programme for maximising participation and expediting the websites to be ready near launch. Mobile applications for smartphones, tablets, and other media devices that will be available at the time of THESEUS will be developed to facilitate the large-scale diffusion of outreach material associated with the THESEUS mission. Communications and outreaching activity from the THESEUS consortium will be coordinated as part of the consortium project office tasks.

The scientific goals of THESEUS include recent Nobel Prize winning fields of research, like cosmology, gravitational waves, black-holes, all of which are fascinating for the general public and most attractive for young students. The excitement generated by the THESEUS mission and its discoveries will provide a topical platform around which to develop educational materials, helping to raise the profile of both the THESEUS mission and the associated scientific activities in general within schools. Curriculum-linked resources will be developed covering a broad range of scientific and technical topics, such as frontiers in the study of the early Universe, physics, detection and cosmic sources of gravitational waves and neutrino, the challenging hunting for electro-magnetic counterparts to high-energy and multi-messenger transients, the extreme physics of GRBs and ultra-relativistic jets. Materials will be disseminated to school students Europe-wide through educational partner networks, and will be supported by continued professional development courses to enable school teachers to use the science and engineering challenges of THESEUS to enliven and illustrate classroom lessons and activities.

Amateur astronomers play a crucial role, both in cascading the outreach efforts of professional scientists by providing a link with the broader general public, and by providing valuable scientific inputs. For instance, amateur observatories are already providing nowadays a significant contribution to the search and identification of optical counterparts to GRBs and also to many other classes of high-energy transients. THESEUS scientists will work to engage the amateur astronomer community, organising workshops and encouraging the community to undertake a programme of observations to support THESEUS. Since THESEUS alert data will be public and easily available, follow-up observations will be feasible, profitable and exciting to both the highly experienced and relatively novice amateur astronomers and schools.

The payload Consortium will execute an active programme to brief and inform policy makers at national and European levels on scientific and technological developments of THESEUS. One-on-one meetings, seminars for politicians and stakeholders, exhibitions at venues such as the European Parliament, and public events that will involve political figures as keynote speakers will be organized to keep policy makers abreast of developments which, although in the "blue-skies" field of space exploration, create indirect economic benefits to society. The fascinating new cosmic frontiers that will be revealed by THESEUS will need visual support to capture the imagination of the public. THESEUS scientists will work together with ESA to produce images, animations, and 3-D simulations suitable for a wide range of online and broadcast media formats. Artistic and musical collaborations will be fostered to spread the impact of the mission through artworks, compositions, writing and performance inspired by the THESEUS mission and its findings. Finally, the synergies of THESEUS with the very large facilities currently being developed (e.g., VRO/LSST, ELT, TMT, SKA, CTA, Athena, next generation GW and neutrino observatories) will be exploited also for further enhancing the outreach and communication aspects of the mission. Indeed, these future observatories are supported by large scientific community and managed by big international organizations. We foresee continuous interactions and resource sharing between the THESEUS Project Office and the corresponding offices at these top-level organizations for maximizing the dissemination of joint results and the efficiency of education efforts.

9 References

[1] ***Costa, E. et al.*** *1997, Nature, Vol. 387, p. 783.*

[2] ***Metzger, M. et al.*** *1997, Nature, Vol. 387, p. 878.*

[3] ***Van Paradijs, J. et al.*** *1997, Nature, Vol. 386, p. 686.*

[4] ***Tanvir, N. R. et al.*** *2007, Roy. Soc. Phil. Trans. A, Vol. 365, p. 1377.*

[5] ***Nakar, E.*** *2020, Phys. Rep., Vol. 886, p. 1.*

[6] ***McGuire, J. et al.*** *2016, ApJ, Vol. 825, p. 135.*

[7] ***Melandri, A. et al.*** *2015, A&A, Vol. 581, p. 86.*

[8] ***Chornock, R. et al.*** *2014, arXiv, p. 1405.7400.*

[9] ***Planck Collaboration.*** *2020, A&A, Vol. 641, p. 6.*

[10] ***Schenker, M. et al.*** *2014, ApJ, Vol. 795, p. 20.*

[11] ***Mondal, R. et al.*** *2020, MNRAS, Vol. 494, p. 4043.*

[12] ***Madau, P. et al.*** *2017, ApJ, Vol. 840, p. 39.*

[13] ***Finkelstein, S. et al.*** *2019, ApJ, Vol. 879, p. 36.*

[14] ***Perley, D. et al.*** *2016, ApJ, Vol. 817, p. 8.*

[15] ***Salvaterra, R. et al.*** *2013, MNRAS, Vol. 429, p. 2718.*

[16] ***Kistler, M. et al.*** *2019, ApJ, Vol. 705, p. 104.*

[17] ***Bouwens, R. et al.*** *2015, ApJ, Vol. 803, p. 34.*

[18] ***Tanvir, N. et al.*** *2012, ApJ, Vol. 754, p. 46.*

[19] ***Hartoog, O. et al.*** *2015, A&A, Vol. 580, p. 139.*

[20] ***Schady, P. et al.*** *2012, A&A, Vol. 537, p. 15.*

[21] ***Zafar, T. et al.*** *2018, MNRAS, Vol. 480, p. 108.*

[22] ***Fynbo, J. P. U. et al.*** *2014, A&A, Vol. 572, p. 12.*

[23] ***Zafar, T. et al.*** *2011, Vol. 735, p. 2.*

[24] ***Friis, M. et al.*** *2015, MNRAS, Vol. 451, p. 167.*

[25] ***De Cia, A., et al.*** *2018, A&A, Vol. 611, p. 76.*

[26] ***Bolmer, J., et al.*** *2018, A&A, Vol. 609, p. 62.*

[27] ***Heintz, K. et al.*** *2019, A&A, Vol. 629, p. 131.*

[28] ***Tanvir, N. et al.*** *2019, MNRAS, Vol. 483, p. 5380.*

[29] ***Vielfaure, J.-B., et al.*** *2020, A&A, Vol. 641, p. 30.*

[30] ***Steidel, C. et al.*** *2018, ApJ, Vol. 869, p. 123.*

[31] ***Robertson, B. et al.*** *2013, ApJ, Vol. 768, p. 71.*

[32] ***Atek, H. et al.*** *2015, ApJ, Vol. 814, p. 69.*

[33] ***Liu, C. et al.*** *2016, MNRAS, Vol. 462, p. 235.*

[34] ***McQuinn, M., et al.*** *2008, MNRAS, Vol. 388, p. 1101.*

[35] ***Bromm, V. et al.*** *2011, ARA&A, Vol. 49, p. 373.*

[36] ***Mészaros, P. et al.*** *2010, ApJ, Vol. 715, p. 967.*

[37] ***Toma, K., et al.*** *2011, ApJ, Vol. 731, p. 127.*

[38] ***Yoon, S-C. et al.*** *2015, ApJ, Vol. 802, p. 16.*

[39] ***Burlon, D., et al.*** *2016, MNRAS, Vol. 459, p. 3356.*

[40] ***Ma, Q. et al.*** *2015, MNRAS, Vol. 449, p. 3006.*

[41] ***Wang, F.Y., et al.*** *2012, ApJ, Vol. 760, p. 27.*

[42] ***Amati, L. et al.*** *2002, A&A, Vol. 390, p. 81.*

[43] ***Yonetoku, D. et al.*** *2004, ApJ, Vol. 609, p. 935.*

[44] ***Ghirlanda, G. et al.*** *2004, ApJ, Vol. 613, p. 13.*

[45] ***Amati, L. et al.*** *2008, MNRAS, Vol. 391, p. 577.*

[46] ***Ascenzi, S. et al.*** *2020, A&A, Vol. 641, p. 61.*

[47] ***Abbott, B. et al.*** *2016, ApJL, Vol. 826, p. 8.*

[48] ***Abbott, B. et al.*** *2019a, PRL, Vol. 9, p. 031040.*

[49] ***Abbott, B. et al.*** *2020a, arXiv2010.14527.*

[50] ***Abbott, B. et al.*** *2017a, PhRevL, Vol. 119, p. 161101.*

[51] ***Abbott, B. et al.*** *2020b, ApJ, Vol. 892, p. 3.*

[52] ***Abbott, B. et al.*** *2020c, ApJ, Vol. 896, p. 44.*

[53] ***Harry, G.*** *2010, Class. Quant. Grav., Vol. 27, p. 084006.*

[54] ***Acernese, F. et al.*** *2015, Class. Quant. Grav., Vol. 32, p. 024001.*

[55] ***Abbott, B. et al.*** *2017b, ApJL, Vol. 848, p. 12.*

[56] ***Abbott, B. et al.*** *2017c, ApJL, Vol. 848, p. 13.*

[57] ***Ghirlanda, G. et al.*** *2019, Science, Vol. 363, p. 968.*

[58] ***Kasen, D. et al.*** *2017, Nature, Vol. 551, p. 80.*

[59] ***Mooley, K. et al.*** *2018, Nature, Vol. 554, p. 207.*

[60] ***Aartsen, A. et al.*** *2013, Science, Vol. 342, p. 1242856.*

[61] ***Aartsen, M. et al.*** *2019, Eur. Phys. J. C, Vol. 79, p. 234.*

[62] ***Albert, A. et al.*** *2020, ApJ, Vol. 892, p. 1.*

[63] ***Aartsen, M. et al.*** *2018, Science, Vol. 361, p. 1378.*

[64] ***Somiya, K. et al.*** *2012, Class. Quant. Grav., Vol. 29, p. 124007.*

[65] ***Abbott, B. et al.*** *2020e, Living Reviews in Relativity, Vol. 23, p. 3.*

[66] ***Punturo, M. et al.*** *2010, Class. Quant. Grav., Vol. 27, p. 194002.*

[67] ***Reitze, D. et al.*** *2019, arXiV:1907.04833.*

[68] ***Adrian-Martinez, S. et al.*** *2016, Journal of Physics, Vol. G43(8), p. 084001.*

[69] ***Avrorin, A. et al.*** *2019, EPJWC , Vol. 20701003A.*

[70] ***Maggiore, M. et al.*** *2020, Journal of Cosmology and Astroparticle, Vol. 3, p. 50.*

[71] ***Chan, M. et al.*** *2018, PhRD, Vol. 97, p. 12.*

[72] ***Norris, J. et al.*** *2006, ApJ, Vol. 643, p. 266.*

[73] ***Norris, J. et al.*** *2010, ApJ, Vol. 717, p. 411.*

[74] ***Bostanci, Z. et al.*** *2013, MNRAS, Vol. 428, p. 1623.*

[75] ***Kaneko, Y. et al.*** *2015, MNRAS, Vol. 452, p. 824.*

[76] ***Lien, A. et al.*** *2016, yCat, Vol. 18290007L.*

[77] ***Kisaka, S. et al.*** *2017, ApJ, Vol. 846, p. 142.*

[78] ***Barthelmy, S. et al.*** *2005, Nature, Vol. 438, p. 994.*

[79] ***Bucciantini, N.*** *2011, A&A, Vol. 528, p. 101.*

[80] ***Metzger, B. et al.*** *2012, ApJ, Vol. 746, p. 48.*

[81] ***Evans, P. et al.*** *2016, MNRAS, Vol. 462, p. 1591.*

[82] ***Sari, R.*** *1998, ApJ, Vol. 494, p. 49.*

[83] ***Siegel, D. et al.*** *2016, ApJ, Vol. 819, p. 15.*

[84] ***Oganesyan, G.*** *2020, ApJ, Vol. 893, p. 88.*

[85] ***Beniamini, P. et al.*** *2020, MNRAS, Vol. 493, p. 3521.*

[86] ***Metzger, B. et al.*** *2014, MNRAS, Vol. 439, p. 3916.*

[87] ***Piro, A. et al.*** *2017, ApJ, Vol. 844, p. 19 .*

[88] ***Drago, A. et al.*** *2018, ApJ, Vol. 852, p. 32.*

[89] ***Evans, P. et al.*** *2017, Science, Vol. 358, p. 1565.*

[90] ***Sugita, S. et al.*** *2018, PASJ, Vol. 70, p. 81.*

[91] ***Rossi, A. et al.*** *2020, MNRAS, Vol. 493, p. 3379.*

[92] ***Metzger, B. et al.*** *2020, ApJ, Vol. 902, p. 22.*

[93] ***Tanvir, N. et al.*** *2013, Nature, Vol. 500, p. 547.*

[94] ***Coulter, D. et al.*** *2017, Science, Vol. 358, p. 1556.*

[95] ***Tanvir, N. et al.*** *2017, ApJL, Vol. 848, p. 27.*

[96] ***Pian, E. et al.*** *2017, Nature, Vol. 551, p. 67.*

[97] ***Smartt, S. et al.*** *2017, Nature, Vol. 551, p. 75.*

[98] ***Riess, A. et al.*** *2020, arXiv, Vol. 2012.08534.*

[99] ***Abbott, B. et al.*** *2017d, Nature, Vol. 551, p. 85.*

[100] ***Belgacem, E. et al.*** *2019, JCAP, Vol. 24, p. 7.*

[101] ***Powell, J. et al.*** *2016, PhRevD, Vol. 94, p. 123012.*

[102] ***Cutler, C. et al.*** *2002, PhRvD, Vol. 66, p. 4025.*

[103] ***Corsi, A. et al.*** *2009, MNRAS, Vol. 720, p. 1171.*

[104] ***Dall'Osso, S. et al.*** *2018, MNRAS, Vol. 480, p. 1353 .*

[105] ***Virgili, F. et al.*** *2009, MNRAS, Vol. 392, p. 91.*

[106] ***Waxman, E. et al.*** *1999, Phys.Rev.D, Vol. 59, p. 023002.*

[107] ***Ghisellini, G. et al.*** *2020, A&A, Vol. 636, p. 82.*

[108] ***Aartsen, M. et al.*** *2016, ApJ, Vol. 824, p. 2.*

[109] ***Adrián-Martínez, S. et al.*** *2013, A&A, Vol. 559, p. 9.*

[110] ***Albert, A.*** *2017, ApJL, Vol. 850, p. 35.*

[111] ***Denton, P. et al.*** *2018, ApJ, Vol. 855, p. 37 .*

[112] ***Kimura, S. et al.*** *2017, ApJ, Vol. 848, p. 4.*

[113] ***Piran, T.*** *2005, Rev. Mod. Phys., Vol. 76, p. 1143.*

[114] ***Preece, R. et al.*** *1998, ApJ, Vol. 506, p. 23.*

[115] ***Sari, R. et al.*** *1996, ApJ, Vol. 473, p. 204.*

[116] ***Rees, M. et al.*** *2005, ApJ, Vol. 628, p. 847.*

[117] ***Asano, K. et al.*** *2009, ApJ, Vol. 705, p. 1714.*

[118] ***Oganesyan, G. et al.*** *2017, ApJ, Vol. 860, p. 137.*

[119] ***Oganesyan, G. et al.*** *2018, A&A, Vol. 616, p. 138.*

[120] ***Oganesyan, G. et al.*** *2019, A&A, Vol. 628, p. 59.*

[121] ***Ravasio, M. et al.*** *2018, A&A, Vol. 613, p. 16.*

[122] ***Ravasio, M. et al.*** *2019, A&A, Vol. 625, p. 60.*

[123] ***Ronchi, M. et al.*** *2020, A&A, Vol. 636, p. 35.*

[124] ***Ghirlanda, G. et al.*** *2013, MNRAS, Vol. 432, p. 3237.*

[125] ***Daigne, F. et al.*** *2002, MNRAS, Vol. 336, p. 1271.*

[126] ***Levinson, A. et al.*** *2020, PhR, Vol. 866, p. 1.*

[127] ***Amati, L. et al.*** *2000, Science, Vol. 290, p. 953.*

[128] ***Janiuk, A.*** *2014, A&A, Vol. 568, p. 105.*

[129] ***Fenimore, E. et al.*** *1998, ApJ, Vol. 473, p. 998.*

[130] ***Kumar, P. et al.*** *2000, ApJ, Vol. 541, p. 9.*

[131] ***D'Alessio, V. et al.*** *2006, A&A, Vol. 460, p. 3.*

[132] ***Ronchini, M. et al.*** *2020, Nat. Comm. (submitted), Vol. arXiv200903913R.*

[133] ***Sakamoto, T. et al.*** *2008, ApJ, Vol. 679, p. 570.*

[134] ***Liang, E. et al.*** *2007, ApJ, Vol. 662, p. 1111.*

[135] ***Pescalli, A. et al.*** *2015, MNRAS, Vol. 447, p. 1911.*

[136] ***Salafia, M. et al.*** *2016, MNRAS, Vol. 461, p. 3607.*

[137] ***Reichart, D. et al.*** *2001, ApJ, Vol. 552, p. 57.*

[138] ***Rizzuto, D. et al.*** *2007, MNRAS, Vol. 379, p. 619.*

[139] ***Beloborodov, A. et al.*** *1998, ApJ, Vol. 508, p. 25.*

[140] ***Guidorzi, C. et al.*** *2012, MNRAS, Vol. 422, p. 1785.*

[141] ***Dichiara, S. et al.*** *2016, A&A, Vol. 589, p. 97.*

[142] ***Guidorzi, C. et al.*** *2015, ApJ, Vol. 801, p. 57.*

[143] ***Aschwanden, M. et al.*** *2018, Space Sci. Rev., Vol. 214, p. 55.*

[144] ***Wang, F. et al.*** *2013, Nat. Phys., Vol. 9, p. 465.*

[145] ***Greco, G. et al.*** *2011, Nat Sci. Rep., Vol. 1, p. 91.*

[146] ***De Luca, A. et al.*** *2010, MNRAS, Vol. 402, p. 1870.*

[147] ***Cenko, B. et al.*** *2010, AJ, Vol. 140, p. 224.*

[148] ***Dichiara, S. et al.*** *2013, ApJ, Vol. 777, p. 132.*

[149] ***Guidorzi, C. et al.*** *2016, A&A, Vol. 589, p. 98.*

[150] ***Bernardini, M. et al.*** *2017, A&A, Vol. 607, p. 121.*

[151] ***Bolmont, J. et al.*** *2008, ApJ, Vol. 676, p. 532.*

[152] ***Ellis, J. et al.*** *2008, Astroparticle Physics, Vol. 29, p. 158.*

[153] ***Franckowiak, A. et al.*** *2018, A&A, Vol. 609, p. 120.*

[154] ***Osborne, J.*** *2015, JHEAP, Vol. 7, p. 117.*

[155] ***Starrfield, S. et al.*** *2020, ApJ, Vol. 895, p. 70.*

[156] ***Metzger, B. et al.*** *2015, MNRAS, Vol. 450, p. 2739.*

[157] ***Sala, G. et al.*** *2005, A&A, Vol. 439, p. 1061.*

[158] ***Wolf, W. et al.*** *2013, ApJ, Vol. 777, p. 136.*

[159] ***Kato, M. et al.*** *2015, ApJ, Vol. 808, p. 52.*

[160] ***Kato, M. et al.*** *2016, ApJ, Vol. 830, p. 40.*

[161] ***Shafter, A.*** *2017, ApJ, Vol. 834, p. 196.*

[162] ***Bode, M. et al.*** *2006, ApJ, Vol. 652, p. 629.*

[163] ***Osborne, J. et al.*** *2011, ApJ, Vol. 727, p. 124.*

[164] ***Cappellaro, E. et al.*** *2015, A&A, Vol. 584, p. 62.*

[165] ***Höflich, P. et al.*** *2009, ApJ, Vol. 705, p. 483.*

[166] ***Dragulin, P. et al.*** *2016, ApJ, Vol. 818, p. 26.*

[167] ***Hsiao, E. et al.*** *2020, ApJ, Vol. 900, p. 140.*

[168] ***HI4PI, Collaboration.*** *2016, A&A, Vol. 594, p. 116.*

[169] ***Mereghetti, S. et al.*** *2020, ApJ, Vol. 898, p. 29.*

[170] ***Mereghetti, S. et al.*** *2015, SSRv, Vol. 191, p. 315.*

[171] ***Frederiks, D. et al.*** *2007, AstL, Vol. 33, p. 19.*

[172] ***Ofek, E. et al.*** *2008, ApJ, Vol. 681, p. 1464.*

[173] ***Svinkin, D. et al.*** *2021, Nature, Vol. 589, p. 211.*

[174] ***Roberts, O. et al.*** *2021, Nature, Vol. 589, p. 207.*

[175] ***Saxton, R. et al.*** *2020, SSRv, Vol. 216, p. 85.*

[176] ***Komossa, S. et al.*** *1999, A&A, Vol. 343, p. 775.*

[177] ***Mockler, B. et al.*** *2019, ApJ, Vol. 872, p. 151.*

[178] ***Lin, D. et al.*** *2018, Nature Astronomy, Vol. 2, p. 656.*

[179] ***Jonker, P. et al.*** *2020, ApJ, Vol. 889, p. 166.*

[180] ***Zauderer, B. et al.*** *2011, Nature, Vol. 476, p. 425.*

[181] ***Cenko, B. et al.*** *2012, ApJ, Vol. 753, p. 77.*

[182] ***Khabibullin, I. et al.*** *2014, MNRAS, Vol. 437, p. 327.*

[183] ***Yuan, W. et al.*** *2015, arXiv, Vol. 1506.07735.*

[184] ***van Velzen, S. et al.*** *2011, ApJ, Vol. 741, p. 73.*

[185] ***Schawinski, K. et al.*** *2015, MNRAS, Vol. 451, p. 2517.*

[186] ***Ricci, C. et al.*** *2020, ApJ, Vol. 898, p. 1.*

[187] ***Miniutti, G. et al.*** *2019, Nature, Vol. 573, p. 381.*

[188] ***Janiuk, A. et al.*** *2015, A&A, Vol. 574, p. 92.*

[189] ***Janiuk, A. et al.*** *2000, MNRAS, Vol. 318, p. 180.*

[190] ***Nakaniwa, N. et al.*** *2019, MNRAS, Vol. 488, p. 5104.*

[191] ***Zemko, P. et al.*** *2014, MNRAS, Vol. 445, p. 869.*

[192] ***Sidoli, L.*** *2017, arXiv, Vol. 1710.03943.*

[193] ***Galloway, D. et al.*** *2017, arXiv, Vol. 1712.06227.*

[194] ***Papitto, A. et al.*** *2020, arXiv, Vol. 2010.09060.*

[195] ***Kaaret, P. et al.*** *2017, ARAA, Vol. 55, p. 303.*

[196] ***Bahramian, A. et al.*** *2020, arXiv, Vol. 2009.10322.*

[197] ***Sharykin, I. et al.*** *2015, AstL, Vol. 41, p. 53.*

[198] ***Kuerster, M. et al.*** *1996, A&A, Vol. 311, p. 211.*

[199] ***Osten, R. et al.*** *2007, ApJ, Vol. 654, p. 1052.*

[200] ***Osten, R. et al.*** *2010, ApJ, Vol. 721, p. 785.*

[201] ***Caramazza, M. et al.*** *2007, A&A, Vol. 471, p. 645.*

[202] ***Tsuboi, Y. et al.*** *2016, PASJ, Vol. 68, p. 90.*

[203] ***Neupert, W.*** *1968, ApJ, Vol. 153, p. 59.*

[204] ***Güdel, M. et al.*** *2004, A&A, Vol. 716, p. 713.*

[205] ***Fender, R. et al.*** *2015, MNRAS, Vol. 446, p. 66.*

[206] ***Caballero-Garcia, M. et al.*** *2015, MNRAS, Vol. 452, p. 4195.*

[207] ***Osten, R. et al.*** *2016, ApJ, Vol. 832, p. 174.*

[208] ***Mitra, S. et al.*** *2018, MNRAS, Vol. 473, p. 945.*

[209] ***Gehrels, N. et al.*** *2004, ApJ, Vol. 611, p. 1005.*

[210] ***Totani, T. et al.*** *2006, PASJ, Vol. 58, p. 485.*

[211] ***Gallerani, S. et al.*** *2008, MNRAS, Vol. 388, p. 84.*

[212] ***Xu, Y. et al.*** *2011, MNRAS, Vol. 410, p. 2025.*

[213] ***Abell, P. et al.*** *2009, arXiv, Vol. 0912.0201.*

[214] ***Cherenkov Telescope Array, Consortium.*** *2019, arXiv, Vol. 1709.07997.*

[215] ***Abdalla, H. et al.*** *2019, Nature, Vol. 575, p. 464.*

[216] ***Acciari, V. et al.*** *2019, Nature, Vol. 575, p. 455.*

[217] ***Ghirlanda, G. et al.*** *2015, MNRAS, Vol. 448, p. 2514.*

[218] ***Salvaterra, R. et al.*** *2012, ApJ, Vol. 749, p. 68.*

[219] ***D'Avanzo, P. et al.*** *2015, JHEAp, Vol. 7, p. 73.*

[220] ***Wanderman, D. et al.*** *2010, MNRAS, Vol. 406, p. 1944.*

[221] ***Jonker, P. et al.*** *2013, ApJ, Vol. 779, p. 14.*

[222] ***Salvaterra, R. et al.*** *2007, MNRAS, Vol. 380, p. 45.*

[223] ***Heger, A. et al.*** *2001, ApJ, Vol. 560, p. 307.*

[224] ***Yoon, S. et al.*** *2006, A&A, Vol. 460, p. 199.*

[225] ***Madau, P. et al.*** *2014, ARA&A, Vol. 52, p. 415.*

[226] ***Cole, S. et al.*** *2001, MNRAS, Vol. 326, p. 255.*

[227] ***Nava, L.*** *2012, MNRAS, Vol. 421, p. 1256.*

[228] ***Ghirlanda, G. et al.*** *2016, A&A, Vol. 594, p. 84.*

[229] ***Ryan, J. et al.*** *2020, ApJ, Vol. 896, p. 23.*

[230] ***O'Brien, P. et al.*** *2021, Proc of SPIE, Vol. 11444, p. 304.*

[231] ***Angel, J.*** *1979, ApJ, Vol. 233, p. 364.*

[232] ***Amati, L. et al.*** *2021, JATIS, Vol. submitted.*

[233] ***Labanti, C et al.*** *2021, Proc. of SPIE, Vol. 11444.*

[234] ***Gasent-Blesa, J.-L. et al.*** *2021, Proc. of SPIE, Vol. 11444.*

[235] ***Campana, R. et al.*** *2021, Proc. of SPIE, Vol. 11444.*

[236] ***Fuschino, F. et al.*** *2021, Proc. of SPIE, Vol. 11444.*

[237] ***Guidorzi, C.*** *2015, Astronomy and Computing, Vol. 10, p. 54.*

[238] ***Kinugawa, T., et al.*** *2019, ApJ, Vol. 878, p. 128.*

[239] ***Nestor, D. et al.*** *2013, ApJ, Vol. 765, p. 47.*

[240] ***Robertson, B. E. et al.*** *2012, ApJ, Vol. 744, p. 95.*

[241] ***Sparre, M. et al.*** *2014, ApJ, Vol. 785, p. 150.*

[242] ***Bernardini, M. et al.*** *2015, MNRAS, Vol. 446, p. 1129.*

[243] ***Abbott, B. et al.*** *2019b, PhRv, Vol. 100, p. 4004.*

[244] ***Abbott, B. et al.*** *2019c, ApJ, Vol. 886, p. 7.*

[245] ***Abbott, B. et al.*** *2020d, PhRv, Vol. 101, p. 4002.*

[246] ***Aartsen, M. et al.*** *2019, Science, Vol. 361, p. 1378.*

[247] ***Aartsen, M. et al.*** *2014, arXiv:1412.5106.*

[248] ***Bartos, I. et al.*** *2017, ApJ, Vol. 835, p. 2.*

[249] ***Ando, S. et al.*** *2013, Reviews of Modern Physics, Vol. 85, p. 1401.*

[250] ***Pagliaroli, G. et al.*** *2016, Journal of Cosmology and Astroparticle Physics, Vol. 11, p. 4.*

[251] ***Ahlers, M. et al.*** *2018, Progress in Particle and Nuclear Physics, Vol. 102, p. 73.*

[252] ***Albert, A. et al.*** *2020, Nature Review Physics, Vol. 2, p. 10.*

[253] ***Albert, A. et al.*** *2017, MNRAS, Vol. 469, p. 906.*

[254] ***Beniamini, P. et al.*** *2018, MNRAS, Vol. 476, p. 5621.*

[255] ***Mukai, K. et al.*** *2017, PASP, Vol. 129, p. 062001.*

[256] ***Bachetti, M. et al.*** *2014, Nature, Vol. 514, p. 202.*

[257] ***Fürst, F. et al.*** *2016, ApJL, Vol. 831, p. 14.*

[258] ***Israel, G. et al.*** *2017, Science, Vol. 355, p. 817.*

[259] ***Tsygankov, S. et al.*** *2016, MNRAS, Vol. 457, p. 1101.*

[260] ***Benz, A. et al.*** *2010, ARA&A, Vol. 48, p. 241.*

[261] ***Tsuboi, Y. et al.*** *2014. Suzaku-MAXI 2014: Expanding the Frontiers of the X-ray Universe. p. 138.*

[262] ***Carrington, R.*** *1859, MNRAS, Vol. 20, p. 13.*

[263] ***Aulanier, G. et al.*** *2013, A&A, Vol. 549, p. 66.*

[264] ***Kitze, M. et al.*** *2014, MNRAS, Vol. 442, p. 3769.*

[265] ***Candelaresi, S. et al.*** *2014, ApJ, Vol. 792, p. 67.*

[266] ***Wu, C. et al.*** *2015, ApJ, Vol. 798, p. 92.*

[267] ***Koch, D. et al.*** *2010, ApJ, Vol. 713, p. 79.*

[268] ***Sillanpaa, A. et al.*** *1988, ApJ, Vol. 325, p. 628.*

[269] ***Domingo, A. et al.*** *2003, Highlights of Spanish Astrophysics, Vol. III, p. 470.*

[270] ***Bolmer, J. et al.*** *2019, A&A, Vol. 623, p. 43.*

[271] ***Hartoog, O. et al.*** *2015 : s.n., A&A, Vol. 580, p. 139.*

[272] ***Mereghetti, S. et al.*** *2021, Proc. of SPIE, Vol. 11444.*

10 List of Acronyms

2/3G	Second/Third Generation
AC	Alert Centre
AGILE	Astrorivelatore Gamma a Immagini LEggero
[CL]AGN	[Changing-Look] Active Galactic Nucleus
AO	Announcement of Opportunity
AOCS	Attitude and Orbit Control System
ASI	Agenzia Spaziale Italiana
ASIC	Application-Specific Integrated Circuit
ATHENA	Advanced Telescope for High-Energy Astrophysics
BAT	Burst Alert Telescope
BATSE	Burst And Transient Source Experiment
BEE	Back-End Electronics
BeppoSAX	Beppo [Occhialini] Satellite per Astronomia X
[SM]BH	[Super-Massive] Black Hole
CBC	Compact Binary Coalescences
CE	Cosmic Explorer
CF	Cold Finger
CGRO	Cosmic Gamma Ray Observatory
CMOS	Complementary Metal Oxide Semiconductor
CNES	Centre National dâ€™Etudes Spatiales
CTA	Cherenkov Telescope Array
CUA	Control Unit Assembly
DHU	Data Handling Unit
DLA	Dumped Lyman Alpha
DYN	DYNamical [pointing strategy]
ECP	EClipctic Pole [pointing strategy]
ECU	Electronics Control Unit
EE	Extended Emission
ELT	Extremely Large Telescope
EM	Electro-Magnetic
EoL	End-of-Life
EoR	Epoch of Reionization
EP	Einstein Probe
eROSITA	extended ROentgen Survey with an Imaging Telescope Array
ESA	European Space Agency
ESAC	European Space Astronomy Centre
ESDC	ESAC Science Data Centre
ESOC	European Space Operation Centre
ET	Einstein Telescope
EXOSAT	European X-ray Observatory Satellite
eXTP	extended X-ray Timing and Polarimetry mission

FAST	First G-APD Cherenkov Telescope
FDIR	Fault Detection Isolation and Recovery
FEE	Front-End Electronics
FM	Folding Mirror
FoR	Field of Regard
FoV	Field of View
FPA	Focal Plane Array
FRB	Fast Radio Bursts
FWHM	Full Width Half Maximum
GBM	Gamma-ray Burst Monitor
GNSS	Global Navigation Satellite System
GO	Guest Observer
GRB	Gamma-Ray Bursts
GWE	Gravitational Wave Event
HERMES	High Energy Rapid Modular Ensemble of Satellites
HK	HouseKeeping
HST	Hubble Space Telescope
H/SW	Hard/SoftWare
KAGRA	Kamioka Gravitational Wave Detector
KM3NeT	Cubic Kilometre Neutrino Telescope
JWST	James Webb Space Telescope
IACT	Imaging Air Cherenkov Telescope
IBIS	Imager on Board of the INTEGRAL Satellite
IGM	InterGalactic Medium
IMF	Initial Mass Function
INTEGRAL	INTErnational Gamma-Ray Astrophysics Laboratory
IOC	Instrument Operation Centre
ISM	InterStellar Medium
[N]IR	[Near] Infra-Red
IRT	InfraRed Telescope
IRT-CAM	Cubic Kilometre Neutrino Telescope
IRT-CUA	IRT Calibration Unit Assembly
IRT-WA	IRT Wheel Assembly
IRT-WCU	IRT Wheel Control Unit
ΛCDM	Lambda Cold Dark Matter
LEO[P]	Low-Earth Orbit [Phase]
LF	Luminosity Function
LGA	Low-Gain Antenna
[a]LIGO	[advanced] Laser Interferometer Gravitational-Wave Observatory
LIV	Lorentz InVariance
LMC	Large Magellanic Cloud
LOFT	Large Observatory for X-ray Timing

LoS	Line of Sight
LSST	Large Synoptic Survey Telescope
MAGIC	Major Atmospheric Gamma Imaging Cherenkov Telescope
MAXI	Monitor of All-sky X-ray Image
MLD	Meander-Line Dipole
MLI	Multi-Layer Insulator
MOC	Mission Operation Center
MOS	Mission Observation Simulator
MPO	Micro-Pore Optics
MTL	Mission TimeLine
MXT	Microchannel X-ray Telescope
MW	Milky Way
NASA	National Aeronautics and Space Administration
NISP	Near Infrared Spectrometer and Photometer
NS	Neutron Star
OBC	On-Board Computer
OCR	Operational Change Request
PC	Partially Coded
PCB	Processing Control Board
PI	Principle Investigator
PICsIT	Pixellated Imaging CaeSium Iodide Telescope
PLM	PayLoad Module
PPS	Pulse Per Second
PS	Project Scientist
PSF	Point Spread Function
PSU	Power Supply Unit
QPE	Quasi-Periodic Eruptions
RAAN	Right Ascension of the Ascending Node
RASS	ROSAT All-Sky Survey
ROI	Region Of Interest
ROSAT	Roentgen SATellite
S/C	SpaceCraft
SAA	South Atlantic Anomaly
SN[R]	Signal to Noise [Ratio]
SDC	Science Data Centre
SDD	Silicon Drift Detector
SDPT	Spin-Down Powered Transient
SFR	Star Formation Ratio
SFXT	Supergiant Fast X-ray Transient
SGR	Soft Gamma-ray Repeater
[C][S]GS	[Consortium] [Science] Ground Segment
SKA	Square Kilometre Array
SLA	Source Location Accuracy
SMC	Small Magellanic Cloud
SMILE	Solar wind Magnetosphere Ionosphere Link Explorer
[CC]SN	[Core-Collapse] SuperNova
SOA	SXI Optics Assembly
SRG	Spectrum Roentgen Gamma
SST	Science Study Team
SVM	SerVice Module
SVOM	Space Variable Objects Monitor
SXI	Soft X-ray Imager
TAC	Time Allocation Committee
TBAGS	THESEUS Burst Alert Ground Stations
TBU	Trigger Broadcasting Unit
TCS	Thermal Control System
TDE	Tidal Disruption Events
TEC	Thermo-Electric Coolers
TM	TeleMetry
TMT	Thirty Meter Telescope
ToO	Target of Opportunity
THESEUS	Transient High-Energy Sky and Early Universe Surveyor
TSST	THESEUS Science Study Team
TT&C	Telemetry, Tracking & Command
ULX	Ultra-Luminous X-ray source
[F]UV	[Far] Ultra-Violet
VERITAS	Very Energetic Radiation Imaging Telescope Array System
VHE	Very High-Energy
VHF	Very-High Frequency
VLT	Very Large Telescope
VRO	Vera Rubin Observatory
XDF	eXtreme Deep Field
XGIS	X-Gamma rays Imaging Spectrometer
XRT	X-Ray Telescope
XSU	XGIS Supply Unit
WD	White Dwarf
WFC-3	Wide Field Camera 3
WHIM	Warm-Hot Intergalactic Medium
WISE	Wide-field Infrared Survey Explorer